

สำนักหอสมุดกลาง พระจอมเกล้าลาดกระบัง

**MATHEMATICAL MODEL FOR THE ADSORPTION OF
SULFUR DIOXIDE BY CALCIUM CARBONATE**



T
ค
ค
ค

เลขหม.....
เลขทะเบียน..... 37746
วัน, เดือน, ปี 16 ส.ค. 2544

**A THESIS SUBMITTED IN PARTIAL FULFILLMENT
OF THE REQUIREMENT FOR THE DEGREE OF
MASTER OF ENGINEERING IN MECHANICAL ENGINEERING
SCHOOL OF GRADUATE STUDIES
KING MONGKUT'S INSTITUTE OF TECHNOLOGY LADKRABANG**

2000

This material is reserved for educational use only, not allowed for commercial use.

ISBN 974 - 622 - 916 - 8

Forbidden to modify the content, and cite the document when use.



COPYRIGHT 2000

SCHOOL OF GRADUATE STUDIES

KING MONGKUT'S INSTITUTE OF TECHNOLOGY LADKRABANG

This material is reserved for educational use only, not allowed for commercial use.

Forbidden to modify the content, and cite the document when use.

หัวข้อวิทยานิพนธ์	แบบจำลองทางคณิตศาสตร์ของการดูดซับก๊าซซัลเฟอร์ไดออกไซด์ด้วยแคลเซียมคาร์บอเนต
นักศึกษา	นายวิภู ศรีสีบสาย
รหัสประจำตัว	41062004
ปริญญา	วิศวกรรมศาสตรมหาบัณฑิต
สาขาวิชา	สาขาวิศวกรรมเครื่องกล
พ.ศ.	2543
อาจารย์ผู้ควบคุมวิทยานิพนธ์	ผศ.ดร.จารุวัตร เจริญสุข

บทคัดย่อ

วิทยานิพนธ์ฉบับนี้เสนอการสร้างแบบจำลองทางคณิตศาสตร์สำหรับการดูดซับก๊าซซัลเฟอร์ไดออกไซด์ในห้องเผาไหม้ด้วยผงแคลเซียมคาร์บอเนต ซึ่งประกอบไปด้วย 2 กระบวนการคือการแตกตัวของแคลเซียมคาร์บอเนตเป็นแคลเซียมออกไซด์และการรวมตัวของแคลเซียมออกไซด์กับก๊าซซัลเฟอร์ไดออกไซด์ซึ่งเกิดปฏิกิริยาไม่พร้อมกัน แบบจำลองดังกล่าวถูกนำไปผสมผสานกับแบบจำลองการก่อตัวและการกระจายตัวของออกไซด์ของกำมะถัน ซึ่งเกิดจากการเผาไหม้ถ่านหินผงที่ได้พัฒนาแล้วโดยนายปัญญา แดงวิไลลักษณ์ โดยพิจารณาการถ่ายเทเอนทัลปี มวล โมเมนตัม และการเผาไหม้ถ่านหินผง ลักษณะของห้องเผาไหม้เป็นทรงกระบอกแนวตั้งและเปลวไฟชนิดลงด้านล่าง มีเส้นผ่านศูนย์กลางภายใน 0.6 เมตร และความยาวรวม 3.0 เมตร เส้นผ่านศูนย์กลางของหัวเผา 0.056 เมตร จากการศึกษาผลของตำแหน่งและขนาดอนุภาคของแคลเซียมคาร์บอเนตที่ปล่อย รวมไปถึงอุณหภูมิของผนังห้องเผาไหม้ต่อปริมาณการดูดซับก๊าซซัลเฟอร์ไดออกไซด์ ได้ข้อสรุปว่าอนุภาคของแคลเซียมคาร์บอเนตควรจะถูกฉีดเข้าไปในกระแสหมุนวนภายนอกของก๊าซเพื่อให้อนุภาคอยู่ในห้องเผาไหม้ได้นาน และอนุภาคควรจะเดินทางผ่านช่วงอุณหภูมิในห้องเผาไหม้ที่สูง และพบว่าตำแหน่งที่ปล่อยอนุภาคและขนาดของอนุภาคมีผลต่อการดูดซับน้อย ข้อมูลดังกล่าวจะเป็นประโยชน์ในการศึกษาเพื่อลดปริมาณก๊าซซัลเฟอร์ไดออกไซด์ในห้องเผาไหม้ต่อไป

Thesis Title Mathematical Model for The Adsorption of Sulfur
 Dioxide by Calcium Carbonate
Student Mr.Wipoo Sriseubsai
Student ID. 41062004
Degree Master of Engineering
Programme Mechanical Engineering
Year 2000
Thesis Advisor Asst.Prof.Dr.Jaruwat Charoensuk

ABSTRACT

This thesis presents a study on mathematical modeling for sulfur dioxide adsorption by calcium carbonate, which consists of calcination and sulfation processes. Those processes are assumed insimultaneous reaction. The model is incorporated with the existing model involving enthalpy, mass, momentum transfer equations, the mathematical model of sulfur oxide formation and distribution in pulverized coal combustion that is developed by Daungviluilux P. The vertically down-fire combustion chamber has a cylindrical shape with 0.6 m. inside diameter, 0.3 m. in length and equipped with the 0.056 m. diameter burner. The results show the effects of inlet locations, particle size and wall temperature on the amount of sulfur dioxide adsorption. The residence time and temperature surrounding calcium carbonate particles are found to be the primary parameters for sulfur dioxide adsorption, whereas, the inlet locations and particle sizes of calcium carbonate have less effect. This study is an informative data for further study about the reduction of sulfur dioxide emissions from the pulverized coal combustion.

ACKNOWLEDGEMENTS

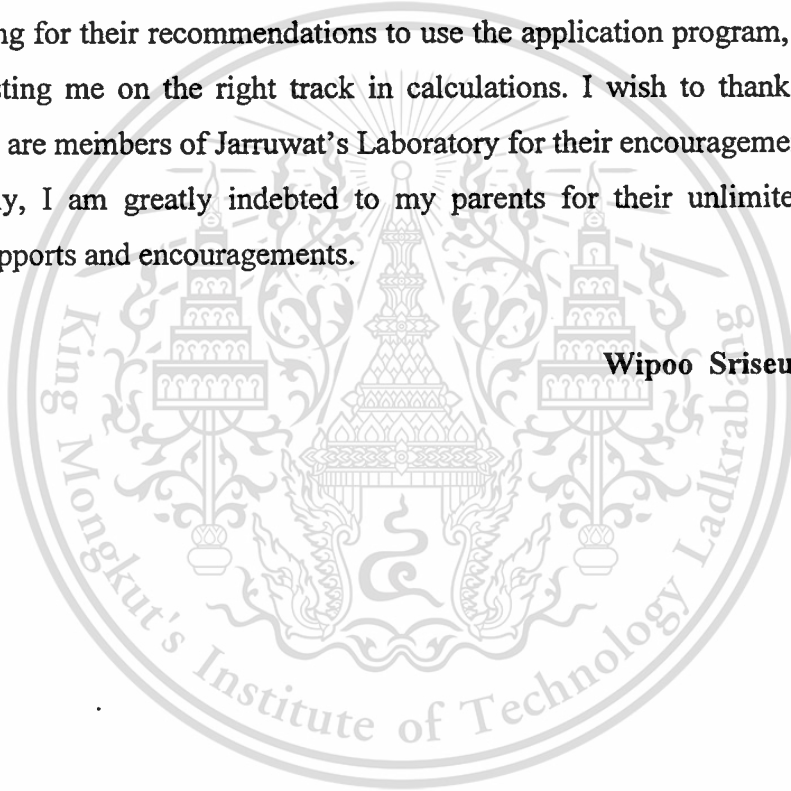
There are numerous individuals whose assistance was crucial to the successful completion of this thesis.

First of all, I would like to express my profoundly invaluable gratitude to my advisor, Asst.Prof.Dr. Jarruwat Charoensuk, for his continuously valuable guidance, helpful suggestions and consistent encouragement since the first day I was his advisee.

I am particularly grateful to Mr. Panya Daungviluilux and Ms. Sudarat Kwankaomeng for their recommendations to use the application program, MATLAB, and for assisting me on the right track in calculations. I wish to thank my fellow students who are members of Jarruwat's Laboratory for their encouragements.

Finally, I am greatly indebted to my parents for their unlimited patience, consistent supports and encouragements.

Wipoo Sriseubsai



CONTENTS

	Page
Thai abstract	I
English abstract	II
Acknowledgements	III
Contents	IV
List of tables	VI
List of figures	VII
Nomenclatures	XI
CHAPTER 1 INTRODUCTION	
1.1 Background of coal utilization in Thailand.....	1
1.2 Purpose and scope of the thesis.....	2
1.3 Outlines of the remaining chapters	2
CHAPTER 2 LITERATURE REVIEW	
2.1 Introduction.....	3
2.2 General descriptions of flue gas desulfurization technologies.....	3
2.3 Important researches for establishing adsorption model.....	5
CHAPTER 3 MATHEMATICAL MODEL	
3.1 Introduction.....	9
3.2 The governing equations in polar co – ordinate forms for gas phase model	9
3.3 Numerical handling at boundaries	11
3.4 Mathematical modeling of gas – phase combustion	14
3.5 Particulate phase model.....	14
3.6 Thermal radiation model.....	21
3.7 Sulfur oxides formation model	22

CONTENTS (continued)

	Page
CHAPTER 4 ADSORPTION MODEL	
4.1 Introduction	23
4.2 Calcination model	23
4.3 Sulfation model	28
4.4 Integration of calcination and sulfation models into FAFNIR.....	40
CHAPTER 5 COMPUTATIONAL SIMULATION	
5.1 Introduction	43
5.2 Numerical set – up for coal combustion in furnace	43
5.3 The simulation of coal combustion (base case)	46
5.4 Computational simulation for adsorption	49
5.5 Modified boundary for coal combustion (base case)	67
5.6 Modified simulation for adsorption	70
5.7 Summary	81
CHAPTER 6 CONCLUSIONS AND DISCUSSIONS	
6.1 Summary of the preceding chapters.....	83
6.2 Conclusions.....	84
6.3 Remarks for further studies.....	84
REFERENCES.....	85
APPENDICES	88
AUTHOR BIOGRAPHY.....	101

LIST OF TABLES

Tables	Page
4.1 Summary of activation energy, reaction rates and frequency factors of dolomites, Borgwardt, 1970.....	30
4.2 Effect of particle sizes on reaction rate at the sulfate loading of 2×10^{-3} mol/g, 870°C	32
4.3 Empirical values of reaction rate at 870°C , sulfate loading of 1×10^{-3} mol/g of 150/170 – mesh particle size (0.0096 cm.).....	32
4.4 Reaction rate at zero sulfation and β for 1337, 1351, 1343 and 1360 stones.....	32
5.1 Characteristics of bituminous coal.....	45
5.2 Furnace operating conditions.....	45
5.3 Kinetic parameters for coal combustion model.....	46
5.4 Numerical set – up for desulfurization properties in case 1.....	50
5.5 Numerical set – up for desulfurization properties in case 2.....	50
5.6 Numerical set – up for desulfurization properties in case 3.....	51
5.7 Numerical set – up for desulfurization properties in case 4.....	51
5.8 Numerical set – up for desulfurization properties in case 5.....	70
5.9 Numerical set – up for desulfurization properties in case 6.....	71
5.10 Numerical set – up for desulfurization properties in case 7.....	71

LIST OF FIGURES

Figures	Page
2.1 Various flue gas desulfurization systems and processes, with characteristics descriptions.....	4
3.1 Dissipation of particle passing a cell.....	15
4.1 Overall concepts for adsorption	23
4.2 Schematic diagram of the calcination model	24
4.3 Model of sulfation process on porous CaO particle.....	28
4.4 Graphical representation of r_0 and β	33
4.5 Sorption of sulfur dioxide for different particle sizes of dolomite 1351, Borgwardt, 1970	33
4.6 Graphical representation of r_0 and β with η_0^* modification.....	35
4.7 Effect of zero – sulfation diffusion resistance on sorption of sulfur oxides against experimental data, dolomite 1351, $D_p = 0.0096$ cm.	36
4.8 Effect of zero – sulfation diffusion resistance on sorption of sulfur oxides against experimental data, dolomite 1351, $D_p = 0.025$ cm.	37
4.9 Comparison between mathematical simulation at $\eta_0^* = 0.35$ and measurement for dolomite 1351, $D_p = 0.025$ cm	37
4.10 Comparison between mathematical simulation at $\eta_0^* = 0.09$ and measurement for dolomite 1351, $D_p = 0.13$ cm	38
4.11 Effect of zero – sulfation diffusion resistance on sorption of sulfur oxides against experimental data, dolomite 1351, $D_p = 0.13$ cm	38
4.12 Effect of β on sorption of sulfur oxides against experimental data, dolomite 1351, $D_p = 0.0096$ cm	39
4.13 Comparison between mathematical simulation and the measurement for dolomite 1351	40
4.14 Flowchart for CaCO_3 particle tracking	41
5.1 Schematic diagram of the top segment of the ICSTM furnace.....	44
5.2 Schematic diagram of the burner	44

This material is reserved for educational use only, not allowed for commercial use.

Forbidden to modify the content, and cite the document when use.

LIST OF FIGURES (continued)

Figures	Page
5.3 Distribution of temperature (K) (a) entire furnace (b) in the near burner zone	47
5.4 Coal particle trajectories (a) entire furnace (b) in the near burner zone	48
5.5 Concentration of sulfur oxides (in % $m_{SO_2} / m_{mixture}$) near the burner zone	49
5.6 Section of the burner and additional $CaCO_3$ inlets	52
5.7 Sorption of sulfur dioxide for dolomite 1351 diameter of 0.0096 cm. (case 1)....	54
5.8 Sorption of sulfur dioxide for dolomite 1351 diameter of 0.025 cm. (case 2).....	54
5.9 $CaCO_3$ particle trajectories in case 1 (a) entire furnace (b) in the near burner zone	55
5.10 $CaCO_3$ particle trajectories in case 2 (a) entire furnace (b) in the near burner zone	56
5.11 Distribution of temperature (K) in case 1 (a) entire furnace (b) in the near burner zone.....	57
5.12 Distribution of temperature (K) in case 2 (a) entire furnace (b) in the near burner zone.....	58
5.13 $CaCO_3$ particle trajectories in case 3 (a) entire furnace (b) in the near burner zone	59
5.14 Distribution of temperature (K) in case 3 (a) entire furnace (b) in the near burner zone.....	60
5.15 Sorption of sulfur dioxide for dolomite 1351 diameter of 0.0096 cm. (case 3)...	61
5.16 $CaCO_3$ particle trajectories in case 4 (a) entire furnace (b) in the near burner zone	62
5.17 Sorption of sulfur dioxide for dolomite 1351 diameter of 0.0096 cm. (case 4)...	63
5.18 Distribution of temperature (K) in case 4 (a) entire furnace (b) in the near burner zone.....	64
5.19 Concentration of sulfur oxides, case 1 (in % $m_{SO_2} / m_{mixture}$), in the near burner zone.....	65
5.20 Concentration of sulfur oxides, case 2 (in % $m_{SO_2} / m_{mixture}$), in the near burner zone.....	65

This burner zone.....

LIST OF FIGURES (continued)

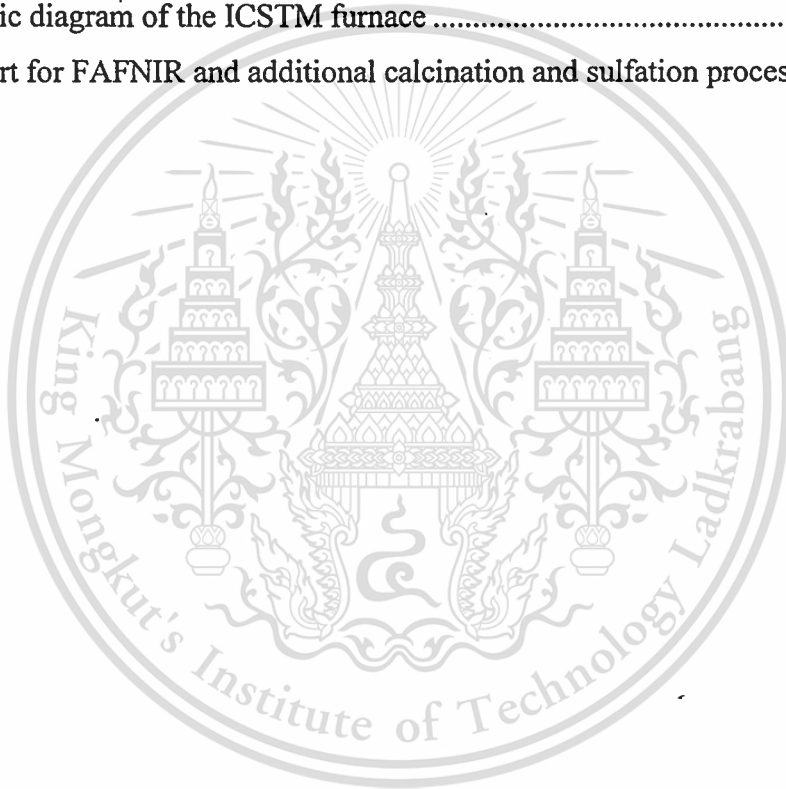
Figures	Page
5.21 Concentration of sulfur oxides, case 3 (in % $m_{SO_2} / m_{mixture}$), in the near burner zone.....	66
5.22 Concentration of sulfur oxides, case 4 (in % $m_{SO_2} / m_{mixture}$), in the near burner zone.....	66
5.23 Distribution of modified temperature (K) (a) entire furnace (b) in the near burner zone.....	68
5.24 $CaCO_3$ particle trajectories in the near burner under modified wall temperature.....	69
5.25 Concentration of sulfur oxides (in % $m_{SO_2} / m_{mixture}$) in the near burner zone under modified wall temperature	69
5.26 $CaCO_3$ particle trajectories in case 5 (a) entire furnace (b) in the near burner zone	72
5.27 $CaCO_3$ particle trajectories in case 6 (a) entire furnace (b) in the near burner zone	73
5.28 $CaCO_3$ particle trajectories in case 7 (a) entire furnace (b) in the near burner zone	74
5.29 Distribution of temperature (K) in case 5 (a) entire furnace (b) in the near burner zone.....	75
5.30 Distribution of temperature (K) in case 6 (a) entire furnace (b) in the near burner zone.....	76
5.31 Distribution of temperature (K) in case 7 (a) entire furnace (b) in the near burner zone.....	77
5.32 Sorption of sulfur dioxide for dolomite 1351 diameter of 0.0096 cm. (case 5)...	78
5.33 Sorption of sulfur dioxide for dolomite 1351 diameter of 0.0096 cm. (case 6)...	78
5.34 Sorption of sulfur dioxide for dolomite 1351 diameter of 0.0096 cm. (case 7)...	79
5.35 Concentration of sulfur oxides, case 5 (in % $m_{SO_2} / m_{mixture}$), in the near burner zone.....	79

This material is reserved for educational use only, not allowed for commercial use.

Forbidden to modify the content, and cite the document when use.

LIST OF FIGURES (continued)

Figures	Page
5.36 Concentration of sulfur oxides, case 6 (in % $m_{SO_2} / m_{mixture}$), in the near burner zone.....	80
5.37 Concentration of sulfur oxides, case 7 (in % $m_{SO_2} / m_{mixture}$), in the near burner zone.....	80
A-1 Schematic diagram of the ICSTM furnace	90
A-2 Flowchart for FAFNIR and additional calcination and sulfation processes	91



NOMENCLATURES

Roman symbols

A	Frequency factor of CaCO_3 particle
A_p	Projected area of the particle
$ACOMB$	Model constant
$BCOMB$	Model constant
C_a	Constant of order unity
C_b	Constant of order unity
C_{1d}	Empirical constant
C_{2d}	Empirical constant
$C_{\varepsilon 1}$	Model constant
$C_{\varepsilon 2}$	Model constant
C_D	Drag coefficient
C_μ	Constant for the $k - \varepsilon$ turbulence model
c	Concentration of SO_2
c_p	Specific heat of gas at constant pressure
D	Diffusion coefficient
D_0	Value of binary diffusion
D_c	Diffusion coefficient for $\text{O}_2 - \text{N}_2$ mixture
D_K	Knudsen diffusion
D_{AB}	Molecular diffusion coefficient for CO_2
D_ϕ, D_{eff}	Laminar and Effective diffusion coefficients of scalar property
D_p	Diameter of CaCO_3 particle
d_p	Diameter of coal particle
E	Effective activation energy of char reaction
E_{dvol}	Activation energy for devolatilization
F	External force
F_d	Drag force

This material is reserved for educational use only, not allowed for commercial use.

Forbidden to modify the content, and cite the document when use.

NOMENCLATURES (continued)

G	Generation of turbulent kinetic energy
H_C	char calorific value
h	Specific enthalpy
h_{tran}	Heat transfer coefficient
K	Turbulent kinetic energy
K_c	Chemical coefficient for char reaction model
K_d	Diffusion coefficient for char reaction model
K_e	Equivalent absorption coefficient
K_g	Gas absorption coefficient
K_t	Total rate coefficient for char reaction
K_0	Frequency factor for char reaction
K_p	Particle absorption coefficient
K'_p	Cumulative projected area of particle
k	Turbulent kinetic energy
k_A	Rate constant
k_D	Rate constant for decomposition of CaCO_3
k_f	Mass transfer coefficient
k_0	Pre – exponential factor
k_v	Rate constant for sulfation model
L_v	Latent heat of devolatilization
M	Molecular mass
M_c	Atomic mass carbon
m	Mass
m	Order of reaction
N_u	Nusselt number
n'	Amount of sulfate in solid particle
P	Pressure

This material is reserved for educational use only, not allowed for commercial use.

Forbidden to modify the content, and cite the document when use.

NOMENCLATURES (continued)

P_i	Partial pressure at node I
P_e	Equilibrium dissociation pressure of CO ₂
P_b	Partial pressure in bulk gas of CO ₂
P_t	Total pressure
\dot{Q}	Heat transfer between particulate and gaseous phases
\dot{q}_w	Heat flux at across the wall
\dot{q}_b	Heat flux across the boundary layer
R_{cc}	Kinetic reaction rate of the coal char
R_{cox}	Reaction rate due to the diffusion of oxygen
R_d	Mean particle diameter
R_u	Universal gas constant
R_e	Reynolds number
R_D	Rate of CaCO ₃ decomposition
R_{SO_2}	Rate of SO ₂ formation
R_m	Rate of mass efflux from particulate to the gaseous phase
R_v	Volumetric reaction rate of volatilizes
r	Radial co-ordinate
r_{sul}	Reaction rate of sulfation
r_w	Radiation reflectivity at the wall
S_{st}	Stoichiometric value of volatile gas
S	Source term of transport equation
S_{BET}	BET surface area
S_m	Mass contribution from particulate of gas phase
$S_{v,j}$	Momentum contribution from the particulate phase to the gas phase
T	Absolute temperature

This material is reserved for educational use only, not allowed for commercial use.

Forbidden to modify the content, and cite the document when use.

NOMENCLATURES (continued)

T_R	Radiation temperature
\bar{T}_w	particle mean emission temperature
t	Time
U	Characteristic velocity, usually referred to the value at the burner inlet
$\Delta U_{p,g}$	Difference of particle velocity referred to that of the gas
u	Velocity components in axial direction
u_τ	Friction velocity
u_{disp}	Particle dispersion velocities in axial direction
V	Cumulative volatile release
V	Characteristic volume of the system
V^*	Potential volatile content of coal
v	Velocity components in radial direction
v_{disp}	Particle dispersion velocities in radial direction
w	Velocity components in angular direction
w_p	Weight of solid particles
X	Molar fraction
x_{s_r}	Mass fraction of SO ₂
x_i	Mass fraction of particle size group I
y	Distance from the stationary wall
y^+	Dimensionless distance from the wall
Σ	Summation

Greek symbols

β	Empirical parameter
ε	Dissipation rate of turbulence kinetic energy
ε_p	Particle emissivity

Γ This material is reserved for educational use only, not allowed for commercial use.

Forbidden to modify the content, and cite the document when use.

NOMENCLATURES (continued)

φ	Mechanism factor for char reaction
κ	Von Karman constant
μ	Absolute viscosity
μ_l	Laminar viscosity
μ_{ed}	Eddy viscosity
μ_{eff}	Effective viscosity
ρ	Density
η	Effectiveness factor
τ	Characteristic residence time
τ_w	Wall shear stress
ϕ	Scalar property
σ	Stefan – Boltzman constant
σ_h	Molecular Prandtl number
$\sigma_{h,t}$	Turbulent Prandtl number
σ_k	Effective Prandtl number
$\sigma_{\phi,t}$	Turbulent Schmidt or Prandtl number of scalar species

Overbars and superscripts

$\bar{\quad}$	Unweighted time averaged mean value
$\tilde{\quad}$	Density – weight time averaged mean value
\cdot	Fluctuating component in unweighted averaging
\cdot^{ρ}	Fluctuating component in density – weight averaging
$+$	Normalized quantity near a wall in Couette flow analysis
n	Order of reaction rate coefficient for char reaction model
$*$	Parameter modification

NOMENCLATURES (continued)

Subscripts

<i>a</i>	Absorbing
<i>as</i>	Asymptotic
<i>convec</i>	Convection
<i>comb</i>	Combustion
<i>D</i>	Decomposition
<i>e</i>	Equilibrium
<i>eff</i>	Effective value
<i>g</i>	Gas phase; gas
<i>i, j, k</i>	Space co – ordinate
<i>l</i>	Laminar
<i>N</i>	Number of nodes or number of shells
<i>ox, o₂</i>	Oxygen
<i>p</i>	Particulate phase or particle
<i>pr</i>	Product
<i>rad</i>	Radiation
<i>tot</i>	total
<i>turb, t</i>	Turbulent
<i>vol</i>	Volumetric
<i>v</i>	Coriolis force
<i>wall</i>	Wall
<i>φ</i>	Quantity φ
<i>0</i>	Zero sulfation
<i>ref</i>	Reference

CHAPTER 1

INTRODUCTION

Contained in with this chapter is the background of coal utilization in Thailand and its consequence on air pollution. The objective of the research and the scope of the thesis will be discussed. The outlines of the remaining chapters, which summarize the information of the succeeding chapters, are given.

1.1 Background of coal utilization in Thailand

Fossil fuel has been long used as energy sources. Although today, the leading part of the energy sources used all over the world consists of fossil fuel such as coal and heavy oil. When any kind of the fossil fuel is converted into energy, it always generates nitrogen oxide (NO_x), dust and sulfur oxide (SO_x), all of which cause air pollution. Eiichi YUGETA [1] reports that the results of the three-year investigation technology in Thailand found that the activities of coal are:

- Coal utilization in the power industry, such as Mae Moh power station at Lampang province where sulfur dioxide (SO_2) pollution is caused by lignite combustion.
- Coal utilization in the cement industry the pulverized coal is applied to the cement-burning kiln in order to reduce the fuel cost. The environmental problem will not to be caused, if pulverized coal burning technology is used.
- Coal utilization in the non-power industries such as coal used as fuel for boilers in the paper and pulp industry, the chemical industry and the food industry. However, it appears that coal will be replaced with kerosene or LPG due to easy combustion control in the future.
- Coal utilization in residential and commercial sectors, the majority of this consists of firewood and charcoal. There are many investigations of wood fuel but they have stopped because of unresolved problem on cost, smoke, odor and other elements of quality.

The SO_2 pollution has been becoming big social issues. Thus, the establishment of mathematical model for SO_2 adsorption is developed in this.

1.2 Purpose and scope of the thesis

Sulfur dioxide adsorption consists of the calcination and sulfation processes. The purpose of this thesis is to develop the mathematical model for each process, calcination and sulfation model. The equations and experimental results, which are validated against these models, are based on the publications of Silcox [2] and Borgwardt [3]. This mathematical model includes with the mathematical model of sulfur oxide formation in pulverized coal combustion (FAFNIR) developed by Charoensuk J. [4] and Daungvilailux P. [5]. The effects of inlet locations of calcium oxide (CaO) particles and particle sizes are also discussed.

1.3 Outlines of the remaining chapters

This thesis consists of six chapters including this introduction. As mentioned earlier, the objective of this thesis concerns about the derivation of the mathematical model for SO₂ adsorption, the details of the derivation procedures are summarized in the remaining chapters as follows:

Chapter 2 describes in general the flue gas desulfurization technologies and extensive literatures for establishing of the mathematical model.

Chapter 3 describes the mathematical equations for coal combustion and sulfur oxide formation involving the governing equation for gas phase, the boundary equations, the devolatilization, the conservation of momentum, including the sulfur oxide formation model which are developed by Charoensuk J. [4] and Daungvilailux P. [5].

Chapter 4 presents the adsorption model which consists of calcination model and sulfation model. The equations and experimental results for establishment of the mathematical model including the validation study are shown in this chapter.

Chapter 5 displays the calculations of SO₂ adsorption with 7 case studies of different inlet locations of calcined CaO particles and their particle sizes.

Chapter 6 summarizes the consequence of the preceding chapters together with the discussions of the further study.

Subsequently, the flowchart for the calculation procedures and figure of ICSTM furnace are shown in the appendices.

CHAPTER 2

LITERATURE REVIEW

2.1 Introduction

The development of computer hardware leads to an establishment of numerical methods for the solutions of complex mathematical equations, such as those governing flow, combustion and heat transfer. One of its applications is the simulation of such processes in industrial combustors. The solution is obtained in conjunction with an experimental assessment to help engineers and researchers distinguishing the differences between theoretical assumptions and what actually happen during combustion, which helps them gaining a better understanding on such process. There have been extensive works on the model development in order to improve many aspects of its predictive quality. Nevertheless, calculation of a validated mathematical model is able to provide the likely results which would be expected from the experiment. So this chapter will present the general descriptions of flue gas desulfurization technologies and the important informations from the literatures which are significant for establishing the adsorption model.

2.2 General descriptions of flue gas desulfurization technologies

The first flue gas desulfurization system in the world was put into operation in 1930 in the Great Britain [6]. It was reported that this first equipment had failed to continue a long-term operation due to scale trouble (solid deposit) on the equipment.

After that, the flue gas desulfurization system was improved in Japan and the United States during 1970s to be manufactured as commercial system since then.

Today, various types of desulfurization systems are proposed so as to be suitable for individual plant conditions. In general, there are three classifications of desulfurization systems—wet type flue gas desulfurization, dry type flue gas desulfurization and semi-dry type flue gas desulfurization. Furthermore, each type of the system can be divided to different desulfurization methods by types of adsorbent used.

Fig.2.1 shows the desulfurization system classifications and their own methods and characteristics descriptions.

This material is reserved for educational use only, not allowed for commercial use.

Forbidden to modify the content, and cite the document when use.

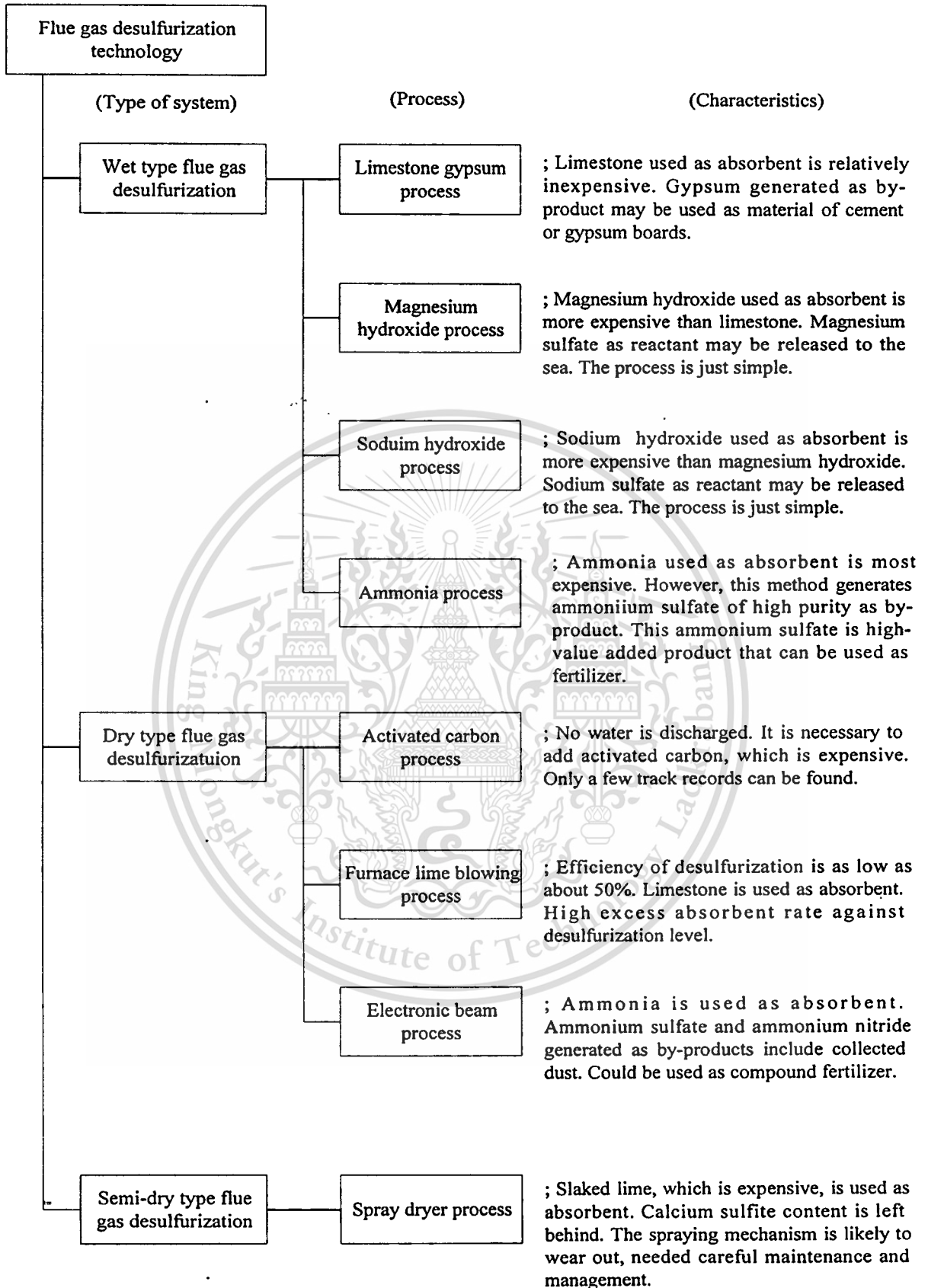


Fig.2.1 Various flue gas desulfurization systems and processes, with characteristic descriptions [6]

This material is reserved for educational use only, not allowed for commercial use.

Forbidden to modify the content, and cite the document when use.

Most of the flue gas desulfurization systems currently used in Japan as well as overseas countries are wet type systems. Of those several wet type systems, particularly the one using limestone as adsorbent for recovering gypsum is the most popular type. In this study, however, the dry type is investigated for achieving the objective that is presented in chapter 1. Despite of low adsorption efficiency, the operating costs involved in dry type flue gas desulfurization is the lowest. It is therefore interesting to fine out what can be done to improve its efficiency. Thus, the mathematical model of dry type flue gas desulfurization must be developed.

2.3 Important researches for establishing adsorption model

Coal is the cheapest and most abundant fossil fuel compared to gas and oil. It is regarded as the major energy resource of the future, at least for the first half of the new century. However, due to environmental impacts of coal combustion, it is necessary to find a clean and efficient way of extracting the energy from it. In recent years, mathematical simulation has played active roles in the development of coal combustion [7 – 13] Recent work by Romo-Millares [11] has incorporated global mechanisms for NO formation and reduction [14] into the model for simulation of combustion heat transfer and NO emission of ICSTM furnace. However, both SO₂ formation and reduction mechanisms have not been incorporated into the combustion model. This study is, therefore, aimed at developing a simplified and reasonably accurate model, which simulates both the formation and reduction of sulfur oxides.

Kinetic studies of sulfur oxides formation reveal that the reaction rate is of the same order of that of combustion. In a non-premixed flame, which typically occurs in coal combustion, where the flame temperature is above 1000°C, kinetic rate is much higher than mixing rate of reactants. Thus, turbulent mixing dominates the overall reaction. Reduction of sulfur oxides, however, mostly takes place at relatively lower temperature and longer residence time. A number of desulfurization techniques have been established. One of them concerns treating of low-grade coal prior to feed into a combustion chamber by blending it with those of higher grade, or separation of pyrite by washing or gravitational method, etc. These techniques have proofed successful in removing pyritic sulfur (FeS₂) but unable to remove those chemically bound with organic matters. Other alternative approaches are treatments during and after combustion. An intermediate treatment involves dry injection of sorbent particles into

a furnace where sulfur oxides are adsorbed under optimum reacting environment. Two types of sorbents are used, which are calcium carbonate, generally known as limestone (CaCO_3), and calcium hydroxide. Post-flame treatments, for example, semi-dry and wet scrubbing are achieved by spraying sulfur-oxide adsorbing solution into exhaust gases. This requires an appropriate device to collect the product of the reaction for disposal or for further use, leading to an increase in initial and operating costs. A semi-dry process also needs careful maintenance due to wearing of the spraying mechanism. Moreover, the cost of adsorbing agents is relatively high [6]. Of these desulfurization techniques, the dry injection of sorbent is the cheapest, but suffers from low adsorption efficiency. SO_2 reduction is reported to be as low as 50% [6] due to short available residence time in a pulverized combustion furnace. Thus, increasing the adsorption efficiency of calcined stone is one of the interesting topics in desulfurization.

Limestone rapidly undergoes the calcination process and produces porous calcined CaO particles and carbon dioxide as shown in the following equation [15].



The high heating rate due to immediate particle suspension in a hot, well-dispersed furnace causes a rapid decomposition of CaCO_3 , leading to formation of CaO whose specific area is reportedly as high as $90 \text{ m}^2/\text{g}$ [16]. The CaO further reacts with SO_2 and oxygen molecules producing CaSO_4 according to the following equation [15].



Although the CaCO_3 -derived calcine is less effective in capturing SO_2 than the $\text{Ca}(\text{OH})_2$ -derived stones [17], the former is more widely used because of its ease of supply. One of the experimental studies, carried out in 1989 by Zarkanitis and Sotirchos [18], revealed that the particle sorptive capacity for SO_2 removal was closely linked to the pore size distribution and the intraparticle mass-transport resistance. They further concluded that the size distribution and the interconnectedness of the pores were important factors rather than the particle

This material is reserved for educational use only, not allowed for commercial use.

Forbidden to modify the content, and cite the document when use.

porosity for adsorption capability of calcined particles. The conversion-versus-time curve was lowered with increasing particle sizes, decreasing calcination temperature and increasing sulfation temperature. This is explained in terms of an increase in diffusion limit due to external plugging. The studies were, however, carried out at the temperature between 750-850°C which was lower than that in a near-flame zone of typical pulverized coal combustors (above 1000°C).

The pore structure also changes while the sulfation reaction is taking place. Newton [19] reported that there were temperature dependent losses in the porosity of calcium based sorbents, due to CO₂ - activated sintering, during high temperature (900 - 1300 °C), short time SO₂ capture (< 1 s). In this process, occurring at temperature around 970°C, many small crystals grew into fewer larger ones, leading to a reduction in internal specific surface area and consequently a decrease in sulfation rate. This result was in good agreement with a study carried out earlier by Borgwardt and Bruce in 1986 [17], which reported a relationship between specific surface area and rate of CaSO₄ formation. Borgwardt [3] also reported an exponential decrease in sulfation rate with an increase in sulfation loading. Several semi-empirical models described this plugging process in terms of diffusion of SO₂ through the porous structure, which led to thicken in product layer in porous structure. [20 – 29] Simons [30] and Simons and Garman [31] found that external or mouth plugging occurred in large pores where reaction was controlled by diffusion. Uniform deposition, however, took place in small pores due to kinetically controlled reaction. Moreover, the SO₂ gas was adsorbed between the temperature range of 900°C and 1300°C, because the diffusion and kinetic rates limit the lower bound of reaction, where the upper one was limited by the reaction stability [19]. Maximum conversion was found to be between 1100°C and 1200°C. Among those investigators, Sotirchos and Yu [32] developed random pore structural models incorporated with an intraparticle and reaction model for simulation of gas-solid reaction. The simulation on sulfation of limestone with SO₂ had been carried out at a reaction temperature of 850 °C with a SO₂ concentration of 0.3% v/v. It is interesting to note here that the reaction temperature was lower than that recommended in an earlier literature that reaction would occur at the temperature between 900 to 1300°C. Nevertheless, the simulation result was in good agreement with an experimental investigation by Hartman and Coughlin [22 – 23]. Latest study of Mahuli et al. [33] combine

This material is reserved for educational use only, not allowed for commercial use.

existing calcination, sintering and sulfation models based on a grain-subgrain concept with first-order calcination kinetics. Validation study carried out by the same researchers against the previous experimental results, i.e., calcination conversion and surface area loss, had been quite satisfactory.



CHAPTER 3

MATHEMATICAL MODEL

3.1 Introduction

This chapter presents a review of the mathematical equations governing combustion in the furnace. A computational code, FAFNIR, is used to numerically solve a number of mathematical equations in polar, two-dimensional co-ordinate domain using structured algorithms [4].

It also briefly describes the governing equations for gas phase model, numerical handling at boundaries, mathematical model of gas phase combustion, particle phase, thermal radiation and sulfur dioxide formation [5].

3.2 The governing equations in polar co – ordinate forms for gas phase model [4]

The FAFNIR code is utilized for calculation in an axi – symmetrical domain. A set of governing equations, polar co – ordinate, are presented as follows:

3.2.1 Continuity

$$\frac{1}{r} \frac{\partial}{\partial r} (r \rho \tilde{v}) + \frac{\partial}{\partial z} (\rho \tilde{u}) = \bar{S}_m \quad (3.1)$$

\bar{S}_m is the source term created from the transport from particulate phase during combustion.

3.2.2 Momentum Conservation

Radial direction:

$$\frac{1}{r} \frac{\partial}{\partial r} (r \rho \tilde{v} \tilde{v}) + \frac{\partial}{\partial z} (\rho \tilde{u} \tilde{v}) = -\frac{\partial \bar{p}}{\partial r} + \frac{1}{r} \frac{\partial}{\partial r} \left(r \mu_{eff} \frac{\partial \tilde{v}}{\partial r} \right) + \frac{\partial}{\partial z} \left(\mu_{eff} \frac{\partial \tilde{v}}{\partial z} \right) + \bar{S}_v + \bar{S}_{m,v} \quad (3.2)$$

where

$$\bar{S}_v = \frac{1}{r} \frac{\partial}{\partial r} \left(r \mu_{eff} \frac{\partial \tilde{v}}{\partial r} \right) + \frac{\partial}{\partial z} \left(\mu_{eff} \frac{\partial \tilde{v}}{\partial z} \right) + \frac{\rho \tilde{w}^2}{r} - 2 \mu_{eff} \frac{\tilde{v}}{r^2} \quad (3.3)$$

This material is reserved for educational use only, not allowed for commercial use.

Forbidden to modify the content, and cite the document when use.

and $\bar{S}_{m,v}$ is the momentum source term due to particulate phase in radial direction.

Axial direction:

$$\frac{1}{r} \frac{\partial}{\partial r} (r \bar{\rho} \tilde{v} \tilde{u}) + \frac{\partial}{\partial z} (\bar{\rho} \tilde{u} \tilde{u}) = -\frac{\partial \bar{p}}{\partial r} + \frac{1}{r} \frac{\partial}{\partial r} \left(r \mu_{eff} \frac{\partial \tilde{u}}{\partial r} \right) + \frac{\partial}{\partial z} \left(\mu_{eff} \frac{\partial \tilde{u}}{\partial z} \right) + \bar{S}_u + \bar{S}_{m,u} \quad (3.4)$$

where

$$\bar{S}_u = \frac{1}{r} \frac{\partial}{\partial r} \left(r \mu_{eff} \frac{\partial \tilde{v}}{\partial z} \right) + \frac{\partial}{\partial z} \left(\mu_{eff} \frac{\partial \tilde{v}}{\partial z} \right) \quad (3.5)$$

and $\bar{S}_{m,u}$ is the momentum source term due to the particulate phase in the axial direction.

Tangential direction:

$$\frac{1}{r} \frac{\partial}{\partial r} (r \bar{\rho} \tilde{v} \tilde{w}) + \frac{\partial}{\partial z} (\bar{\rho} \tilde{u} \tilde{w}) = \frac{1}{r} \frac{\partial}{\partial r} \left(r \mu_{eff} \frac{\partial \tilde{w}}{\partial r} \right) + \frac{\partial}{\partial z} \left(\mu_{eff} \frac{\partial \tilde{w}}{\partial z} \right) + \bar{S}_w + \bar{S}_{m,w} \quad (3.6)$$

where

$$\bar{S}_w = -\tilde{w} \left(\frac{\bar{\rho} \tilde{v}}{r} + \frac{\mu_{eff}}{r^2} + \frac{1}{r} \frac{\partial \mu_{eff}}{\partial r} \right) \quad (3.7)$$

and $\bar{S}_{m,w}$ is the momentum source term due to the particulate phase in the angular direction.

3.2.3 Turbulent transport

Turbulent kinetic energy:

$$\frac{1}{r} \frac{\partial}{\partial r} (r \bar{\rho} \tilde{v} k) + \frac{\partial}{\partial z} (\bar{\rho} \tilde{u} k) = \frac{1}{r} \frac{\partial}{\partial r} \left(r \frac{\mu_{eff}}{\sigma_K} \frac{\partial k}{\partial r} \right) + \frac{\partial}{\partial z} \left(\frac{\mu_{eff}}{\sigma_K} \frac{\partial k}{\partial z} \right) + G + \bar{\rho} \varepsilon \quad (3.8)$$

where

$$G = \mu_{eff} \left\{ 2 \left[\left(\frac{\partial \tilde{u}}{\partial z} \right)^2 + \left(\frac{\partial \tilde{v}}{\partial r} \right)^2 + \left(\frac{\tilde{v}}{r} \right)^2 \right] + \left(\frac{\partial \tilde{u}}{\partial r} + \frac{\partial \tilde{v}}{\partial z} \right) + \left(\frac{\partial \tilde{w}}{\partial z} \right)^2 + \left[r \frac{\partial}{\partial r} \left(\frac{\tilde{w}}{r} \right) \right]^2 \right\} \quad (3.9)$$

Dissipation rate:

$$\frac{1}{r} \frac{\partial}{\partial r} (r \bar{\rho} \tilde{v} \varepsilon) + \frac{\partial}{\partial z} (\bar{\rho} \tilde{u} \varepsilon) = \frac{1}{r} \frac{\partial}{\partial r} \left(r \frac{\mu_{eff}}{\sigma_\varepsilon} \frac{\partial k}{\partial r} \right) + \frac{\partial}{\partial z} \left(\frac{\mu_{eff}}{\sigma_\varepsilon} \frac{\partial k}{\partial z} \right) + C_{\varepsilon 1} \frac{\varepsilon}{k} G + C_{\varepsilon 2} \bar{\rho} \frac{\varepsilon^2}{k} \quad (3.10)$$

3.2.4 Scalar transport

$$\frac{1}{r} \frac{\partial}{\partial r} (r \bar{\rho} \tilde{v} \tilde{\phi}) + \frac{\partial}{\partial z} (\bar{\rho} \tilde{u} \tilde{\phi}) = \frac{1}{r} \frac{\partial}{\partial r} \left(r D_{eff} \frac{\partial \tilde{\phi}}{\partial r} \right) + \frac{\partial}{\partial z} \left(D_{eff} \frac{\partial \tilde{\phi}}{\partial z} \right) + \bar{S}_\phi \quad (3.11)$$

$$D_{eff} = D_\phi + \frac{\mu_{eff}}{\sigma_{\phi,t}} \quad (3.12)$$

3.3 Numerical handling at boundaries [4]

There are two assumptions to be made in the calculation of the momentum conservation, turbulent kinetic energy and heat in the region closed to the wall boundary, i.e.,

- 1) The shear stress in the fluid is equal to the shear stress at the wall.
- 2) Convection and diffusion fluxes are considered to be small so that the production rate of turbulence energy may be equated to its dissipation rate.

The transport of energy is calculated using the effective Prandtl number.

A non-dimensional parameter y^+ is used to characterize the flow near the boundary and is defined by

$$y^+ = \frac{\bar{\rho} u_\tau y}{\mu_1} \quad (3.13)$$

where y is a distance from the stationary wall and u_τ is a friction velocity defined as

This material is reserved for educational use only, not allowed for commercial use.

Forbidden to modify the content, and cite the document when use.

$$u_\tau = \sqrt{\frac{\tau_w}{\rho}} \quad (3.14)$$

where τ_w is the wall shear stress. The flow region is categorized into two zones:

- 1) $0 < y^+ < 11.63$: laminar sub-layer where the molecular diffusion dominates ($\mu_l \gg \mu_t$), and Newtonian flow is assumed.
- 2) $11.63 < y^+ < 300$: turbulent sub - layer where turbulent diffusion dominates ($\mu_t \gg \mu_l$).

3.3.1 Momentum conservation near the wall

The calculation of the contribution of the shear stress to the conservation of momentum closed to a stationary wall recognizes two regions:

- 1) Laminar sub - layer: The shear stress is the product of viscosity and the gradient of the velocity component parallel to the wall $\left(\tau = \mu_l \frac{d\tilde{u}}{dy} = \tau_w \right)$.
- 2) Turbulent sub - layer: the shear stress is given by $\tau = \mu_t \frac{d\tilde{u}}{dy} = \tau_w$, where the eddy viscosity is: $\mu_t = \bar{\rho} \kappa y u_\tau$ and κ is Von Karman constant. The derived form of shear stress is given by

$$\tau = \bar{\rho} k^{1/2} C_\mu^{1/4} \frac{\kappa \tilde{u}}{\ln(y^+)} \quad (3.15)$$

3.3.2 Turbulent kinetic energy and its dissipation near the wall

Neglecting the convection and diffusion fluxes in the equation of kinetic energy, the generation rate of turbulent kinetic energy is equal to its dissipation rate, so that:

$$-\overline{\rho \tilde{u}^* \tilde{v}^*} \frac{\partial \tilde{u}}{\partial y} = \bar{\rho} \varepsilon \quad (3.16)$$

Applying Boussinesq's hypothesis to the flow at the boundary, we have:

This material is reserved for educational use only, not allowed for commercial use.

Forbidden to modify the content, and cite the document when use.

$$\tau_{turb} = -\overline{\rho u'v'} = \mu_t \frac{\partial \tilde{u}}{\partial y} \quad (3.17)$$

By considering the balance of shear stress at the wall and the fluid layer, the kinetic energy and its dissipation rate at locations near the boundary are given by

$$K = C_\mu^{-1/2} \frac{\tau_w}{\rho} \quad (3.18)$$

$$\varepsilon = \frac{C_\mu^{3/4} K^{2/3}}{\kappa y} \quad (3.19)$$

3.3.3 The transport of energy

The assumption that the heat flux, \dot{q}_b , in the boundary layer is constant and equal to that across the wall gives

$$\dot{q}_b = \Gamma_{eff} \frac{dh}{dy} = \dot{q}_w, \Gamma_{eff} = \Gamma + \Gamma_t \quad (3.20)$$

where Γ_{eff} is the effective thermal conductivity.

1) In the laminar sub - layer ($0 < y^+ < 11.63$), $\dot{q}_w = \frac{\mu}{\sigma_h} \frac{dh}{dy}$ where σ_h is the molecular Prandtl number.

2) In the turbulent sub - layer ($11.63 < y^+ < 300$), $\dot{q}_w = \frac{\mu_t}{\sigma_{h,t}} \frac{d\tilde{h}}{dy}$ where

$\sigma_{h,t}$ is the turbulent Prandtl number. The heat flux may be written as:

$$\dot{q}_w = \frac{\overline{\rho} u_\tau (\tilde{h} + h_w)}{\sigma_{\phi,t} \left[u^+ + P \left(\frac{\sigma_\phi}{\sigma_{\phi,t}} \right) \right]} \quad (3.21)$$

where

$$P\left(\frac{\sigma_{\phi}}{\sigma_{\phi,t}}\right) = 9.29 \left[\frac{\sigma_{\phi}^{3/4}}{\sigma_{\phi,t}} + 1 \right] \quad (3.22)$$

3.4 Mathematical model of gas – phase combustion [4]

The model is a function of the concentration of oxygen, fuel and combustion products. The reaction rate can be specified as:

$$R_{vol} = ACOM \rho \frac{\varepsilon}{k} \min\left(\tilde{\phi}_{fuel}, \frac{\tilde{\phi}_{ox}}{S_{st}}, BCOM \frac{\tilde{\phi}_{pr}}{1 + S_{st}}\right) \quad \dots\dots(3.23)$$

where R_{vol} is the volumetric reaction rate of volatilizes, $ACOM$ and $BCOM$ are model constants, ϕ_{fuel} , ϕ_{ox} and ϕ_{pr} are, respectively, the time averaged mass fractions of volatilizes, oxygen and combustion products and S_{st} is the stoichiometric value of volatile gas.

3.5 Particulate phase model [4]

The Lagrangian approach was adopted to describe the particulate phase of the flow. It is assumed that the particles were spherical and of constant initial density. Their distribution was defined by finite number of particle size ranges, each represented by its average size. There is a finite number of locations where the particles enter the computational domain. Particles are released at each location with the same velocity and temperature as that of the surrounding gas. The conservation of mass, momentum and energy between two phases are solved for each inlet location and each particle size group in a Lagrangian framework for discrete time steps. The following sub – section contains more details of the approach.

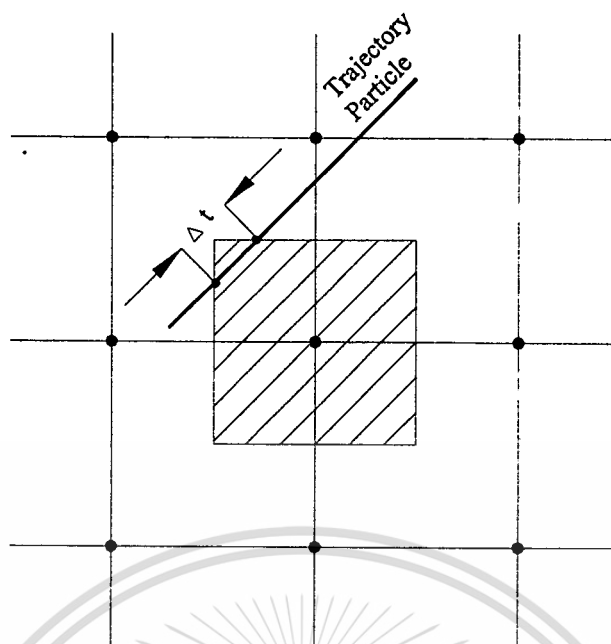


Figure 3.1 Dissipation of particle passing a cell

3.5.1 Conservation of mass

Mass transfer from the particulate phase to the gas phase may be expressed by

$$\frac{dm_p}{dt} = -R_m \quad (3.24)$$

where R_m is the volumetric rate of mass efflux from the particulate phase to the gaseous phase by devolatilization or char combustion. The negative value indicates the mass loss in respect to the particulate phase.

3.5.1.1 The devolatilization model

The single reaction model devolatilization as a simplified Arrhenius function coupled with a group of empirical parameters. The model may be expressed by

$$R_m = \frac{dV}{dt} = k_A (V^* - V) \quad (3.25)$$

This material is reserved for educational use only, not allowed for commercial use.

Forbidden to modify the content, and cite the document when use.

V is the cumulative amount of volatiles release, and V^* is the original or total amount of volatiles in the coal. The rate constant k_A may be expressed in Arrhenius form below:

$$k_A = k_0 \exp\left(-\frac{E_{dvol}}{R_u T}\right) \quad (3.26)$$

R_u is the universal gas constant and T is the absolute temperature. k_0 and E_{dvol} are the pre-exponential factor and the activation energy for devolatilization, respectively.

3.5.1.2 The char combustion model

The model assumes that the primary reaction takes place near the surface of the particle to produce carbon monoxide. This product is assumed to oxidize completely to carbon dioxide within the boundary layer surrounding the coal particles. The overall rate of char combustion is controlled by two competitive rate limiting processes, namely the kinetic reaction of coal char and diffusion rate of the oxygen to the particle surface.

Char reaction due to chemical kinetics

The kinetic reaction rate between coal char and oxygen may be written as:

$$R_{cc} = K_c \{(P_{O_2})_o\}^n \quad (3.27)$$

where

$$K_c = K_0 \exp\left(-\frac{E}{R_u T}\right)^n \quad (3.28)$$

P_{O_2} is the partial pressure of oxygen at the particle surface and K_c is the chemical reaction rate coefficient of order n . K_0 is the frequency factor for char reaction and E is the effective activation energy of char reaction.

Char reaction due to the diffusion of oxygen

$$R_{cox} = K_d \left\{ (P_{O_2})_{\infty} - (P_{O_2})_0 \right\} \quad (3.29)$$

where

$$K_d = \frac{D_c M_c \varphi}{\left\{ \frac{R_d}{2} \left(\frac{T_p + T_g}{2} \right) \right\}} \quad (3.30)$$

and

$$D_c = D_0 \left(\frac{P_0}{P} \right) \left(\frac{T_g}{T_0} \right)^{1.75} \quad (3.31)$$

$(P_{O_2})_{\infty}$ is the partial pressure of oxygen in the surrounding gas and at the particle surface, M_c is the atomic mass of carbon, φ is the mechanism factor of char reaction, defined as 1.0 for carbon monoxide formation, R_d is the mean particle diameter, T_p and T_g are, respectively, the absolute temperature of the particle and the gas. D_0 , P_0 and T_0 are the values of the binary diffusion, pressure and temperature taken as $3.13 \times 10^4 \text{ m}^2/\text{s}$, $1.013 \times 10^5 \text{ Pa}$ and 1500 K , respectively.

The overall rate coefficient for char combustion

The overall reaction rate is controlled by the diffusion rate of oxygen and it may be given as:

$$K_t = \frac{1}{\left\{ \left(\frac{1}{K_c} \right) + \left(\frac{1}{K_d} \right) \right\}} \quad (3.32)$$

The burning rate for a particle of diameter d may be expressed is:

$$\frac{\partial m}{\partial t} = K_t \pi d_p^2 P X_{O_2} \quad (3.33)$$

This material is reserved for educational use only, not allowed for commercial use.

Forbidden to modify the content, and cite the document when use.

where P is the gas pressure. X_{O_2} is the molar fraction of oxygen in the surrounding gas.

3.5.2 Conservation of momentum

3.5.2.1 Mean motion of particle

The momentum balance of particle motion may be expressed as

$$\frac{dm_p \tilde{u}_i}{dt} = \sum \bar{F}_i \quad (3.34)$$

The right hand side of the equation is the result of external forces acting on the particle (the pressure gradient, Coriolis effect, Magnus effect, gravity and the drag force created by the velocity difference between the particle and the turbulent flow). In pulverized coal combustion, it is assumed, however, that the forces due to the pressure gradient, gravity and the Magnus effect are negligible. Therefore, the drag force may be given by the following expression:

$$F_d = C_D \rho \frac{A_p}{2} (\tilde{U}_g - \tilde{U}_p) |\tilde{U}_g - \tilde{U}_p| \quad (3.35)$$

where

$$C_D = \left(1 + 0.15 \text{Re}_p^{0.687}\right) \frac{\text{Re}_p}{24} \quad (3.36)$$

\tilde{U}_g and \tilde{U}_p are, respectively, the time – averaged velocities of gas and coal particle, A_p is the projected area of the particle, ρ is the local gas density, C_D is the drag coefficient and Re_p is the Reynolds number referred to the particle, defined as:

$$\text{Re}_p = \frac{\rho |\tilde{U}_g - \tilde{U}_p| d_p}{\mu} \quad (3.37)$$

where μ is the absolute viscosity of the gas and d_p is the diameter of particle. The equation for momentum balance may be written in three components of polar coordinate system as follows:

$$\text{Axial direction:} \quad \frac{d\tilde{u}_p}{dt} = -\alpha (\tilde{u}_p - \tilde{u}_g) \quad (3.38)$$

$$\text{Radial direction:} \quad \frac{d\tilde{v}_p}{dt} = -\alpha (\tilde{v}_p - \tilde{v}_g) + \frac{\tilde{w}_p^2}{r_p} \quad (3.39)$$

$$\text{Tangential direction:} \quad \frac{d\tilde{w}_p}{dt} = -\alpha (\tilde{w}_p - \tilde{w}_g) + \frac{\tilde{v}_p \tilde{w}_p}{r_p} \quad (3.40)$$

where $\alpha = \frac{18\mu C_D \text{Re}_p}{24\rho_p d_p^2}$ and r_p is the distance from the axis symmetry.

3.5.2.2 Particle dispersion due to turbulence

The dispersion velocity of the particle is assumed to be related to the fluctuations of the gas velocity by the expression:

$$u_{disp.} = c_{1d} \left(\overline{u^{n2}} \right)^{1/2} \quad (3.41)$$

$$v_{disp.} = c_{2d} \left(\overline{v^{n2}} \right)^{1/2} \quad (3.42)$$

where the fluctuation in velocity can be written as:

$$\overline{u^{n2}} = -c_a 2 \frac{\mu_t}{\rho} \left(\frac{\partial \tilde{u}}{\partial z} \right) + \frac{2}{3} k \quad (3.43)$$

$$\overline{v^{n2}} = -c_b 2 \frac{\mu_t}{\rho} \left(\frac{\partial \tilde{v}}{\partial r} \right) + \frac{2}{3} k \quad (3.44)$$

where C_a and C_b are constants also specified as unity. The dispersion velocity can be expressed in term of the mean velocity gradient and kinetic energy as:

$$u_{disp.} = c_1 \left(-c_a 2 \frac{\mu_t}{\rho} \left(\frac{\partial \tilde{u}}{\partial z} \right) + \frac{2}{3} k \right)^{1/2} \quad (3.45)$$

$$v_{disp.} = c_2 \left(-c_b 2 \frac{\mu_t}{\rho} \left(\frac{\partial \tilde{v}}{\partial r} \right) + \frac{2}{3} k \right)^{1/2} \quad (3.46)$$

Thus we have:

$$\frac{d\tilde{u}_p}{dt} = -\alpha \left(\tilde{u}_p \pm u_{disp.} - \tilde{u}_g \right) \quad (3.47)$$

$$\frac{d\tilde{v}_p}{dt} = -\alpha \left(\tilde{v}_p \pm v_{disp.} - \tilde{v}_g \right) + \frac{\tilde{w}^2}{r_p} \quad (3.48)$$

$$\frac{d\tilde{w}_p}{dt} = -\alpha \left(\tilde{w}_p - \tilde{w}_g \right) + \frac{\tilde{v}_p \tilde{w}_p}{r_p} \quad (3.49)$$

3.5.3 Conservation of energy

The change of thermal energy within the particle is the sum of the heat transfer to the particle and the heat generation by char combustion, the heat removed with the mass loss during char combustion and the heat of evaporation during the devolatilization process. The thermodynamic balance equation becomes:

$$\frac{d(m_p c_p T_p)}{dt} = m_p \dot{Q}_t - c_p T_p \left(-\frac{dm_p}{dt} \right) - L_v \frac{dm_p}{dt} \quad (3.50)$$

Where

$$\dot{Q}_{tot} = \dot{Q}_{convec.} + \dot{Q}_{rad.} + \dot{Q}_{comb.} \quad (3.51)$$

L_v - latent heat of devolatilization

c_p - specific heat of gas at constant pressure

This material is reserved for educational use only, not allowed for commercial use.

Forbidden to modify the content, and cite the document when use.

T_p - absolute temperature of particle

The individual components of heat are evaluated as given by the following expressions.

$$\dot{Q}_{convec.} = \frac{\pi d_p^2 h_{tran} (T_g - T_p)}{m_p} \quad (3.52)$$

$$\dot{Q}_{rad} = \pi \sigma \varepsilon_p \frac{d_p^2}{m_p} (T_R^4 - T_p^4) \quad (3.53)$$

$$\dot{Q}_{comb.} = \frac{\eta H_C}{m_p} \left(-\frac{dm_p}{dt} \right) \quad (3.54)$$

Where,

- d_p - the diameter of particle
- m_p - mass of particle
- h_{tran} - the heat transfer coefficient
- Nu - the Nusselt number
- H_C - char calorific value
- η - the ratio of heat absorbed by the particle to heat released
- σ - Stefan – Boltzman constant
- ε_p - particle emissivity
- T_i - temperature of $i = g(\text{gas}), p(\text{particle})$ and R (radiation)

3.6 Thermal radiation model

For the evaluation of the radiation temperature, “Non – equilibrium diffusional Radiation model” is used along with “Truncated moment expansion simplification technique” [34]. The model is given by,

$$\nabla \cdot \left(\frac{1}{3K_e} \nabla T_R^4 \right) = (K_g + \bar{\varepsilon}_p K'_p) T_R^4 - K_g T_g^4 - \bar{\varepsilon}_p K'_p \bar{T}_p^4 \quad (3.55)$$

with the boundary condition (assuming that the enclosing wall is a Grey Lambert surface and is opaque to radiation (transitivity = 0), hence $\varepsilon_w + r_w = 1$)

$$-\frac{1}{3K_e} \frac{\partial T_R^4}{\partial n} = \frac{1}{2} \frac{\left\{ (1 - \bar{r}_w) T_R^4 - \bar{\varepsilon}_w \bar{T}_w^4 \right\}}{(1 + \bar{r}_w)} \quad (3.56)$$

where,

- K_g - gas absorption coefficient
- K_p - particle absorption coefficient
- ε_p - particle emissivity, assuming the particles as opaque spheres
- K_e - equivalent absorption coefficient
- $\bar{\varepsilon}_w$ - wall emissivity
- \bar{r}_w - radiation reflectivity at the wall
- \bar{T}_w - particle mean emission temperature

3.7 Sulfur oxides formation model

This model is investigated by Panya [5] who summarized that typical coals comprise a substantial amount of carbon and hydrogen and small amounts of oxygen, nitrogen, sulfur and solid matters constitute ash. Pulverized coal, when it enters the hot environment of combustion zone, releases the volatile comprising carbon dioxide, water, combustible hydrocarbons, nitrogen and sulfur species. The oxidation of volatile sulfur is assumed that only the SO_2 is occurred. The relationship between the rate of SO_2 formation and volatile combustion can be written as:

$$R_{SO_2} = x_s \cdot R_{vol} \quad (3.57)$$

where R_{SO_2} is the rate of SO_2 formation, x_s is the mass fraction of SO_2 and R_{vol} is the volumetric reaction rate of volatilizes.

CHAPTER 4

ADSORPTION MODEL

4.1 Introduction

Adsorption is the process by which material accumulates at the interface between two phases. These phases can be any of the following combinations: liquid – liquid, gas – liquid and gas – solid. The adsorbing phase is called the adsorbent, and any substance being adsorbed is termed as an adsorbate.

Adsorption onto solid adsorbents has great environmental significance, since it can effectively remove pollutants from both aqueous and gaseous streams due to the high degree of purification that can be achieved.

This chapter presents the reaction between $\text{SO}_2(\text{g})$ and limestone or dolomitic limestone ($\text{CaCO}_3(\text{s})$) that is assumed to occur in two steps. The first step is the calcination, i.e. carbon dioxide is emitted from the carbonate. The second step is the sulfation (pore model) that is a heterogeneous reaction between SO_2 and CaO . The overall concept shows in Fig.4.1.

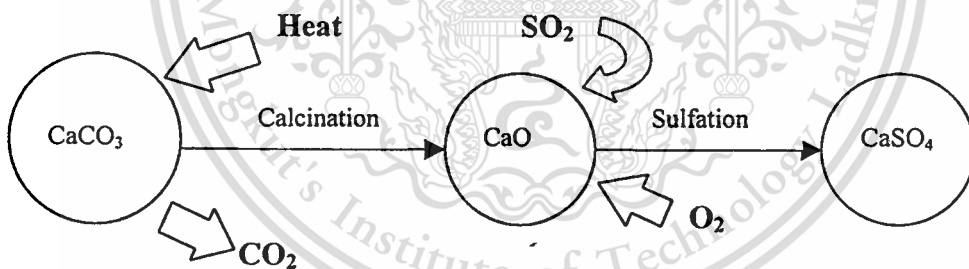


Fig.4.1 Overall concepts for adsorption

4.2 Calcination model [2]

The following steps are included in the model: decomposition of CaCO_3 at the $\text{CaO} - \text{CaCO}_3$ interface, diffusion of CO_2 through the CaO to the particle surface, diffusion of CO_2 from the particle surface to the bulk gas and loss of continuous surface area for all calcined material. The overall concept for the model is shown in Fig.4.2. The particle is assumed to be isothermal. As suggested by Fig.4.2, a CO_2 concentration gradient exists across the CaO layers. The calcination process is

This material is reserved for educational use only, not allowed for commercial use.

Forbidden to modify the content, and cite the document when use.

allowed to occur in steps leading to a layered CaO zone. Each layer is homogeneous, and the physical properties within a given layer are constant. Physical properties are allowed to vary from layer to layer with the most recently formed layer of CaO possessing the highest surface area. The rate of surface area loss is a function of temperature, surface area and CO₂ concentration.

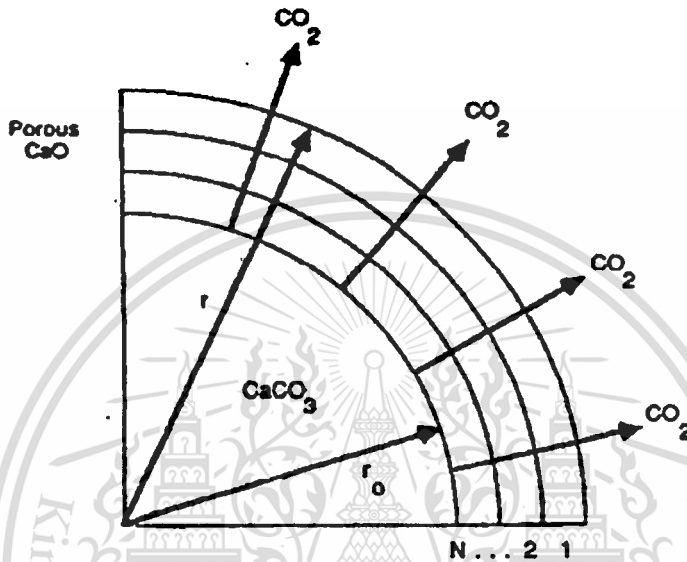


Fig.4.2 Schematic diagram of the calcination model [2]

The equations governing the movement of the calcination front are:

$$\frac{dr}{dt} = -\frac{M}{\rho} R_D \quad (4.1)$$

and at $t = 0$, $r = r_0$

where

$$R_D = k_D (P_e - P_N) \quad (4.2)$$

$$k_D = 0.00122 \exp(-4026/T) \quad (4.3)$$

$$P_e = \exp(17.74 - 0.00108T + 0.332 \ln T - 22020/T) \quad (4.4)$$

and r is the radius (m) of the shrinking core of CaCO_3 , t is time (s), M is the molecular weight of CaCO_3 (kg), ρ is the density (kg m^{-3}), R_D is the rate of decomposition ($\text{kmol m}^{-2} \text{s}^{-1}$), r_0 is the initial particle radius, which is assumed constant, k_D is a rate constant for decomposition of CaCO_3 ($\text{kmol m}^{-2} \text{s}^{-1} \text{atm}^{-1}$), P_e is the equilibrium dissociation pressure of CO_2 (atm), P is the CO_2 partial pressure at the $\text{CaO} - \text{CaCO}_3$ interface, and T is the absolute temperature (K). The diffusion coefficient, which controls transport mechanism for CO_2 in porous lime, is estimated as:

$$D = \left(D_K^{-1} + D_{AB}^{-1} \right)^{-1} \quad (\text{m}^2 \text{s}^{-1}) \quad (4.5)$$

where

$$D_K = 0.00881T^{1/2} S_{BET}^{-1} \quad (\text{m}^2 \text{s}^{-1}) \quad (4.6)$$

and

$$D_{AB} = 0.000139(T/273)^{1.75} P_{tot}^{-1} \quad (\text{m}^2 \text{s}^{-1}) \quad (4.7)$$

Finally, the effective diffusivity for the porous material is estimated by

$$D_e = D\varepsilon^2 \quad (4.8)$$

where $\varepsilon = 0.5$, that is the porosity of the calcined particles. D is the diffusion coefficient for the pore, D_K is Knudsen diffusion coefficient, D_{AB} is the molecular diffusion coefficient for CO_2 in the air, T is absolute temperature (K), S_{BET} is the BET surface area ($\text{m}^2 \text{kg}^{-1}$), and P_{tot} is the total pressure (atm).

The BET surface area, S_{BET} , can be described by the equation

$$\frac{dS_{BET}}{dt} = -k(S_{BET} - S_{as})^2 \quad (4.9)$$

where t is time (s), S_{as} , $5 \text{ m}^2/\text{g}$, is the asymptotic surface area and k ($\text{km}^2 \text{ s}^{-1}$) is the rate constant may be written as:

$$k = 286 \exp\left(\frac{-14500 - 3280P^{-0.111}}{T}\right) \quad (4.10)$$

The differential equation governing the diffusion of CO_2 through the porous lime is

$$\frac{\partial^2 P}{\partial r^2} + \left(\frac{2}{r} + \frac{1}{D_e} \frac{\partial D_e}{\partial r}\right) \frac{\partial P}{\partial r} = \frac{1}{D_e} \frac{\partial P}{\partial t} \quad (4.11)$$

Two boundary conditions are:

at $r = r_0$

$$-D_e \frac{\partial P}{\partial r} = k_f (P - P_b) \quad (4.12)$$

at $r = r$

$$\frac{D_e}{R_u T} \frac{\partial P}{\partial r} = k_D (P_e - P) \quad (4.13)$$

where r (m) is the radial position within the calcined layer, k_f (m s^{-1}) is the mass – transfer coefficient for sphere may be written as :

$$k_f = \frac{D_A}{D_p} (2.0 + 4.9 D_p^{1/2}) \times 10^{-2} \quad (4.14)$$

where D_p (cm) is the diameter of calcined particle and D_A is $2.16 \times 10^{-5} T^{3/2}$ ($\text{cm}^2 \text{ s}^{-1}$), P_b is the CO_2 partial pressure in the bulk gas, and R_u is the gas constant.

Applying the pseudo – steady – state approximation for gas – solid reactions and each shell of calcined particle is assumed to be homogeneous, D_e constant. Equation 4.11 can be simplified to

$$\frac{d^2 P}{dr^2} + \frac{2}{r} \frac{dP}{dr} = 0 \quad (4.15)$$

This equation applies to each shell of calcined particles. The shells or nodes are numbered as illustrated in Fig.4.2. There is a CO_2 generation term at the $\text{CaCO}_3 - \text{CaO}$ interface (Equation 4.13) and a convective boundary condition at the outer surface (Equation 4.12) the solutions to Equation 4.12, 4.13 and 4.15 are:

for node 1

$$P_1 = P_b + \frac{r_N^2 k_D R_u T}{r_1^2 k_f} (P_e - P_N) \quad (4.16)$$

for node 2 through N-1

$$P_i = P_{i-1} + \frac{FR_u T}{4\pi(D_e)_{i-1}} \left(\frac{1}{r_i} - \frac{1}{r_{i-1}} \right) \quad (4.17)$$

where

$$F = 4\pi r_N^2 k_D (P_e - P_N) \quad (4.18)$$

for node N

$$P_N = \frac{P_e + BP_b}{1 + B} \quad (4.19)$$

where

$$B = \frac{A_1 U_1}{4\pi r_N^2 k_D} \quad (4.20)$$

$$A_1 = \frac{4\pi r_1^2}{R_u T} \quad (4.21)$$

$$\frac{1}{U_1} = r_1^2 \sum_{j=1}^{N-1} \frac{1}{(D_e)_j} \left(\frac{1}{r_{j+1}} - \frac{1}{r_j} \right) + \frac{1}{k_f} \quad (4.22)$$

The number of nodes increases by one with each step in time. The layers of CaO are allowed to sinter at each time step, which lead to change in their transport properties. The rate of sintering is also a function of CO₂ partial pressure.

From the above equations, the Gauss – Seidel method and the improvement of convergence using relaxation are used to predict the pressure for each shell. This type of modification known as underrelaxation, $0 \leq \omega \leq 1$, and shown as follows [35]:

$$P_i^{new} = P_i^{old} + \omega \Delta P_i^{new} \quad (4.23)$$

As the first step of calculation, the pressures for each shell are initialized as total pressure of gas phase. Eventually, the calcination rate is predicted by replacing the P_N in Equation 4.2 with a convergent pressure at node N . This rate is a parameter for calculation the sulfation process.

4.3 Sulfation model

The chemical reaction between calcined limestone and sulfur dioxide is

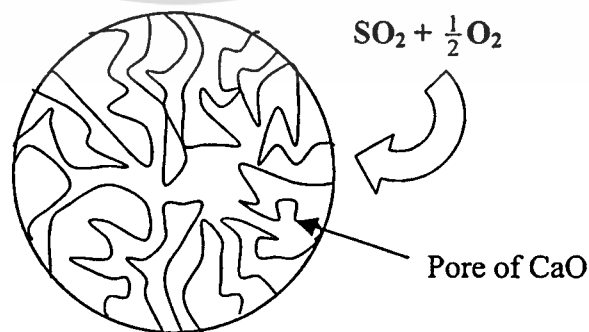
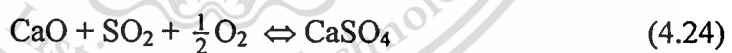


Fig.4.3 Model of sulfation process on porous CaO particle

Due to Borgwardt [3], the reaction rate is defined as

$$r = \frac{1}{w_p} \frac{dn'}{dt} = \frac{\eta}{\rho} k_v c^m \quad (4.25)$$

The rate is in mole per unit gram of calcined particle per second. w_p is the weight of solid particles, n' is the amount of sulfate in solid particle in mole. c and m are concentration of SO_2 and order of reaction respectively. k_v is a rate constant which is a function of temperature in the Arrhenius

$$k_v = A e^{-E/RT} \quad (4.26)$$

Experimental values of k_v are summarized in Table 4.1, along with those of E and A . ρ is the density and η is an effectiveness factor indicating a decrease in adsorption rate due to sulfate loading. This parameter is related to sulfate loading, $\frac{n'}{w_p}$ by the following equation:

$$\ln \eta \frac{Ac^m}{\rho} - \frac{E}{RT} = -\beta \frac{n'}{w_p} + \ln r_0 \quad (4.27)$$

β is an empirical parameter obtained by fitting the experimental data. r_0 is the reaction rate at zero sulfation, defined as

$$r_0 = \eta_0 \frac{A_0 c^m}{\rho_0} e^{-E/RT} \quad (4.28)$$

Table 4.1. Summary of activation energy, reaction rates and frequency factors of dolomites, Borgwardt, 1970 [3]

Dolomites	Activation energy, E, cal/mol	Reaction rate constant, k_v , s^{-1}	Frequency factor, A, s^{-1}
1337	10,000	4.8×10^3	2.4×10^5
1351	18,100	7.2×10^3	9.0×10^6
1343	14,200	4.0×10^3	1.1×10^6
1360	8,100	2.3×10^3	5.5×10^4

From the Equations 4.27 and 4.28, the frequency factor may be expressed as

$$A = \frac{\eta_0 \rho}{\eta \rho_0} A_0 e^{-\beta \frac{n'}{w_p}} \quad (4.29)$$

A_0 from Equation.4.28 is substituted into Equation 4.29. Combining with Equations 4.25 and 4.26, it yields the following relationship:

$$r = \frac{\eta \rho}{\rho \rho_0} r_0 \frac{\rho_0 e^{E/RT}}{\eta_0 c^m} \frac{\eta_0}{\eta} e^{-\beta \frac{n'}{w_p}} e^{-E/RT} c^m \quad (4.30)$$

thus,

$$r = r_0 e^{-\beta \frac{n'}{w_p}} \quad (4.31)$$

As will be shown below, a simple relationship between r, r_0, β and $\frac{n'}{w_p}$ can

be derived from the above Equation (4.31) showing that the reaction rate is a function of only a few parameters which is not the case observed from Borgwardt's experiment [3]. The data at 1×10^{-3} mol/g sulfate loading of the same investigator shows a linear correlation between $\log(r)$ and $1/T$ (K^{-1}), thus the reaction rate should be modified to account for this temperature effect as:

$$r = r_0 e^{-\beta \frac{n'}{w_p}} e^{\frac{-E}{RT} + c_0} \quad (4.32)$$

where

$$c_0 = \frac{E}{RT_{ref}} \quad (4.33)$$

where T_{ref} is the reference temperature which is 1143.15 K (870°C). The above relationship reduces to Equation 4.31 at reference temperature. Moreover, the rate also increases with increasing SO_2 . Thus, an additional term is proposed as follows:

$$r = r_0 e^{-\beta \frac{n'}{w_p}} e^{(-E/RT) + (E/R_{iref})} \frac{c^m}{c_{ref}^m} \quad (4.34)$$

where c_{ref} is the SO_2 concentration which is 2.9×10^{-8} mol/cc (wet basis). The value r_0 for each type of dolomite is obtained by linear interpolation, knowing the reaction rate at 1×10^{-3} sulfation and the correlation of $\log(r)$ with linear $\frac{n'}{w_p}$:

$$\ln r_0 = \ln r_{1 \times 10^{-3}} - \beta (1 \times 10^{-3}) \quad (4.35)$$

β may be obtained by the following expression, knowing the reaction rates at 1×10^{-3} and 2×10^{-3} from the experiment [3] which are summarized in Tables 4.2 and 4.3

$$\beta = \frac{\ln r_{2 \times 10^{-3}} - \ln r_{1 \times 10^{-3}}}{2 \times 10^{-3} - 1 \times 10^{-3}} \quad (4.36)$$

Table 4.2. Effect of particle sizes on reaction rate at the sulfate loading of 2×10^{-3} mol/g, 870°C [3]

Dolomites	Reaction rate (mol/g s) $\times 10^5$		
	D_p 0.0096 cm.	D_p 0.025 cm.	D_p 0.13 cm.
1337	4.2	3.2	1.4
1351	3.2	2.1	1.3
1343	2.1	1.4	0.7
1360	2.5	1.8	1.1

Table 4.3. Empirical values of reaction rate at 870°C , sulfate loading of 1×10^{-3} mol/g of 150/170-mesh particle size (0.0096 cm) [3]

Dolomites	Reaction rate (mol/g s) $\times 10^5$
1337	6.4
1351	5.9
1343	3.6
1360	3.1

The above relationships for the case of dolomite 1337, for instance, may be graphically presented in Fig.4.4. The values of r_0 and β for other types of particles may be obtained in a similar manner, which are summarized in Table 4.4.

Table 4.4. Reaction rate at zero sulfation and β for dolomites 1337, 1351, 1343 and 1360 [3]

Dolomites	$\ln r_0$	β		
		D_p 0.0096 cm.	D_p 0.025 cm.	D_p 0.13 cm.
1337	-9.24	-420	-550	-970
1351	-8.97	-690	-900	-1140
1343	-9.69	-540	-740	-1090
1360	-10.16	-220	-385	-630

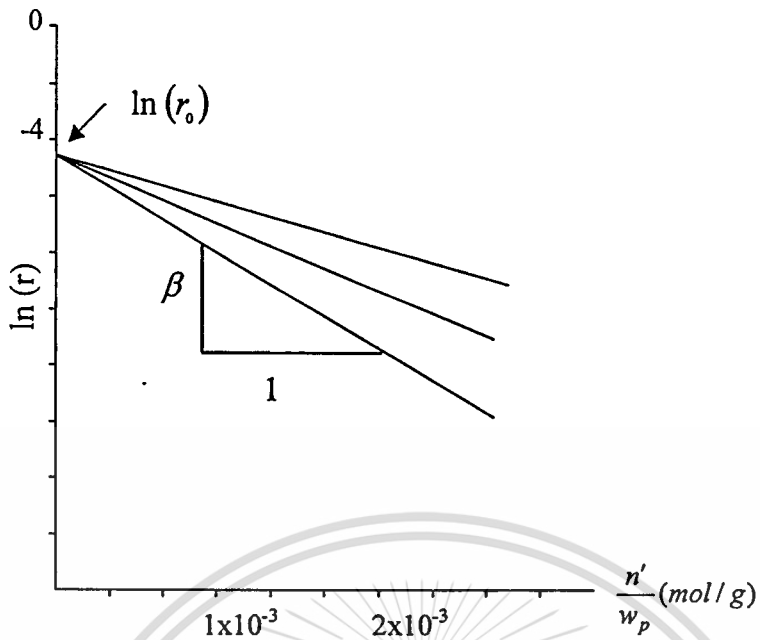


Fig.4.4 Graphical representation of r_0 and β

Apparently from Equation 4.34, the reaction rate is independent of an effectiveness factor. The experimental results, however, suggest that the amount of SO_2 adsorbed per 30 mg of small particles is greater than that of the larger ones, as clearly observed at the beginning of the reaction. This is due to pore diffusion resistance at zero sulfation, which becomes more significant for the larger particle sizes, see Fig.4.5.

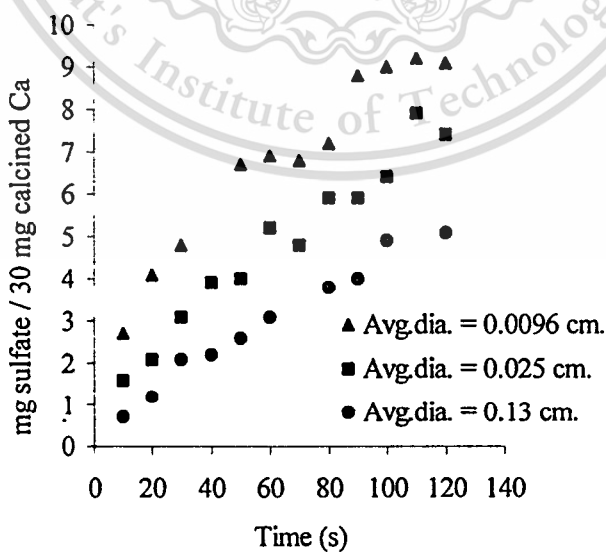


Fig.4.5 Sorption of sulfur dioxide for different particle sizes of dolomite 1351, Borgwardt, 1970 [3]

This material is reserved for educational use only, not allowed for commercial use.

Forbidden to modify the content, and cite the document when use.

Equation 4.26 can be written as

$$\ln \eta_0^* \eta A \frac{c^m}{\rho} - \frac{E}{RT} = -\beta \frac{n'}{w_p} + \ln r_0 \quad (4.37)$$

yielding

$$\ln \eta_0^* + \ln \eta A \frac{c^m}{\rho} - \frac{E}{RT} = -\beta \frac{n'}{w_p} + \ln r_0 \quad (4.38)$$

or

$$\ln \eta A \frac{c^m}{w} - \frac{E}{RT} = -\beta \frac{n'}{w_p} + \ln \left(\frac{r_0}{\eta_0^*} \right) \quad (4.39)$$

All terms, except the last one in the right-hand side of the equation is in the same form as those of Equation 4.27. Thus, a linear relationship between $\ln(r)$ and $1/T$ is maintained. The value η_0^* represents the diffusion resistance at zero sulfation, which differs from η . This latter parameter represents the effectiveness of reaction throughout the reaction period. The former is constant for a particular size of particle whereas the latter decreases with increasing sulfate loading. Therefore, a more general equation for β would be

$$\beta = \frac{\ln r_{2 \times 10^{-3}} - \ln \left(\frac{r_0}{\eta_0^*} \right)_{0.0}}{2 \times 10^{-3}} \quad (4.40)$$

This parameter reflects the overall kinetic rate of reaction (4.24) without intraparticle effects. The value is thus unique for each type of dolomite. The empirical values in logarithmic form are previously given in Table 4.4. The graphical representation of β is given in Fig.4.6.

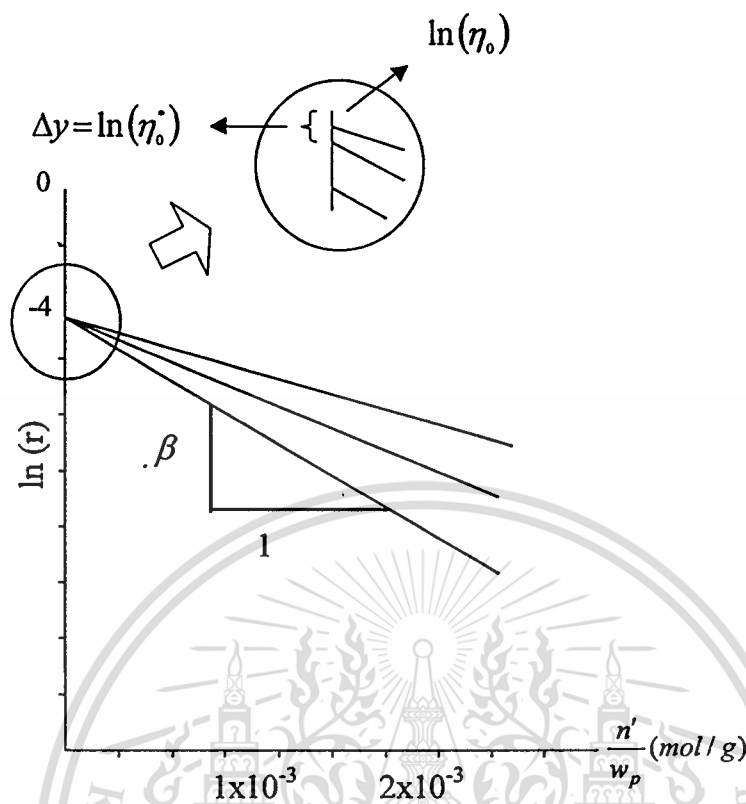


Fig.4.6 Graphical representation of r_0 and β with η_0^* modification

4.3.1 Validation

Fig.4.7 shows the effect of diffusion resistance on sorption of sulfur oxides with η_0^* varying from 1 (no resistance at zero sulfation) to 0.4 for different types of dolomites. Experimental data are compared with the simulation results obtained from Equation 4.34 with the activation energy from Table 4.1, r_0 from Table 4.4 and β from Equation 4.40. It is important to note here that the values of β given in Table 4.4 are determined from Equation 4.36 assuming that the reaction rate at zero sulfation is unique for certain type of dolomite regardless of the effect of particle size variation. Thus, those values only represent the relationship of $\ln(r)$ and the sulfate loading, $\frac{n'}{w_p}$ at the absence of initial diffusion resistance, η_0^* . Generally, the

simulation underpredicts the experimental data. A change in diffusion resistance generally affects the shape of sulfate accumulation with time. A decrease in reaction

rate at zero sulfation leads to a decrease in the amount of sulfate adsorbed, which is most notable at the early stage of reaction. At sulfate loading of 2×10^{-3} the reaction rate equals the value given in Table 4.2. This is a break-even point of the reaction rate where the values are the same for all η_0^* . As the reaction rate decreases linearly with increasing sulfate loading, a decrease in reaction rate, for the case of $\eta_0^* < 1$, is less than that of $\eta_0^* = 1$. This leads to higher reaction rate at sulfate loading greater than 2×10^{-3} . The sulfate accumulation for the case of $\eta_0^* < 1$ is, therefore, greater than that for the case of $\eta_0^* = 1$ after a certain period of time.

Fig.4.8 suggests a similar trend of evolution with change in η_0^* . The reaction rate is generally lower than that for $D_p = 0.0096$ cm., due to lower β . At $t = 0$ s, for $\eta_0^* = 1$, both cases have the same reaction rate. As for t greater than 0 s, the reaction rate of the 0.025-cm particles becomes less than that of the 0.0096-cm one, and the gap becomes greater as the time increases. Its effect on the accumulative amount of sulfate with time, thus, follows this trend. It appears, however, that the simulated result for $\eta_0^* = 0.35$ yields the best fit to the measurement, see Fig.4.9. The measured data clearly shows that there is a significant diffusion resistance at zero sulfation.

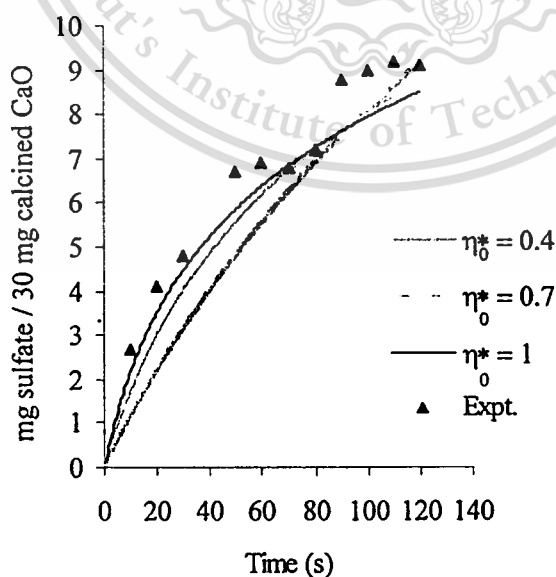


Fig.4.7 Effect of zero-sulfation diffusion resistance on sorption of sulfur oxides

This against experimental data, dolomite 1351, $D_p = 0.0096$ cm. for commercial use.

Forbidden to modify the content, and cite the document when use.

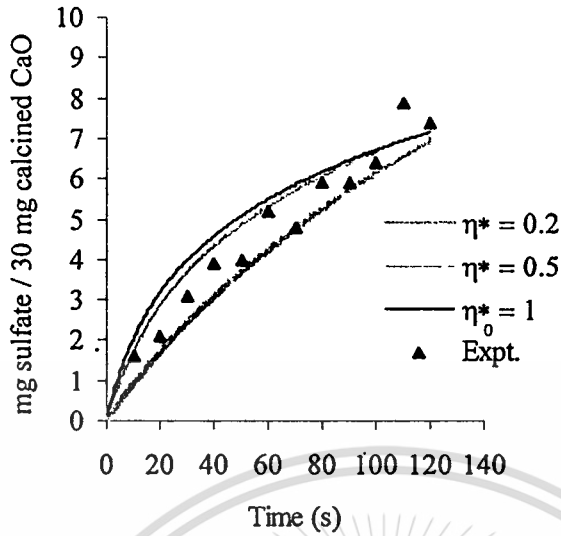


Fig.4.8 Effect of zero-sulfation diffusion resistance on sorption of sulfur oxides against experimental data, dolomite 1351, $D_p = 0.025$ cm.

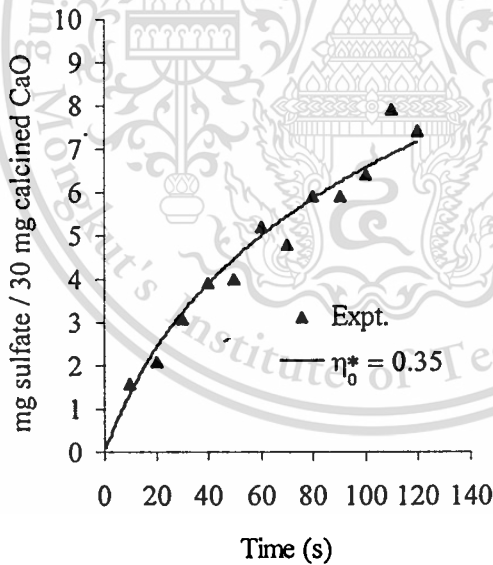


Fig.4.9 Comparison between mathematical simulation at $\eta_0^* = 0.35$ and measurement for dolomite 1351, $D_p = 0.025$ cm.

As for the adsorption of 0.13-cm particle size, the value of $\eta_0^* = 0.09$ yields the best fit to the measured data, see Fig.4.10.

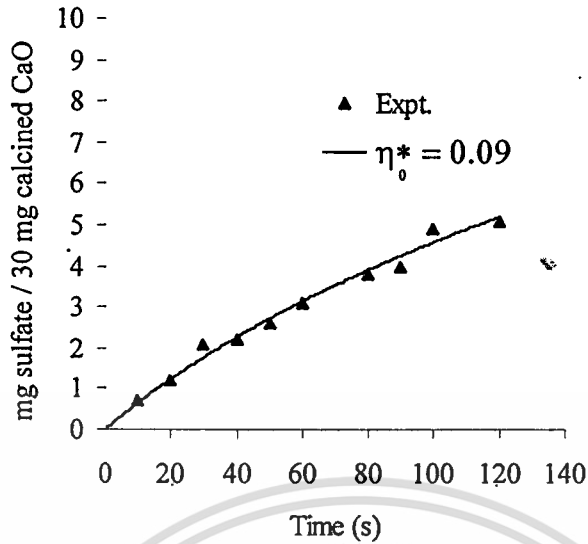


Fig.4.10 Comparison between mathematical simulation at $\eta_0^* = 0.09$ and the measurement for dolomite 1351, $D_p = 0.13$ cm.

At $\eta_0^* = 0.05$, the accumulation level increases almost linearly with time, suggesting that the reaction rate is very much less influenced by the sulfate loading, see Fig.4.11.

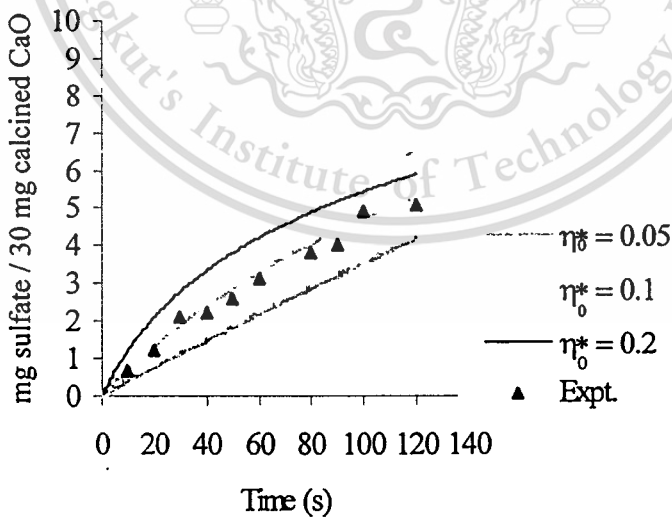


Fig.4.11 Effect of zero-sulfation diffusion resistance on sorption of sulfur oxides against experimental data, dolomite 1351, $D_p = 0.13$ cm.

The effect of β on SO_2 adsorption may be illustrated in Fig.4.12. At a constant value, $\eta_0^* = 1$, a decrease in magnitude of β leads to an increase in the reaction rate. The parameter β indicates that the rate of $\ln(r)$ decreases with sulfate loading, thus the greater the magnitude of β the lesser the rate of reaction.

Fig.4.12 shows an increase in accumulative sulfate loading against the same corresponding time when decreasing the magnitude of β to 90% and 85% of its original (β), respectively. The profile of sulfate loading, which is compared between mathematical simulation and the measurement for dolomite 1351, has already been given in Fig.4.13. For different types of dolomites, the mathematical model for SO_2 adsorption may be obtained in a similar manner. However, the chemical and physical structures of dolomite are different from one dolomite to another, thus specific η_0^* and β values should be identified for different types of particles.

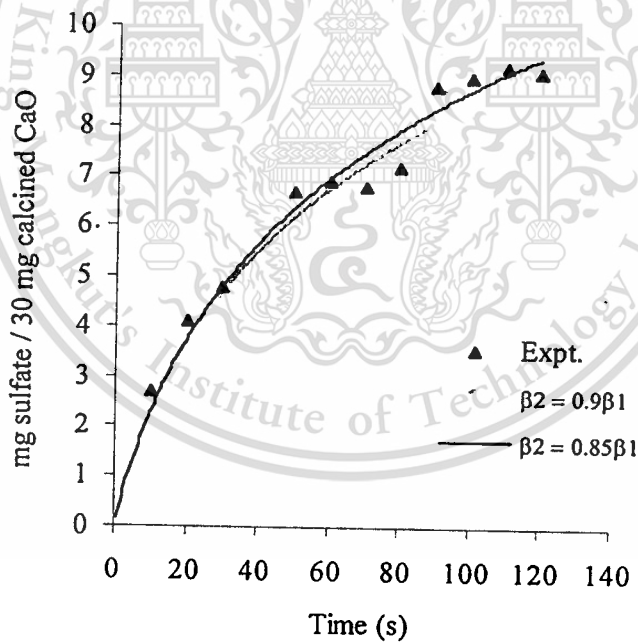


Fig.4.12 Effect of β on sorption of sulfur oxides against experimental data, dolomite 1351, $D_p = 0.0096$ cm.

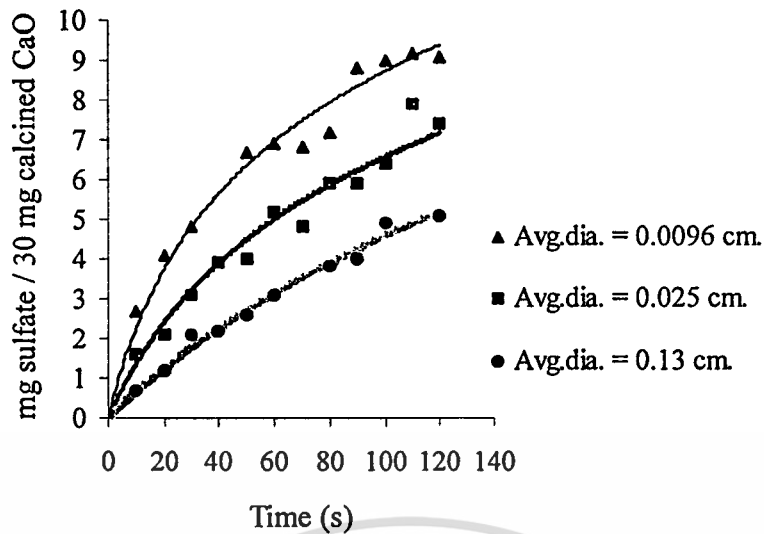


Fig.4.13 Comparison between mathematical simulation and the measurement for dolomite 1351

4.4 Integration of calcination and sulfation models into FAFNIR

The calcination and sulfation models are integrated in FAFNIR by inserting sub-program for each model. The assumptions for these models are insimultaneous. CaCO_3 particles were injected into the furnace by the conditions of inlet locations and particle sizes. Sub-program, PARTIC, that determines the track of coal particle [4], is modified for prediction of CaCO_3 particle path. Algorithm of this sub-program shows in Fig.4.14. The assumptions of particles are:

1. No collision and interaction particles
2. Gray system is assumed for radiation
3. Constant diameter is assumed but the density decreases with time
4. Dispersion of particles in mean turbulent flow is achieved by injecting the particle from different locations within the injection domain / port, incorporated with turbulent dispersion velocity model (Section 3.5).
5. Mass, momentum and heat sources contribute to gas phase via particle-source-in cell technique [4] as mentioned in Section 3.5. Since the mean particle trajectories are different from one iteration to another. With underrelaxation techniques [4] the above source terms are dispersed within the turbulent gaseous stream.

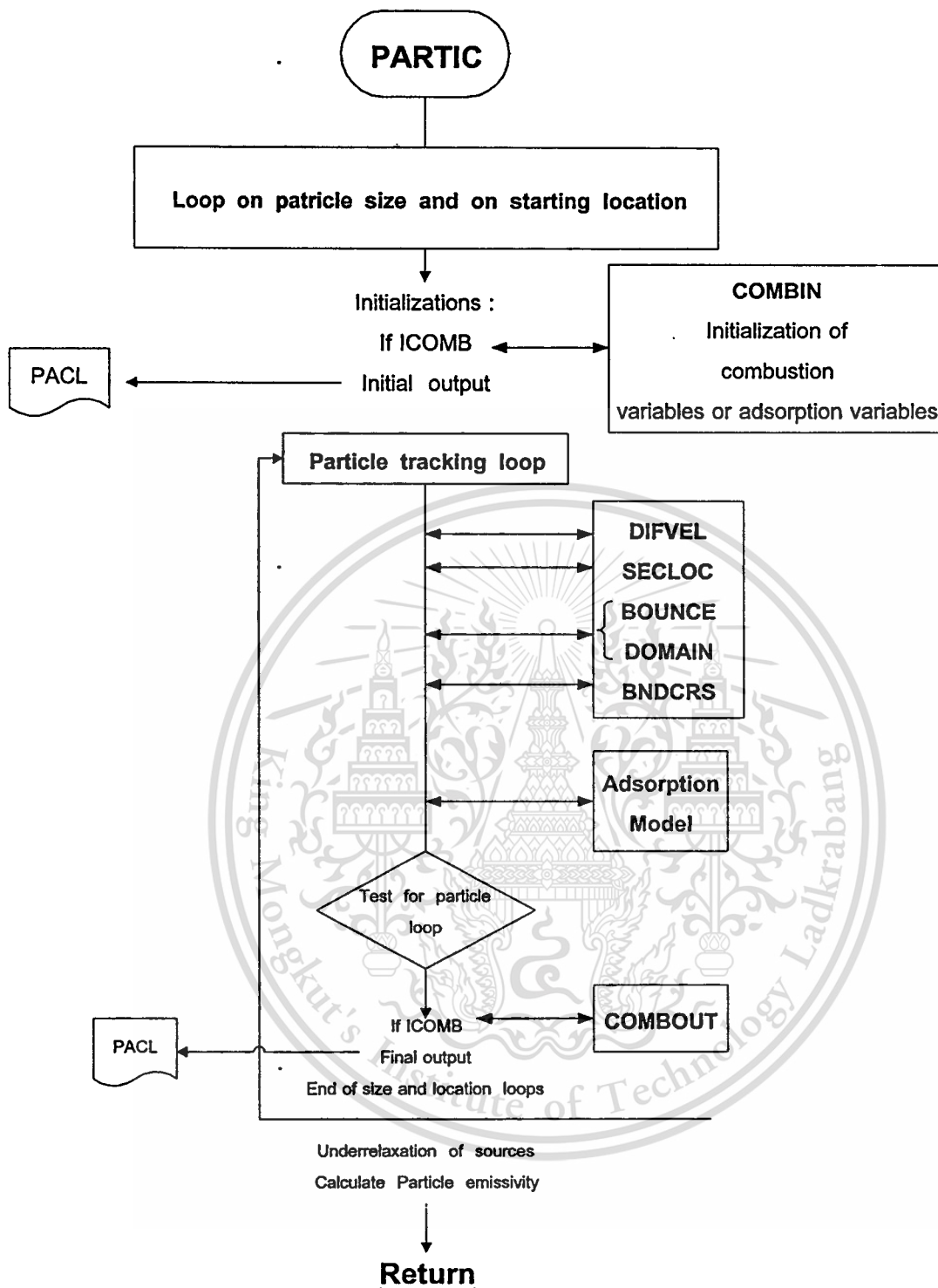


Fig.4.14 Flowchart for CaCO_3 particle tracking

- DIFVEL, this subroutine calculates the local gas velocity and diffusion velocity.
- SECLOC, this subroutine returns the new sector in which particle is giving its new position.

This material is reserved for educational use only, not allowed for commercial use.

Forbidden to modify the content, and cite the document when use.

- **BOUNCE**, this subroutine calculates the position and the velocity of particle after it bounces a boundary.
- **BNDCRS**, this subroutine determines the boundaries of the sector where a particle crosses the grid during each time step.
- **Adsorption model** consists of two models for calcination and sulfation processes.



CHAPTER 5

COMPUTATIONAL SIMULATION

5.1 Introduction

This chapter consists of the results and discussions in 9 cases. Those cases discussed in section 5.3 – 5.6 are a study of the effects of inlet locations, particle sizes and wall temperature on the amount of SO₂ adsorption. The mathematical model is included in FAFNIR while the schematic diagram of the furnace and numerical set – up are illustrated in the following section.

5.2 Numerical set - up for coal combustion in furnace

The detailed numerical set-up has been previously described by Charoensuk J. [4] and Daungvilailux P. [5]. The summary of them are as follows:

1. The furnace is a cylindrical symmetry. It has a diameter of 0.6 m. and a total length of 0.3 m. Fig.5.1 shows the schematic diagram of the top segment of the ICSTM furnace, which is used for simulation and the overview of furnace shown in Fig.A-1 (in appendix A). Dimensions of burner are illustrated in Fig.5.2.
2. The characteristics of bituminous coal given in Table 5.1. The furnace operating conditions are summarized in Table 5.2 with the recommended coal kinetic parameters in Table 5.3.
3. Uniform profiles of temperature and velocities at every component of inlets are assumed. The wall is considered adiabatic from the burner exit plane up to 1.5 meters along the axial distance.
4. In region where the gradient of the velocity is large and suddenly changed in shape of the boundary occurs (e.g., at corner, or at the burner inlet), the cell should be small.

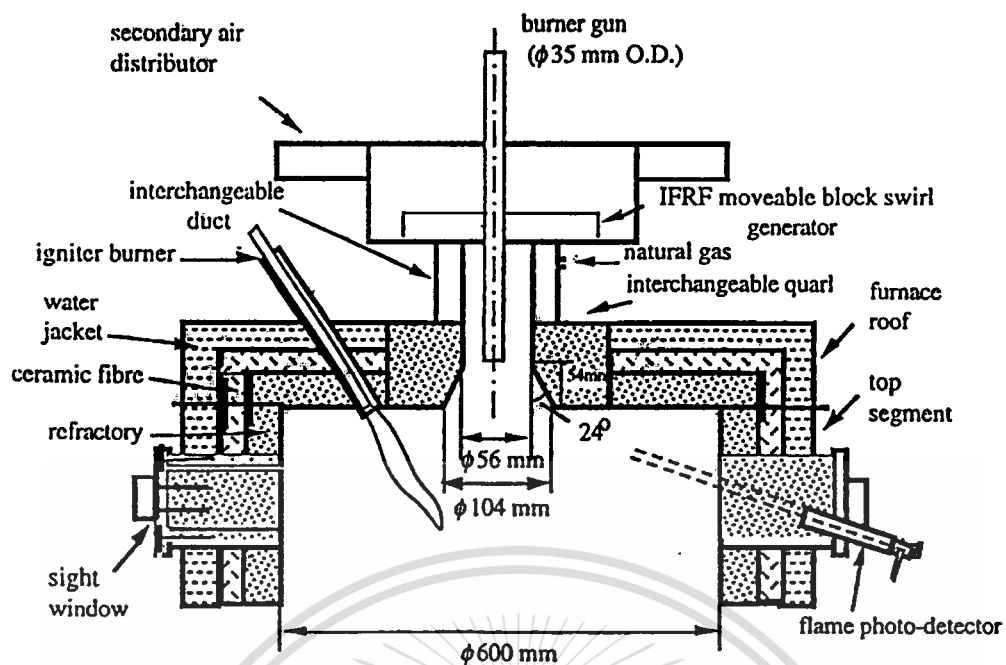


Fig.5.1 Schematic diagram of the top segment of the ICSTM furnace

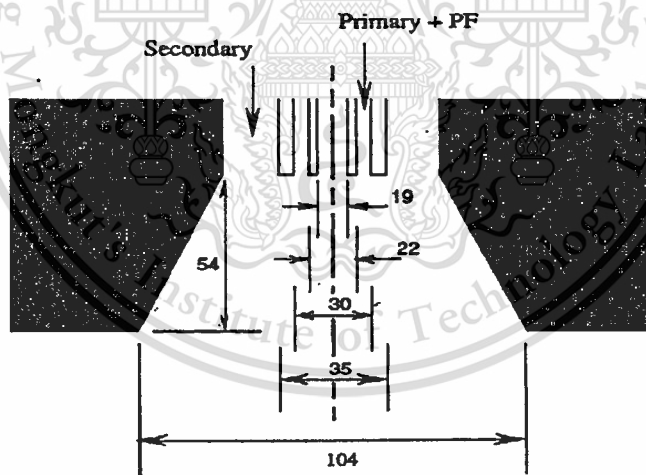


Fig.5.2 Schematic diagram of the burner

Table 5.1 Characteristics of bituminous coal [36]

Proximate analysis:	(wt %)
Volatiles	35.8
Fixed carbon	53.7
Moisture	6.3
Ultimate analysis:	(wt %)
Carbon	72.60
Hydrogen	5.05
Nitrogen	15.31
Sulfur	1.29
Oxygen	1.55
Particle size distribution (μm)	(wt %)
0-10	15.0
10-25	25.0
25-40	20.0
40-75	20.0
>75	20.0
Gross calorific value, MJ/kg	29.29

Table 5.2 Furnace operating conditions

Central pipe: Air flow rate, kg/s	4.777×10^{-4}
Swirl number	0.0
Temperature, K	353
Coal feed rate, kg/s	0.39×10^{-2}
Primary: Air flow rate, kg/s	8.833×10^{-3}
Swirl number	0.0
Temperature, K	353
Secondary: Air flow rate, kg/s	3.344×10^{-2}
Swirl number	1.03
Temperature, K	573
Excess air (%)	15

Table 5.3 Kinetic parameters for coal combustion model

<u>Kinetic parameters</u>	E (J/kmol)	k_0, K_0
Devolatilization	7.4×10^7	$8.36 \times 10^4 \text{ s}^{-1}$
Char reaction	1.02×10^8	$0.86 \text{ kg s N m}^{-4}$

5.3 The simulation of coal combustion (base case)

The simulation of flow, heat transfer and coal combustion are performed as well as formation of sulfur oxides. A contour plot of the temperature distribution in Fig.5.3 describes the role of recirculation on the mechanism of flame stabilization. The heat generated by volatile combustion is transported into the internal recirculation zone and stored in a torroidal vortex closed to the center of the jet, near the burner exit. Fig.5.4 shows the consequential coal particle trajectories. The reverse flow of coal particles is evident at the distance between 0.05 – 0.18 m from the burner exit. The sooner particle is entrained with the local gas velocity, the shorter particle penetrates into the internal recirculation zone. From Fig.5.5, high SO₂ concentration is observed at the distance between 0.03 – 0.18 m from the burner exit.

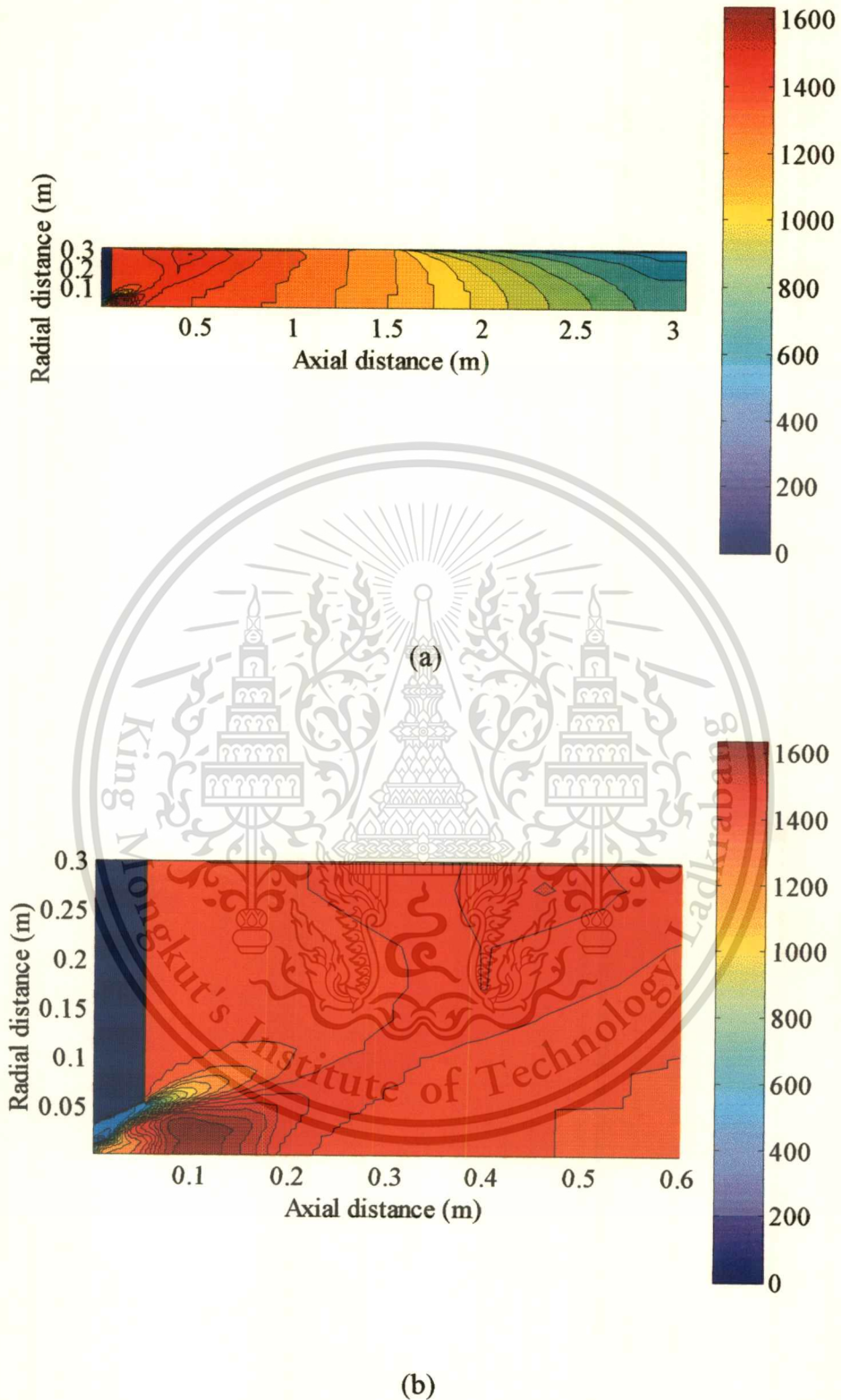
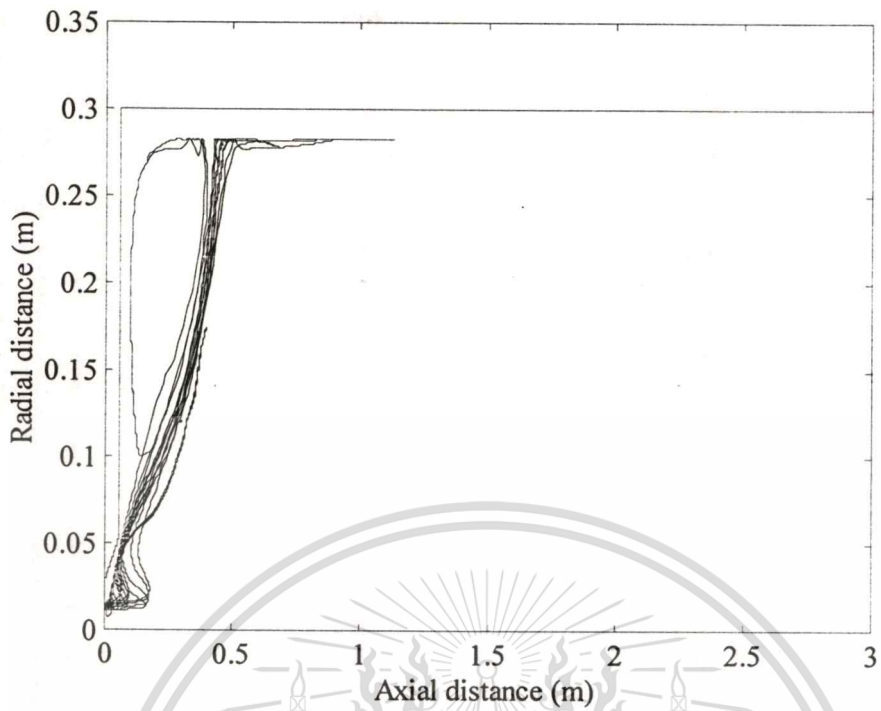
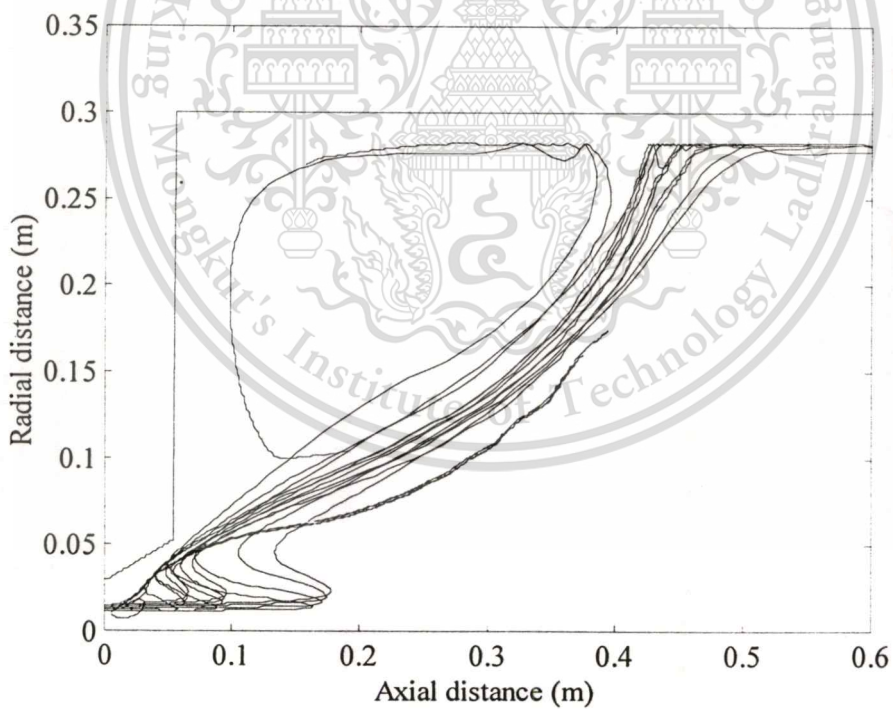


Fig.5.3 Distribution of temperature (K) (a) entire furnace (b) in the near burner zone



(a)



(b)

Fig.5.4 Coal particle trajectories (a) entire furnace (b) in the near burner zone

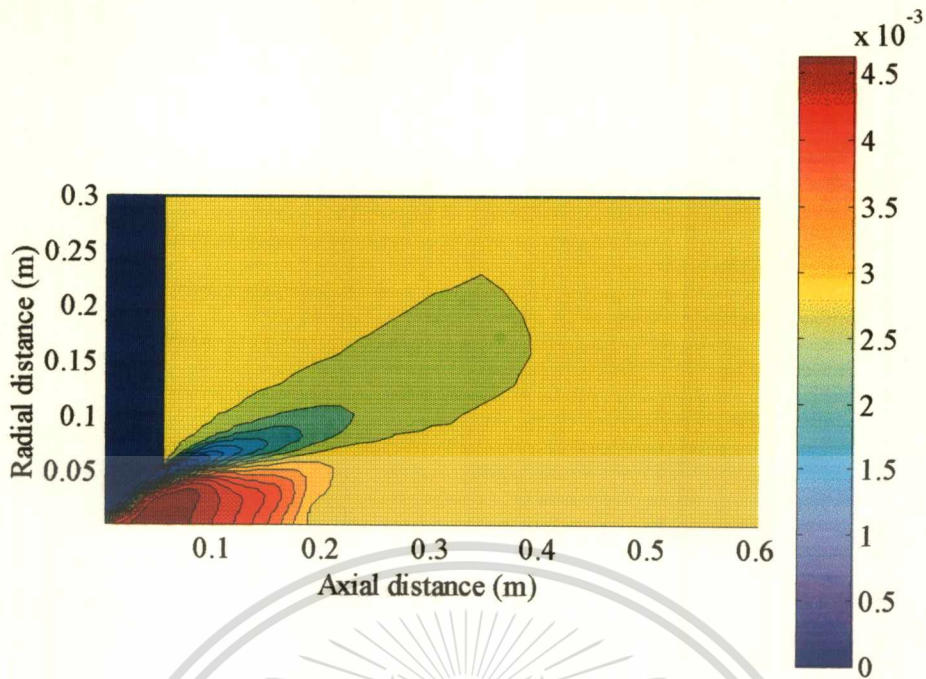


Fig.5.5 Concentration of sulfur oxides (in % $m_{SO_2} / m_{mixture}$) near the burner zone

5.4 Computational simulation for adsorption

From the evidence given in Section 4.2 and 4.3, calcination and sulfation processes are insimultaneous and the conversion is 90% before the sulfation process occurs. Four cases are carried out to achieve the objective of this study. Two cases, as will be discussed in Section 5.4.1 are case 1 and 2 for a study on the effect of particle sizes. Case 1 and 3 will be discussed in Section 5.4.2 for a study on the effect of starting location at side wall with different of 0.056 and 0.201 m from the furnace axis. Case 1 and 4 will be discussed in Section 5.4.3 for a study on the effect of inlet location at side wall and top wall. The numerical set - up are shown in Tables 5.4 – 5.7. Result of these cases will be discussed as follows. Fig.5.6 illustrates the schematic diagram of the burner and additional $CaCO_3$ inlet that consists of side wall and top wall inlets.

Table 5.4 Numerical set – up for desulfurization properties in case 1

Density of CaCO ₃	kg/m ³	2710
Density of CaO	kg/m ³	1590
Particle size	m	96x10 ⁻⁴
Particle temperature	K	1143
Top wall temperature	K	Insulation
Inlet location		Side wall
Axial distance	m	0.054
Radial distance	m	0.056
Flow rate	m ³ /s	0.006
Velocity	m/s	5.3818

Table 5.5 Numerical set – up for desulfurization properties in case 2

Density of CaCO ₃	kg/m ³	2710
Density of CaO	kg/m ³	1590
Particle size	m	25x10 ⁻³
Particle temperature	K	1143
Top wall temperature	K	Insulation
Inlet location		Side wall
Axial distance	m	0.054
Radial distance	m	0.056
Flow rate	m ³ /s	0.006
Velocity	m/s	5.3818

Table 5.6 Numerical set – up for desulfurization properties in case 3

Density of CaCO_3	kg/m^3	2710
Density of CaO	kg/m^3	1590
Particle size	m	96×10^{-4}
Particle temperature	K	1143
Top wall temperature	K	Insulation
Inlet location		Side wall
Axial distance	m	0.054
Radial distance	m	0.201
Flow rate	m^3/s	0.006
Velocity	m/s	5.3818

Table 5.7 Numerical set – up for desulfurization properties in case 4

Density of CaCO_3	kg/m^3	2710
Density of CaO	kg/m^3	1590
Particle size	m	96×10^{-4}
Particle temperature	K	1143
Top wall temperature	K	Insulation
Inlet location		Top wall
Axial distance	m	0.099
Radial distance	m	0.292
Flow rate	m^3/s	0.005
Velocity	m/s	-3.3818

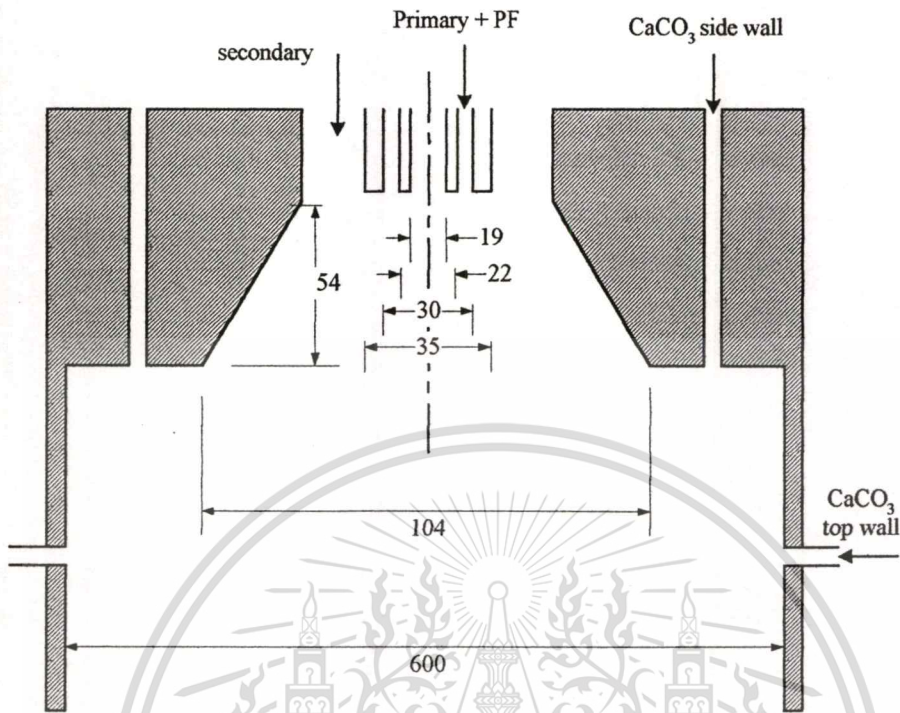


Fig.5.6 Section of the burner and additional CaCO_3 inlets

5.4.1 Effect of particle sizes on the amount of SO_2 adsorption (case 1 and case 2)

The particle trajectories and the amount of SO_2 adsorption of small (0.0096 cm.) and large (0.025 cm.) CaCO_3 particles are compared. In both cases, the particles were injected from side wall at 0.056 m. from the furnace axis. In Fig.5.7, the calcination process of particle size 0.0096 cm. is faster than that of particle 0.025 cm., (see Fig.5.8) because of the size of particles is smaller. After that, the sorption of sulfur oxides for the smaller diameter, 0.0096 cm., is more than that of 0.025-cm particles, see Figs.5.7 and 5.8. Figs.5.9 and 5.10 illustrate the trajectories of particle sizes of 0.0096 cm. and 0.025 cm., respectively. In the near burner zone (< 0.5 m. from the exit plane), the particles caught up with the gas velocity, which was the same as coal particles, see Fig.5.4. The particles moved into the location near the top wall at which the axial location was about 0.45 m. and moved to the low temperature zone, see Figs.5.11 and 5.12. This result is a decrease in the rate of sorption as illustrated in Figs.5.7 and 5.8. When the residence time is higher than 1.5 s., the slopes of the graphs decrease.

This material is reserved for educational use only, not allowed for commercial use.

Forbidden to modify the content, and cite the document when use.

5.4.2 Effect of inlet location at side wall with different of 0.056 and 0.201 m on the amount of SO₂ adsorption (case 1 and case 3)

Fig.5.13a and b illustrate trajectories of 0.0096- μ m particles which were injected into the furnace at side wall and 0.2 m. from the furnace axis. Particles were entrained by the flow of the external recirculation and moved to the top wall at the axial location of 0.45 m. After leaving the top wall, particles moved into the low temperature zone and exited the furnace, see Fig.5.13 and 5.14. Therefore, the kinetic rate of sorption (between 0 – 0.2 s.) is higher than the case of which the particles were injected at 0.056 m. from the furnace symmetry axis, see Fig.5.7 and 5.15. This is due to the longer residence time of moving particles in high temperature zone, see Figs.5.13 and 5.14.

5.4.3 Effect of inlet location at side wall and top wall (case 1 and case 4)

In case 4, the 0.0096- μ m particles were injected at the top wall of the furnace located axially at 0.1 m. from the coal inlet, see Fig.5.16. The particle moved down to the center of the furnace. After that, it moved to the top wall again due to the gas flow at 0.45 m., therefore the kinetic rate of sorption between 0 – 2 s., in Fig.5.17 and 5.7, is higher than that of case 1 because the particles moved through the higher temperature zone in external recirculation zone (ERZ), see Fig.5.16 and 5.18. Finally, the particles move through the low temperature zone, and exited the furnace at the outlet. Then, the low kinetic rate of sorption is seen in Fig.5.17

Moreover, concentration of SO₂ from the cases 1, 2, 3 and 4 can be illustrated in Figs.5.19, 5.20, 5.21 and 5.22.

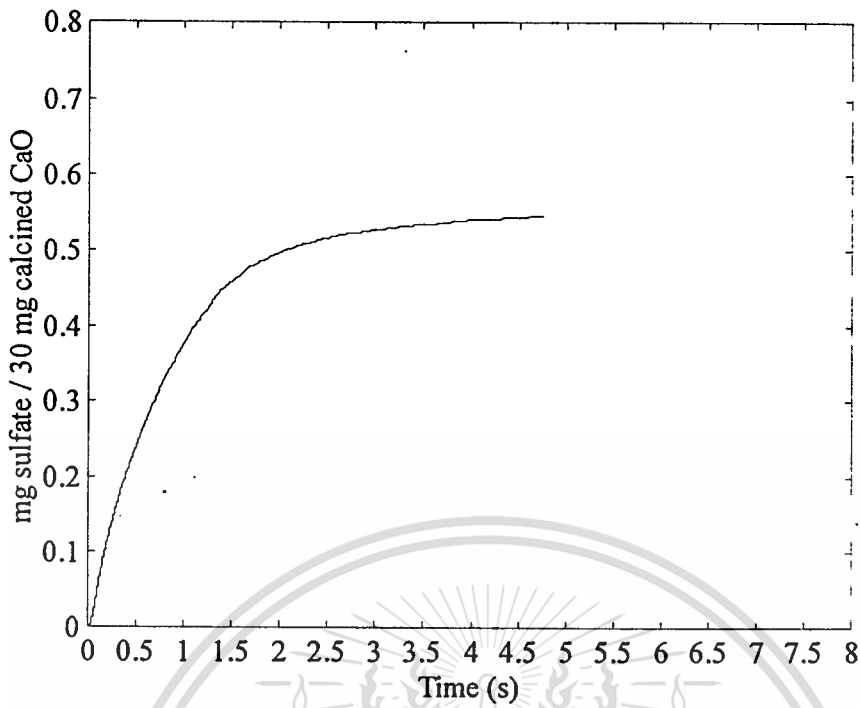


Fig.5.7 Sorption of sulfur dioxide for dolomite 1351 diameter of 0.0096 cm. (case 1)

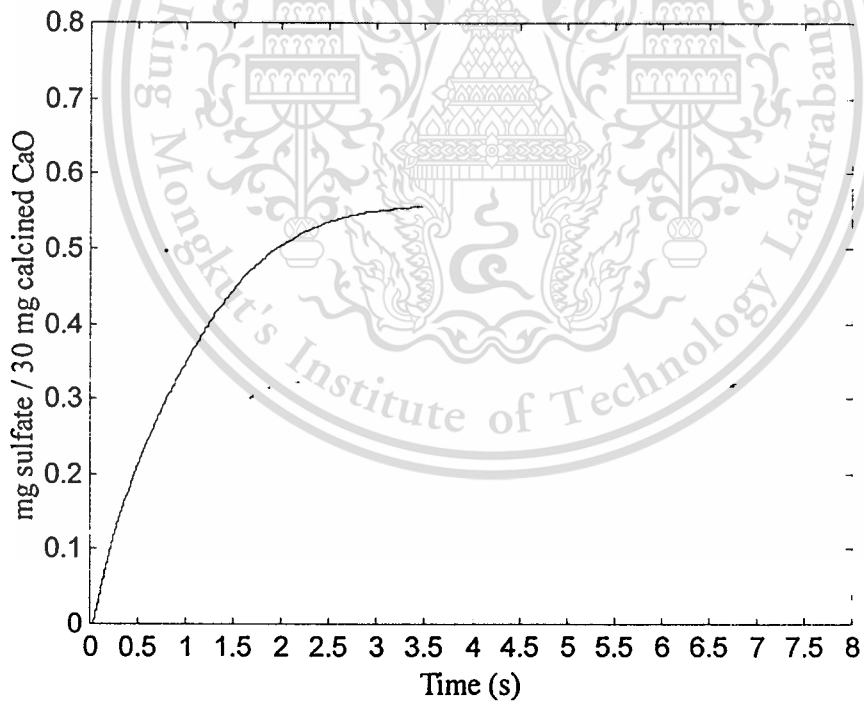


Fig.5.8 Sorption of sulfur dioxide for dolomite 1351 diameter of 0.025 cm. (case 2)

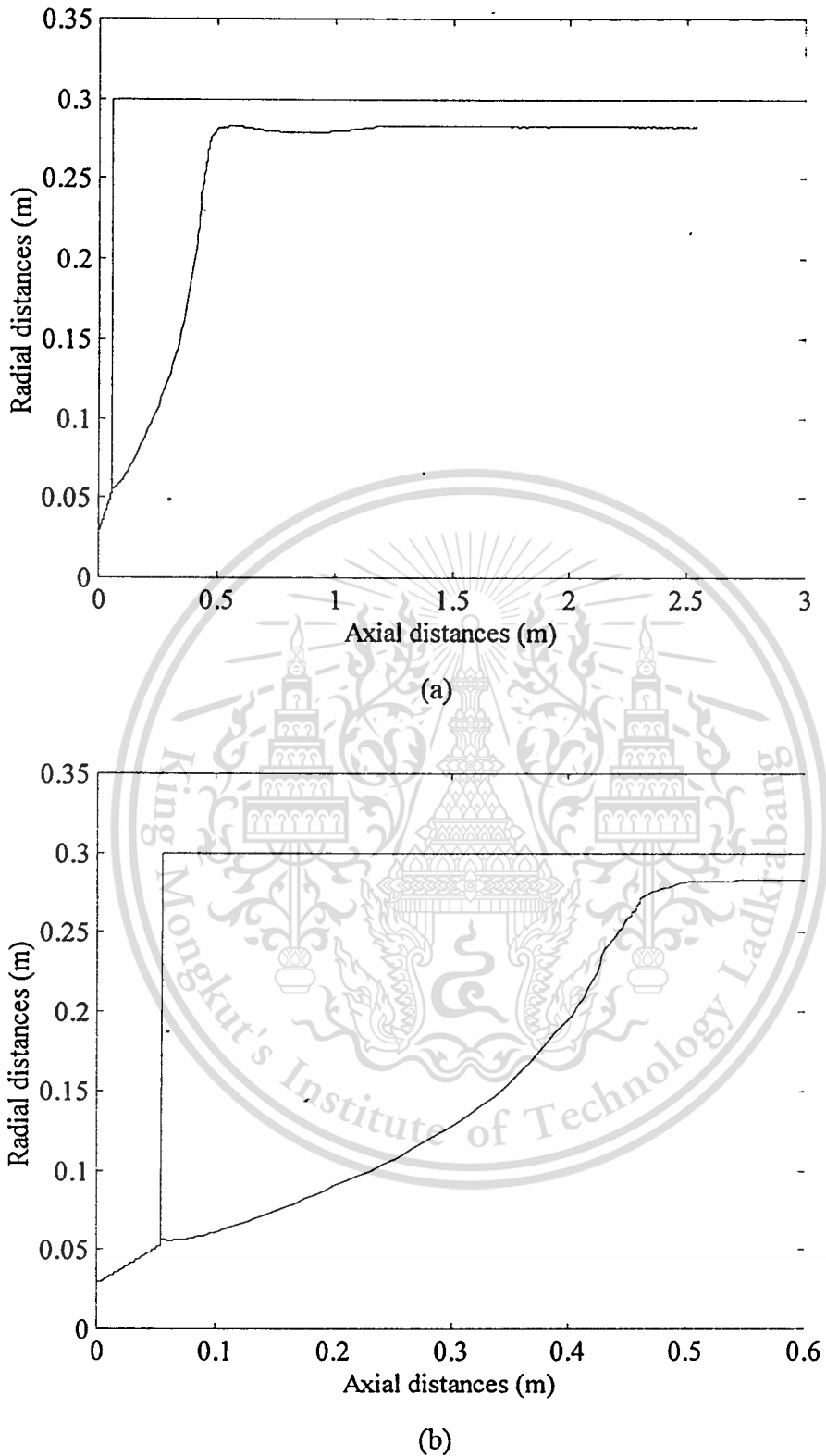
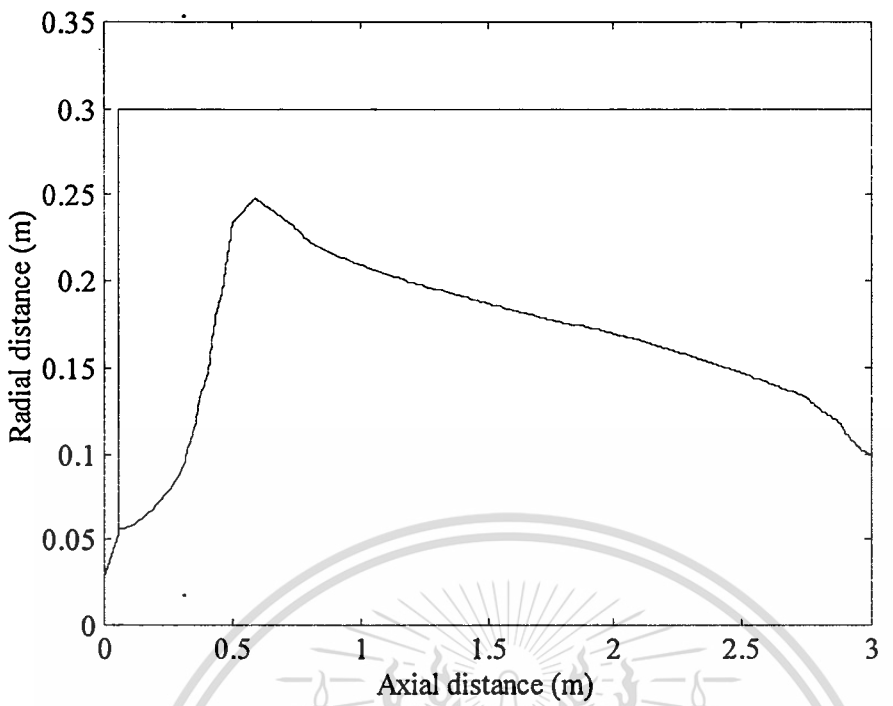
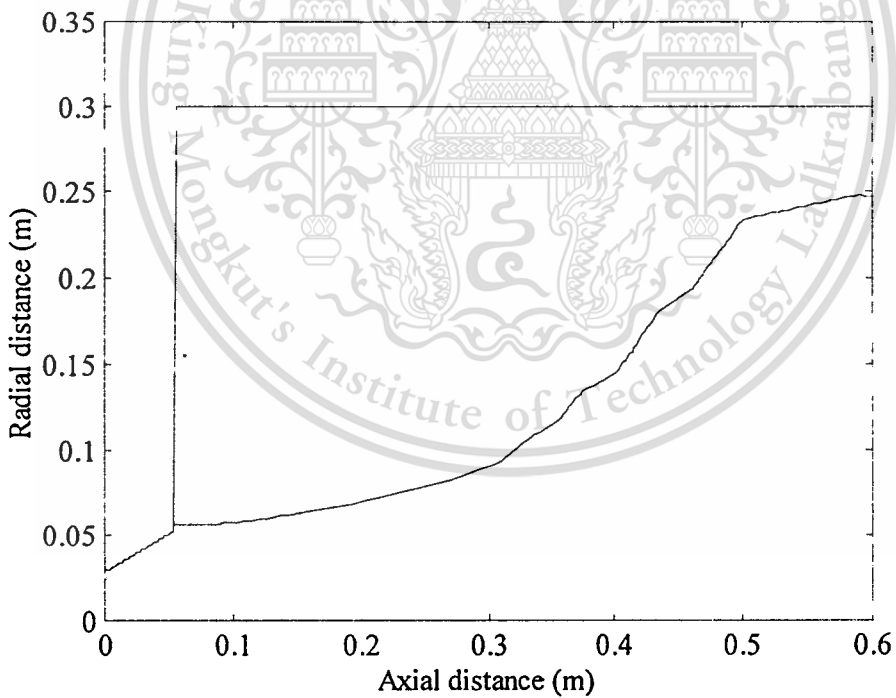


Fig.5.9 CaCO_3 particle trajectories in case 1 (a) entire furnace (b) in the near burner zone

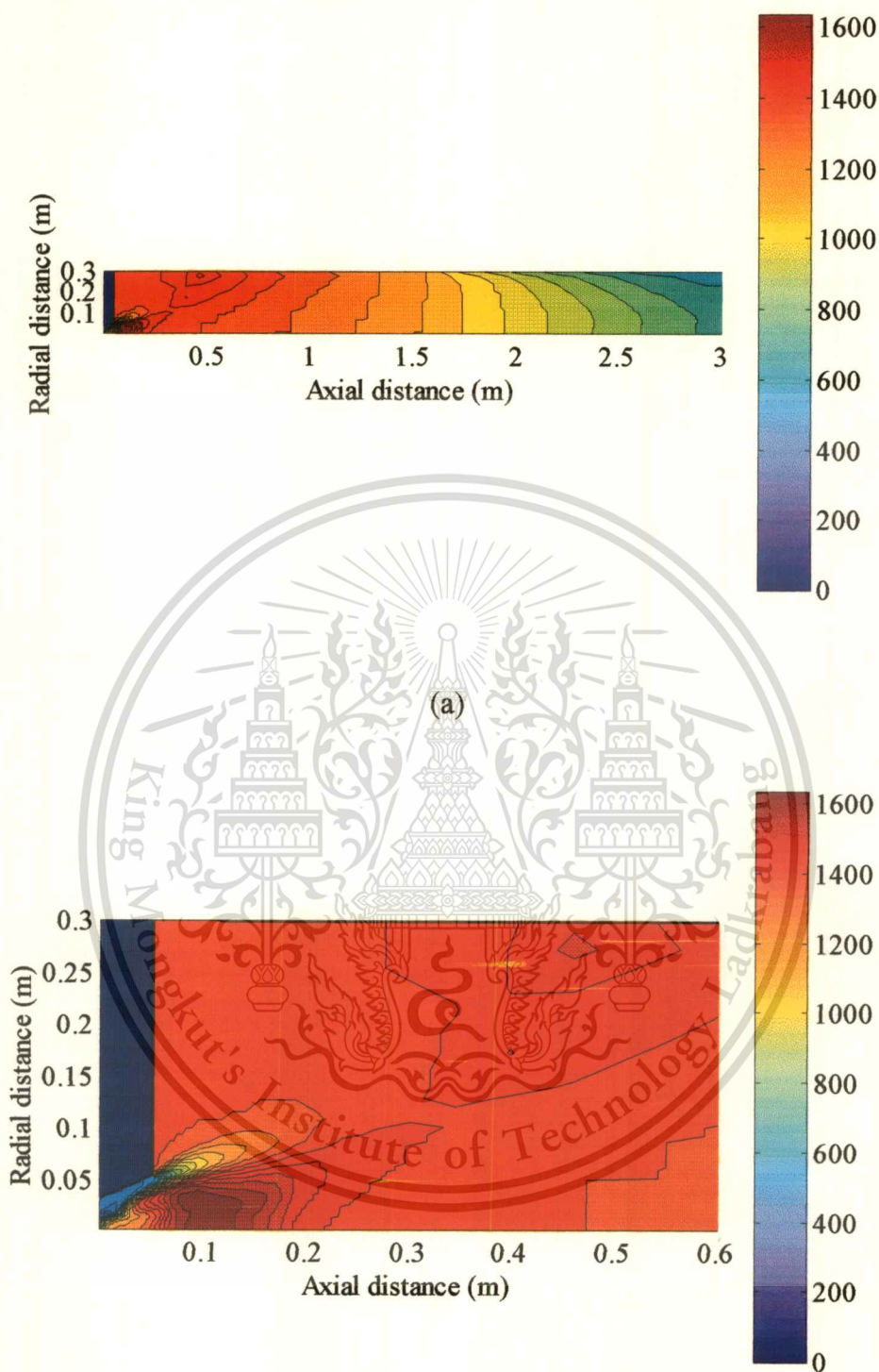


(a)



(b)

Fig.5.10 CaCO_3 particle trajectories in case 2 (a) entire furnace (b) in the near burner zone



(b)

Fig.5.11 Distribution of temperature (K) in case 1 (a) entire furnace (b) in the near burner zone

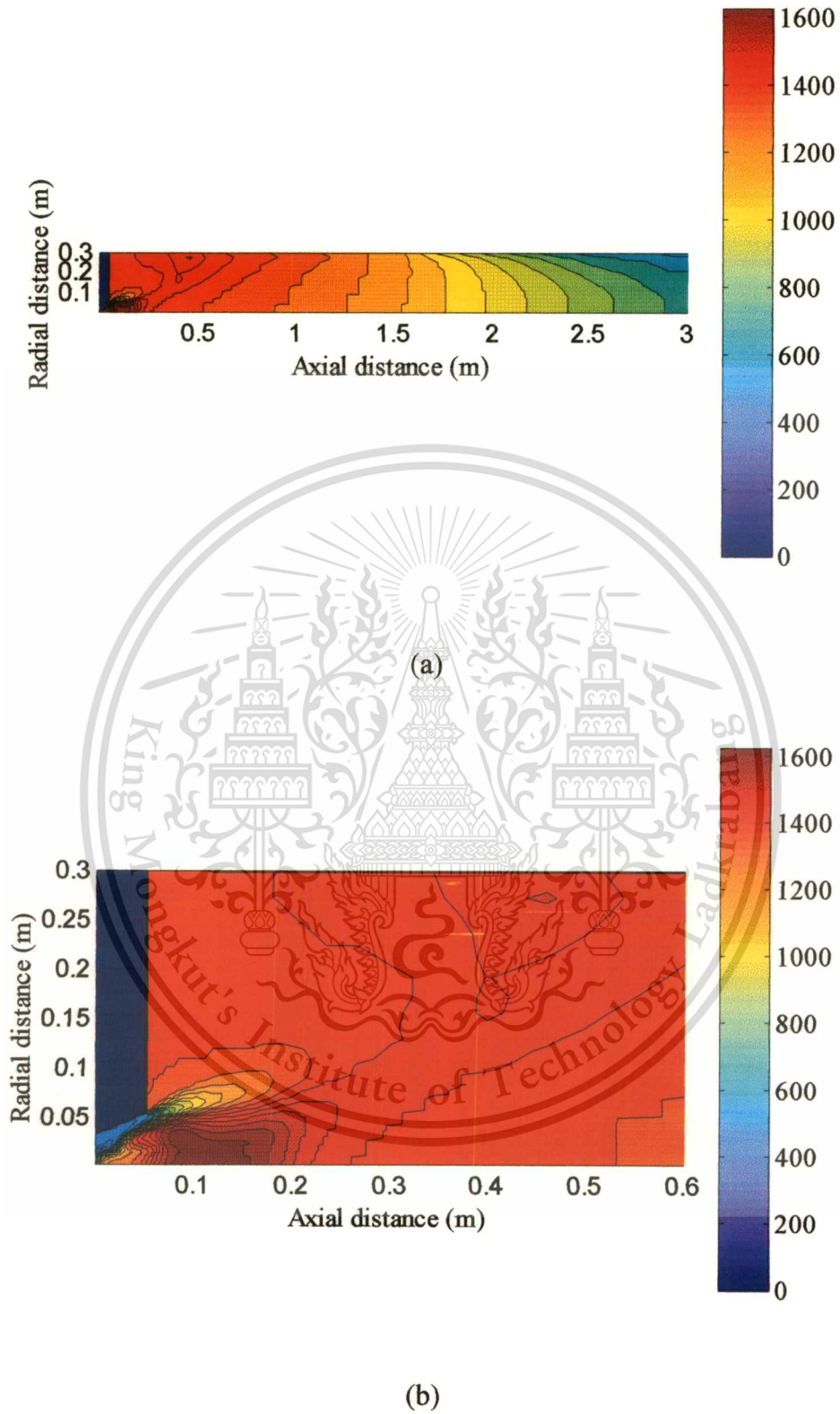
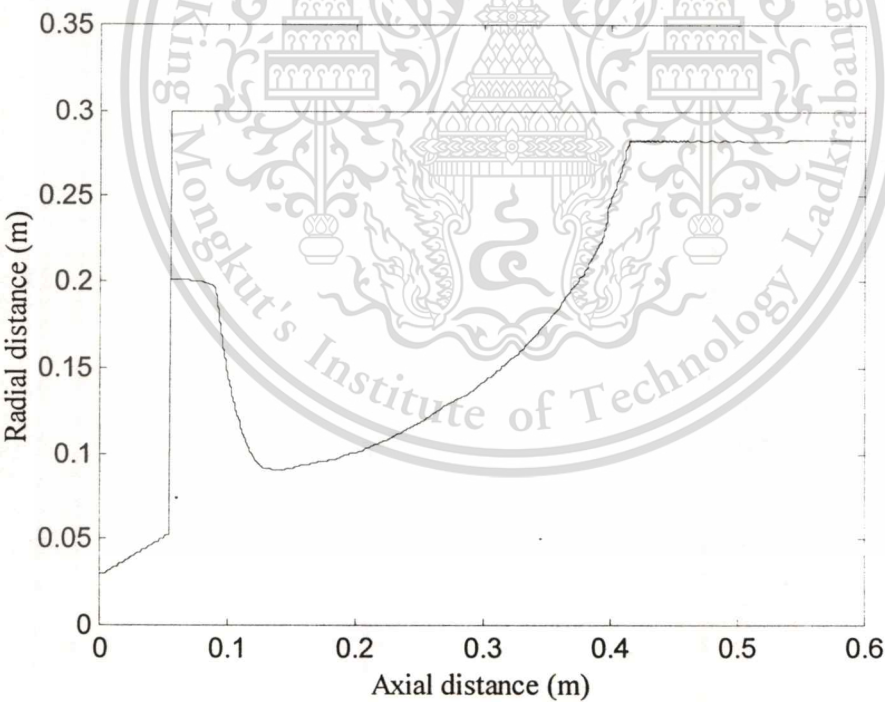
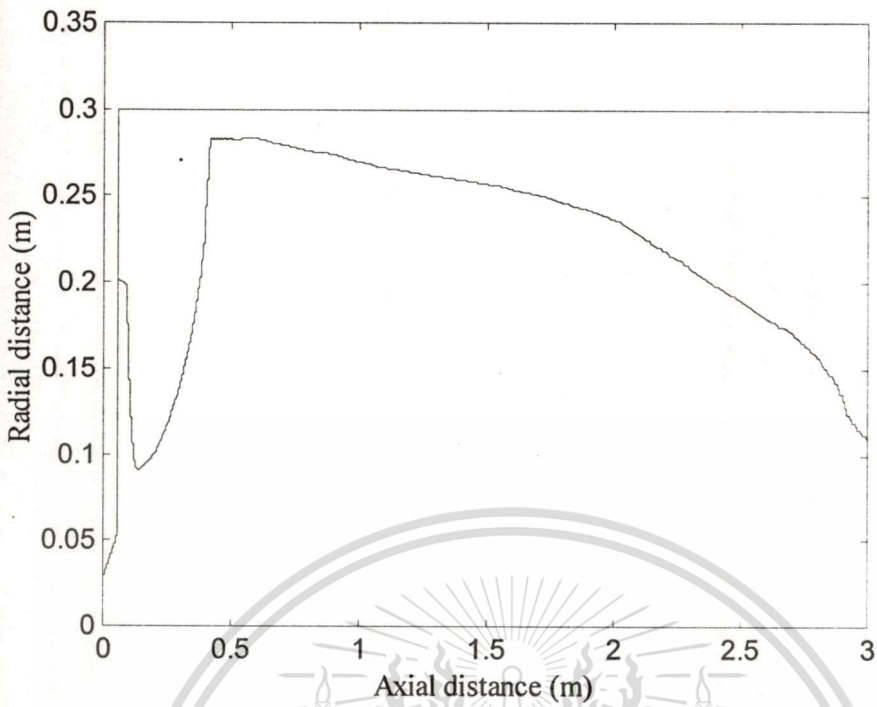


Fig.5.12 Distribution of temperature (K) in case 2 (a) entire furnace (b) in the near burner zone



(b)

Fig.5.13 CaCO_3 particle trajectories in case 3 (a) entire furnace (b) in the near burner zone

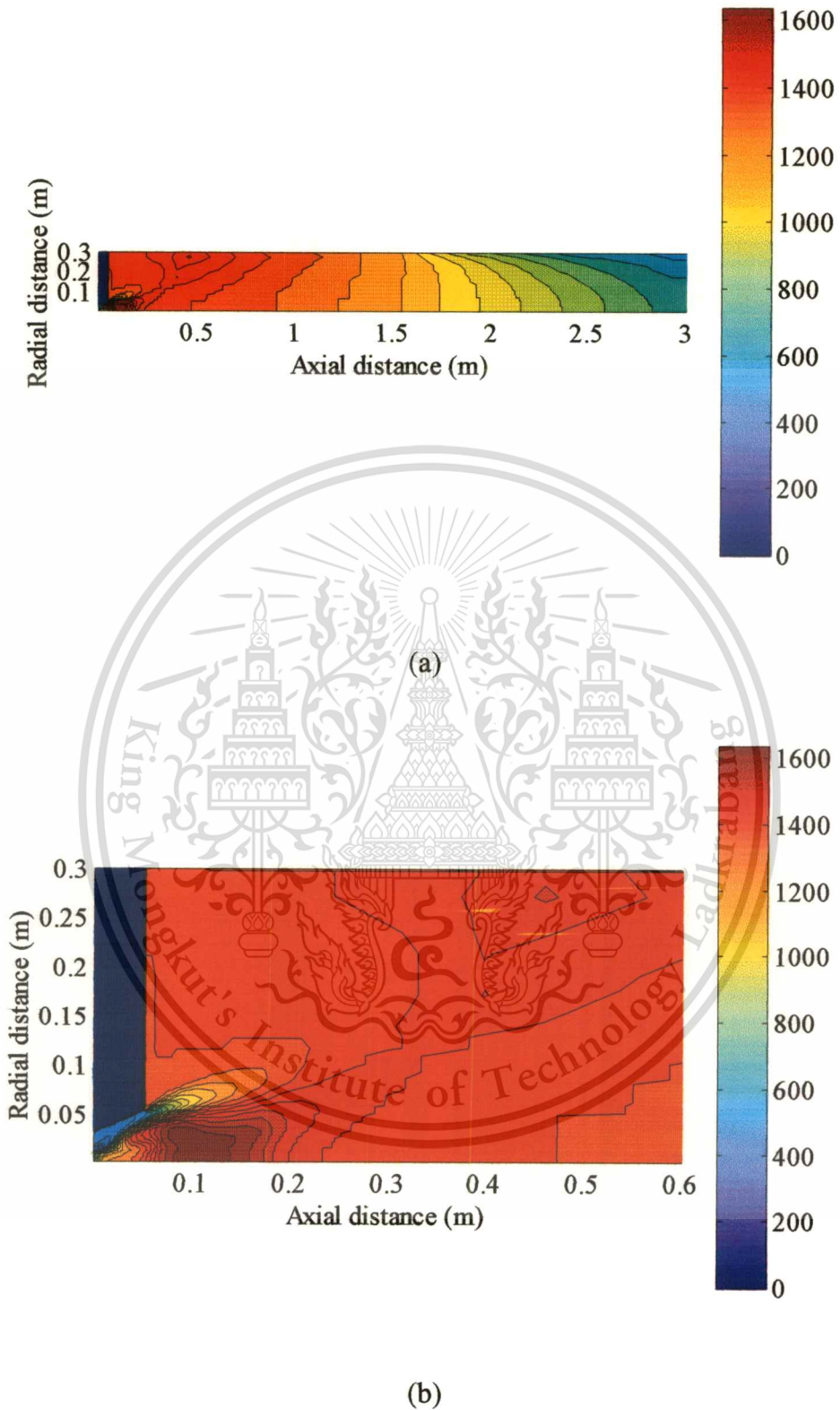


Fig.5.14 Distribution of temperature (K) in case 3 (a) entire furnace (b) in the near burner zone

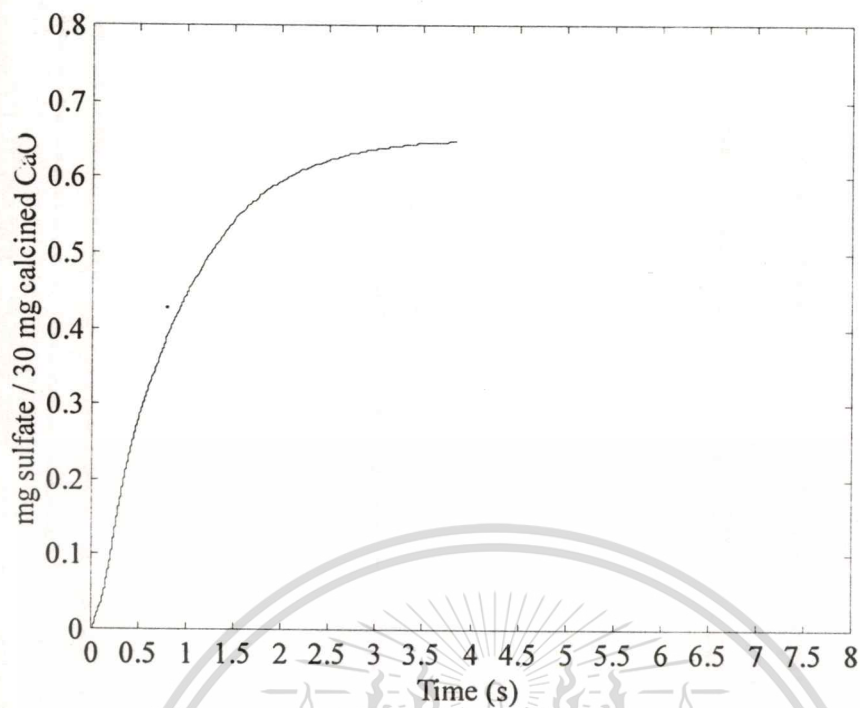
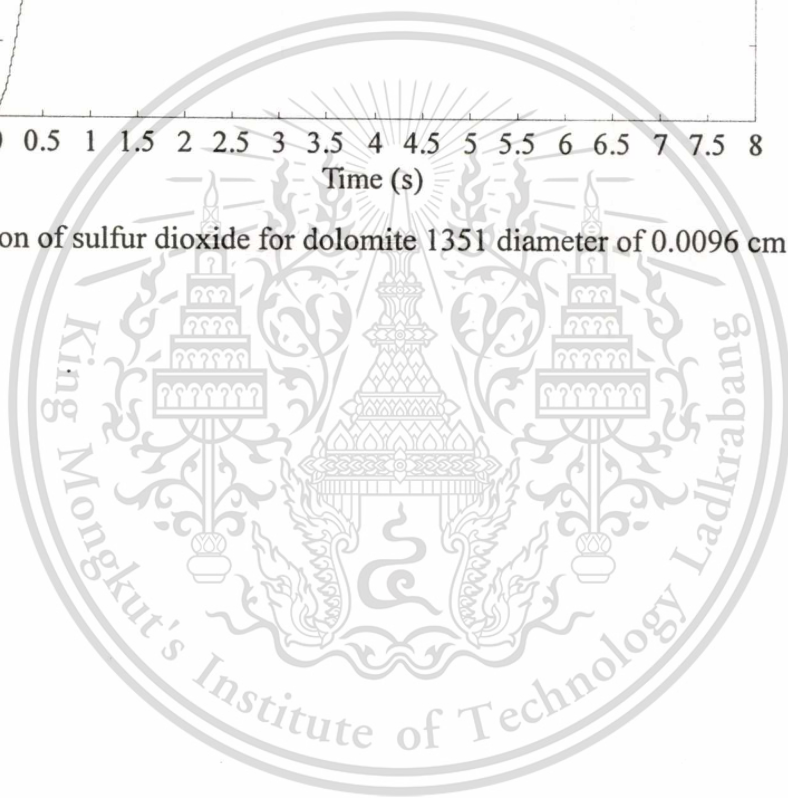
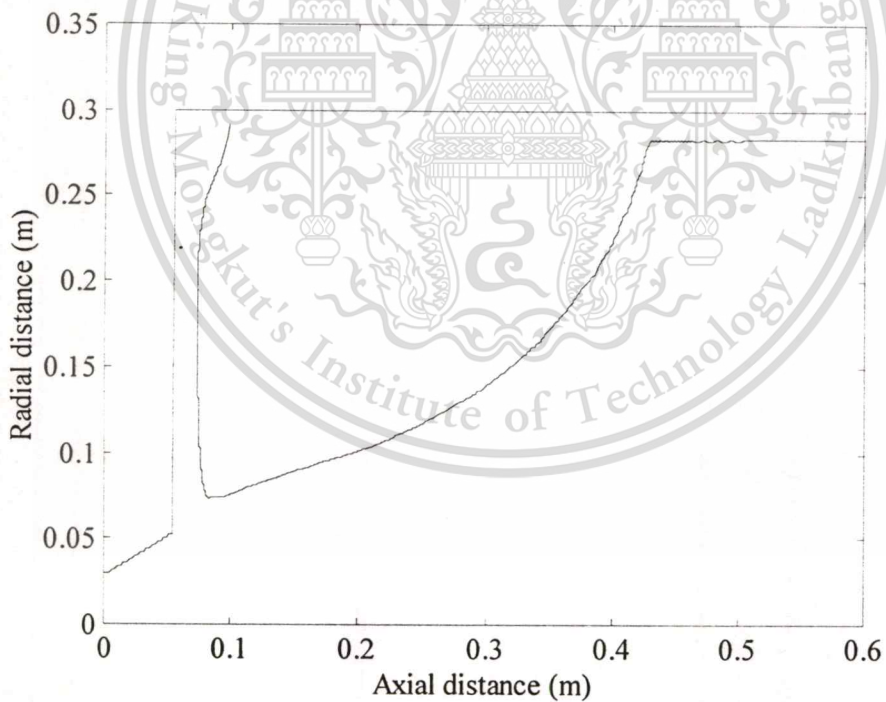
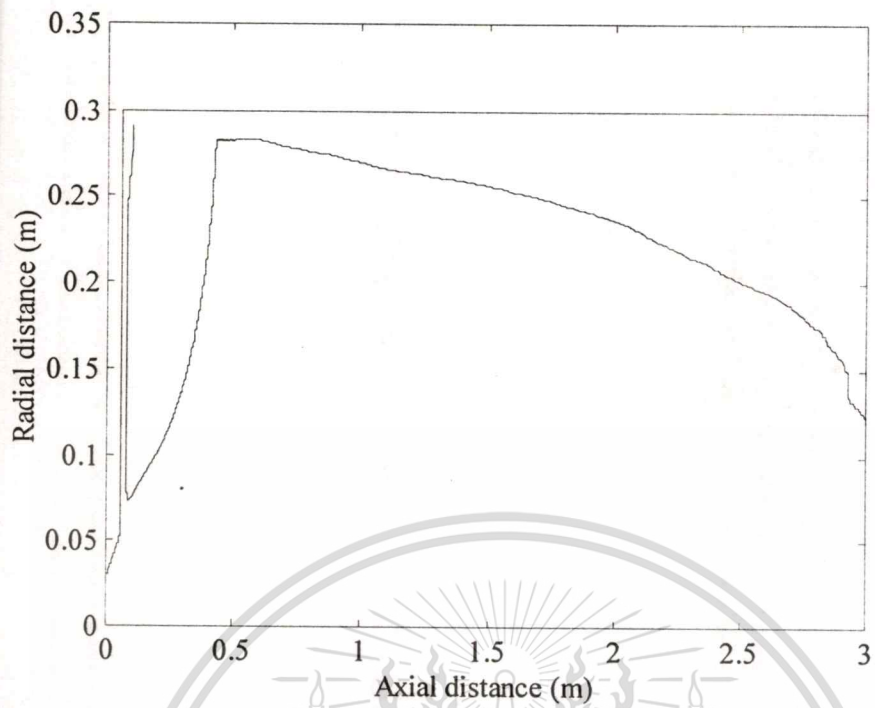


Fig.5.15 Sorption of sulfur dioxide for dolomite 1351 diameter of 0.0096 cm. (case 3)





(b)

Fig.5.16 CaCO_3 particle trajectories in case 4 (a) entire furnace (b) in the near burner zone

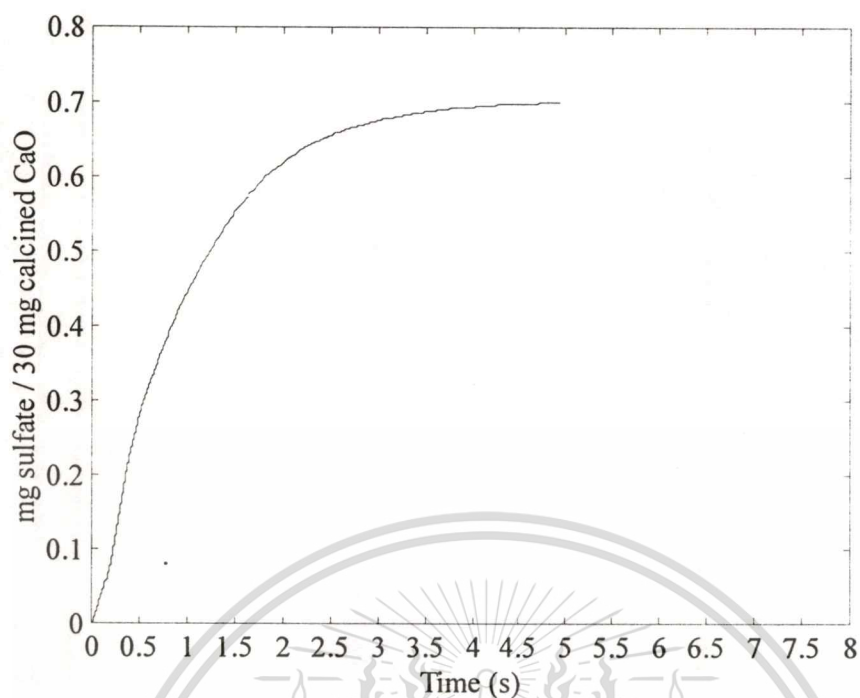
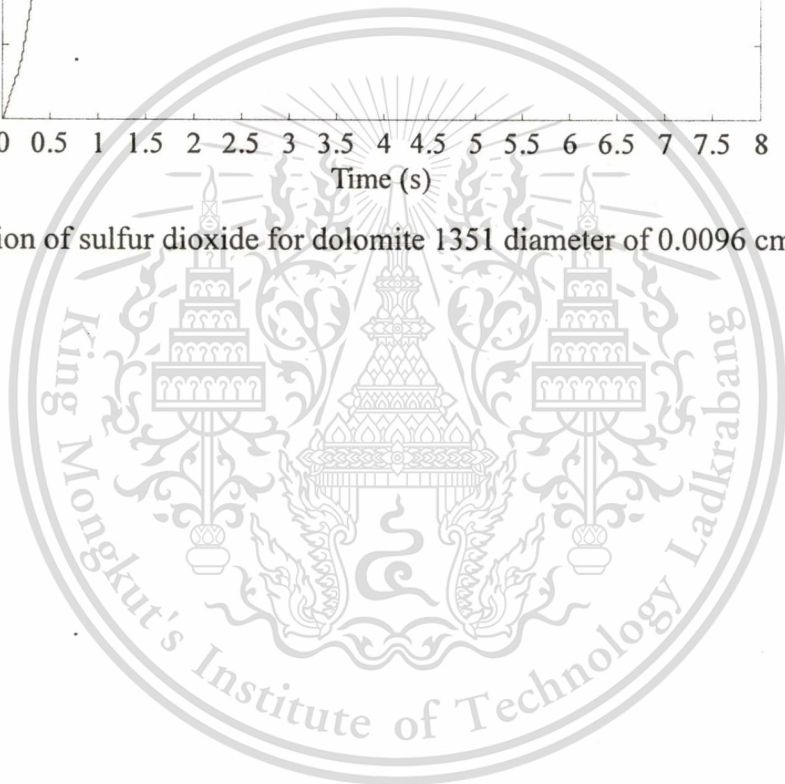


Fig.5.17 Sorption of sulfur dioxide for dolomite 1351 diameter of 0.0096 cm. (case 4)



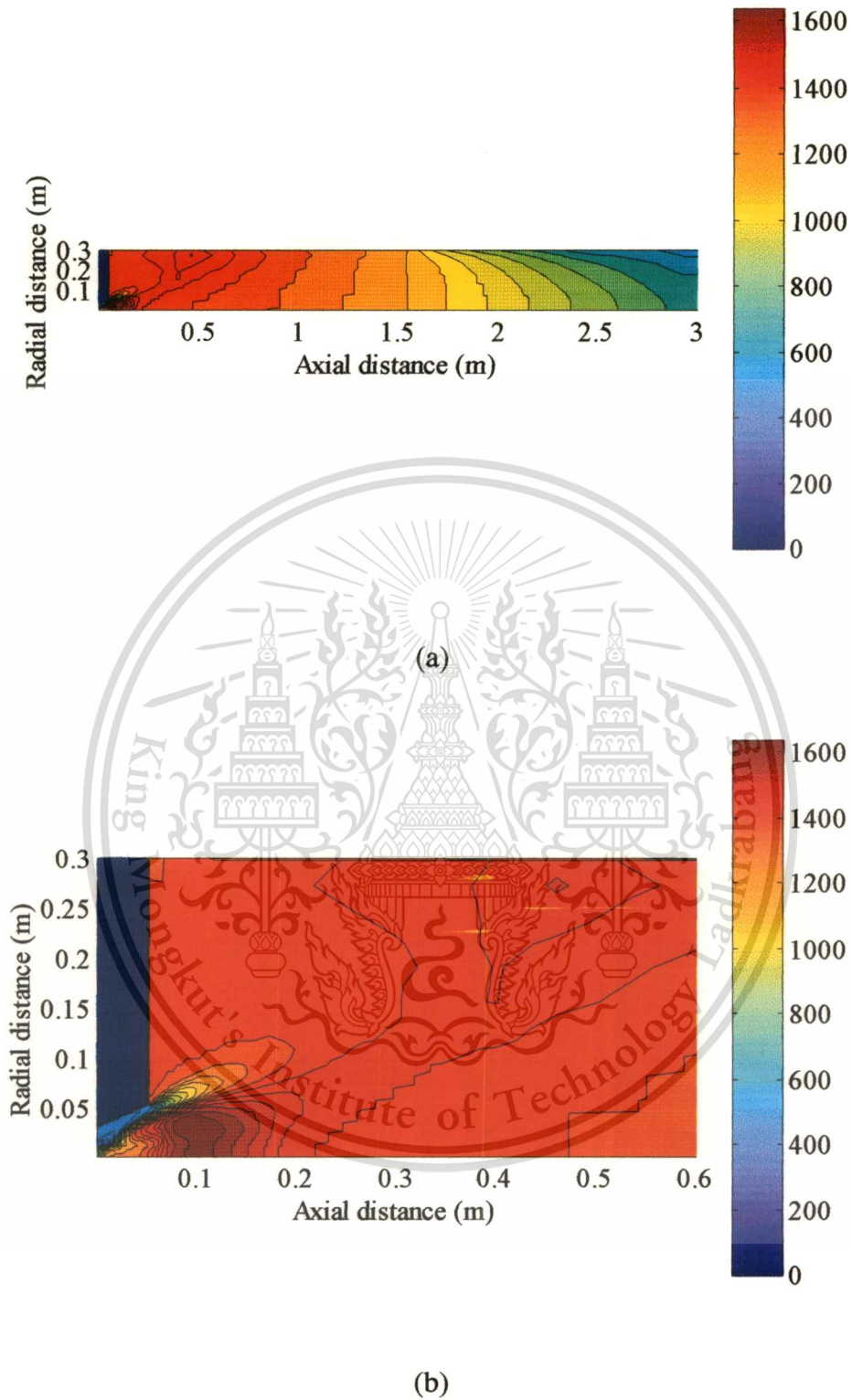


Fig.5.18 Distribution of temperature (K) in case 4 (a) entire furnace (b) in the near burner zone

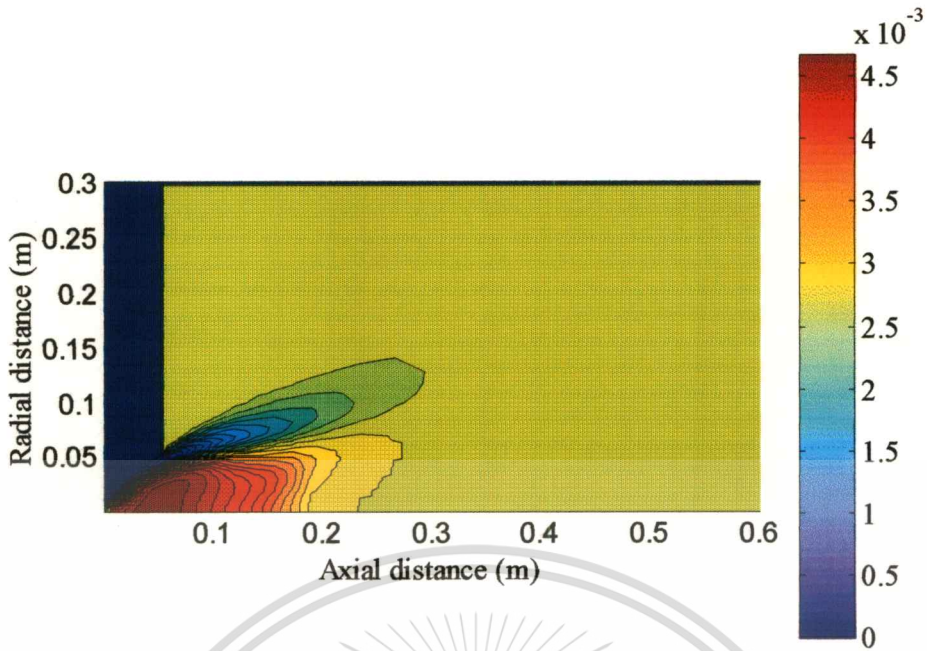


Fig.5.19 Concentration of sulfur oxides, case 1 (in % $m_{SO_2} / m_{mixture}$), in the near burner zone

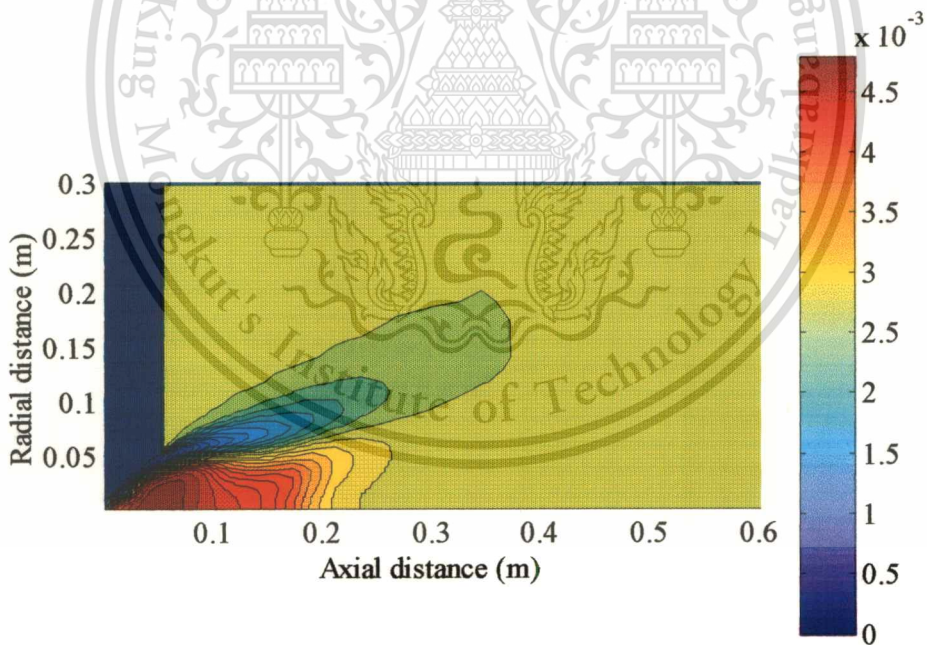


Fig.5.20 Concentration of sulfur oxides, case 2 (in % $m_{SO_2} / m_{mixture}$), in the near burner zone

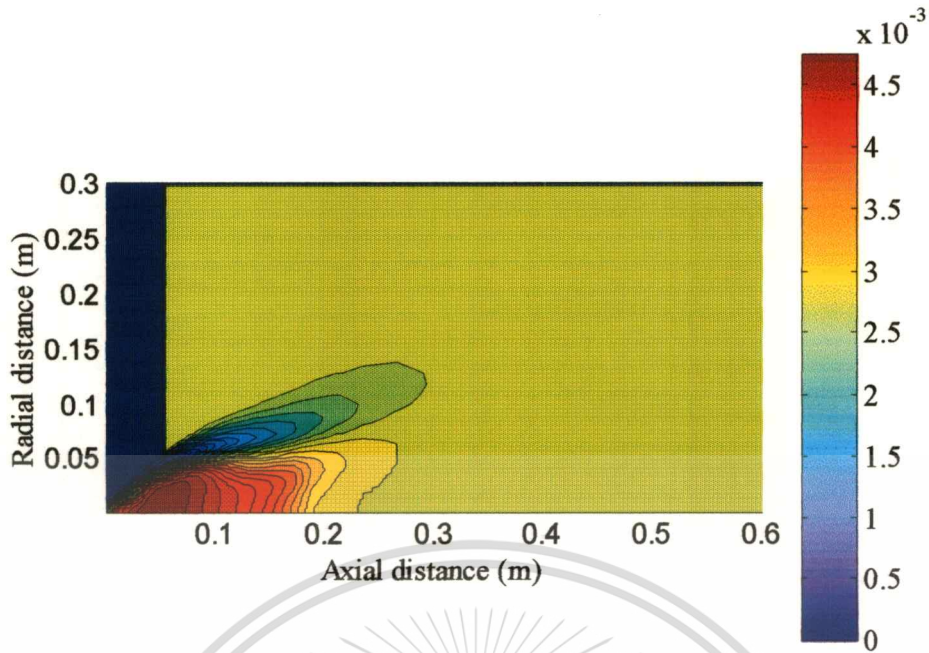


Fig.5.21 Concentration of sulfur oxides, case 3 (in % $m_{SO_2} / m_{mixture}$), in the near burner zone

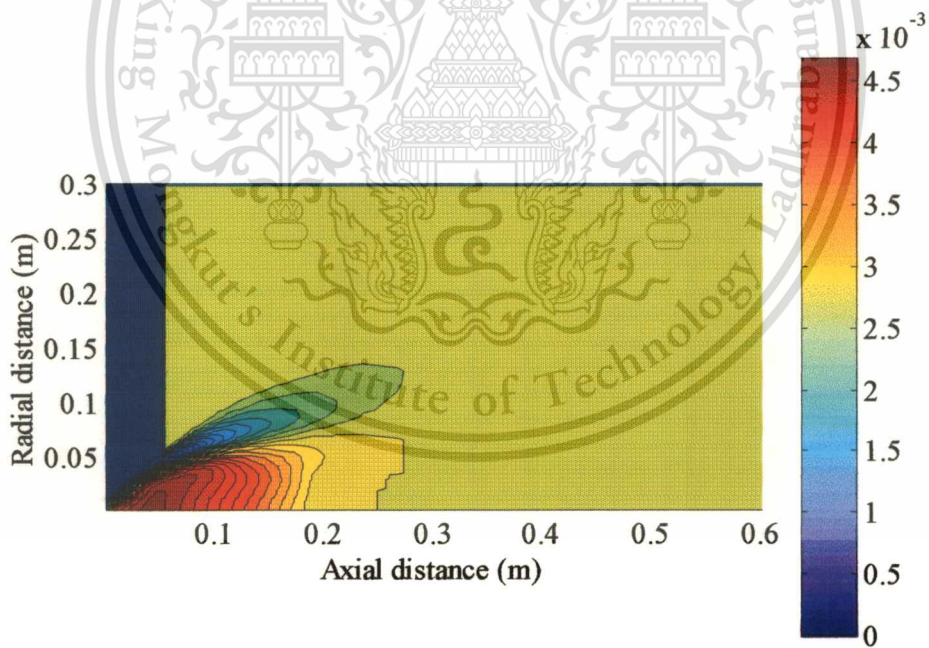
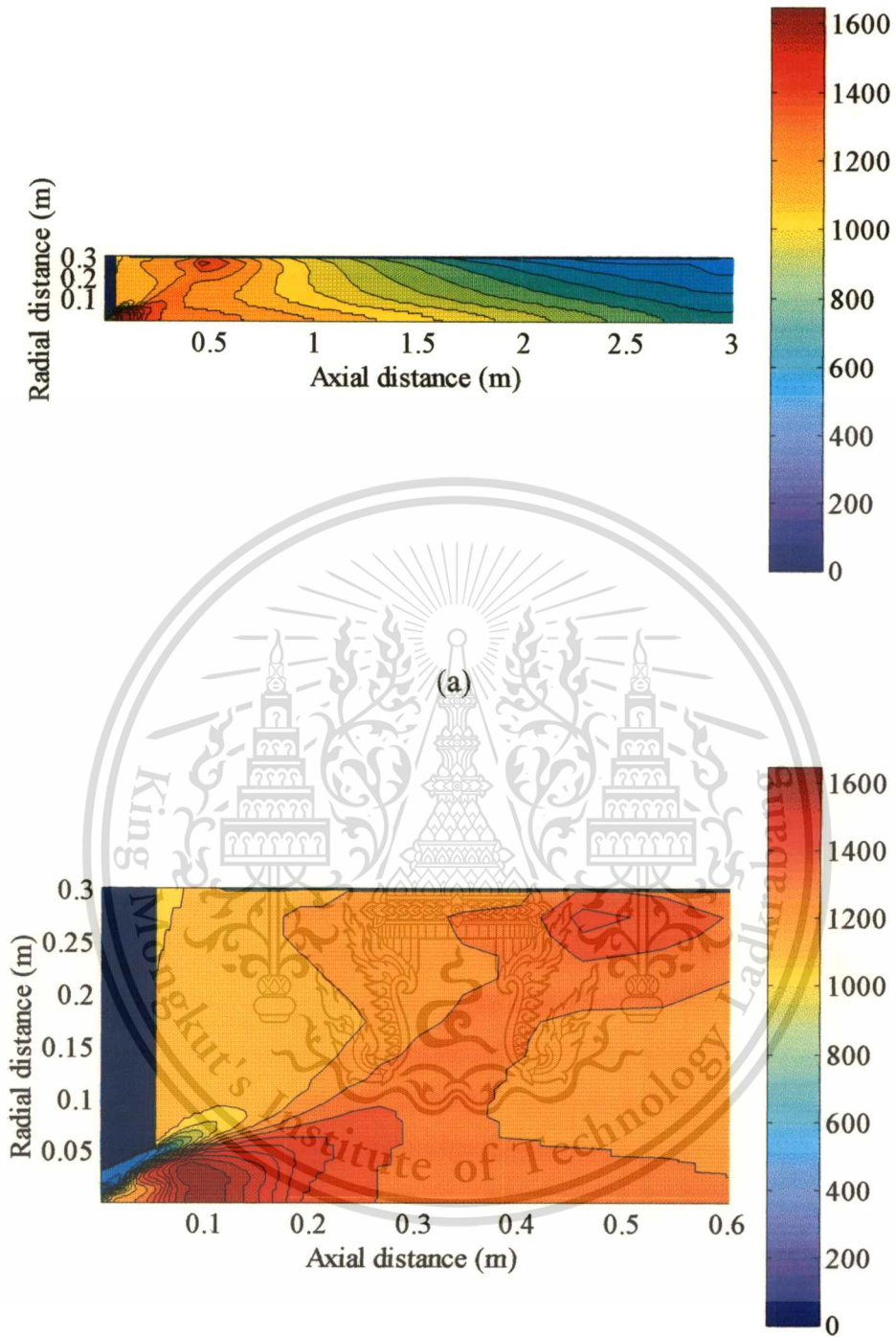


Fig.5.22 Concentration of sulfur oxides, case 4 (in % $m_{SO_2} / m_{mixture}$), in the near burner zone

5.5 Modified boundary for coal combustion (base case)

The simulated results displayed in the series of above figures show that the inlet locations and particle sizes have relationships with the SO_2 adsorption. The high reaction rate of SO_2 adsorption occurs when the CaCO_3 particles move in a high temperature zone and within a long residence time. The sizes of particles have less effect on SO_2 adsorption when compared to effect of the temperature distribution. In section 5.4, the furnace wall was insulated thus the distribution of temperature near the burner was high. The following section will discuss on the results under the conditions which the wall temperature was reduced in order to keep the temperature distribution in the near burner region at about 1000 K. The reason for that is due to the suggestions given by the previous researchers for the maximum allowable adsorption temperature that should not be greater than 1300 K [19]. To achieve such requirement, the temperature of 500 K was applied at the top wall. Fig.5.23 shows a contour plot of the temperature distribution in the furnace under such conditions. Coal particle trajectories are illustrated in Fig.5.24 and sulfur oxide concentration in Fig.5.25. CaCO_3 particles are not yet injected into the furnace. The result serves as a base case for the comparison in the next section.



(b)

Fig.5.23 Distribution of modified temperature (K) (a) entire furnace (b) in the near burner zone

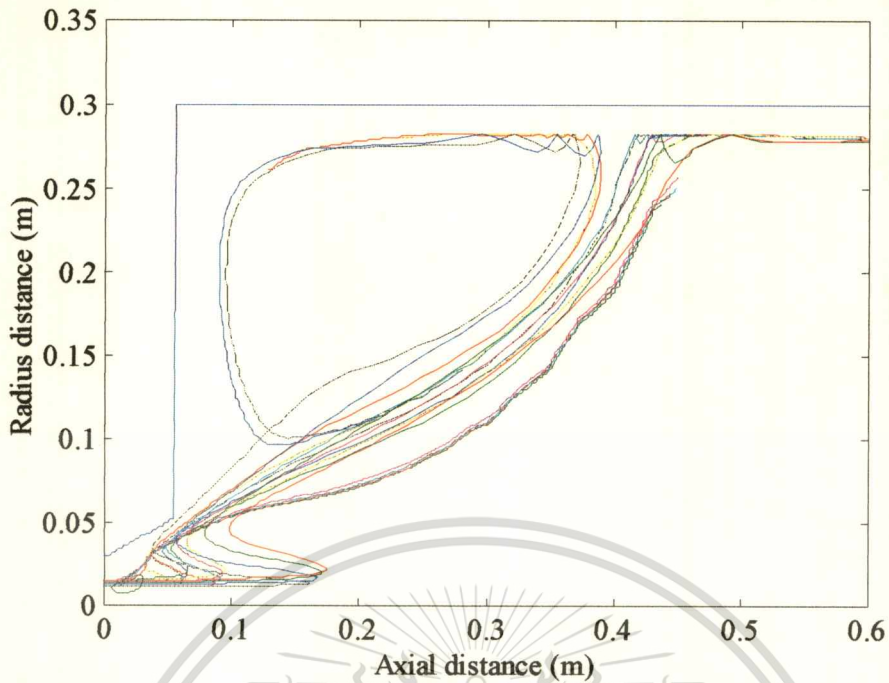


Fig.5.24 CaCO_3 particle trajectories in the near burner under modified wall temperature

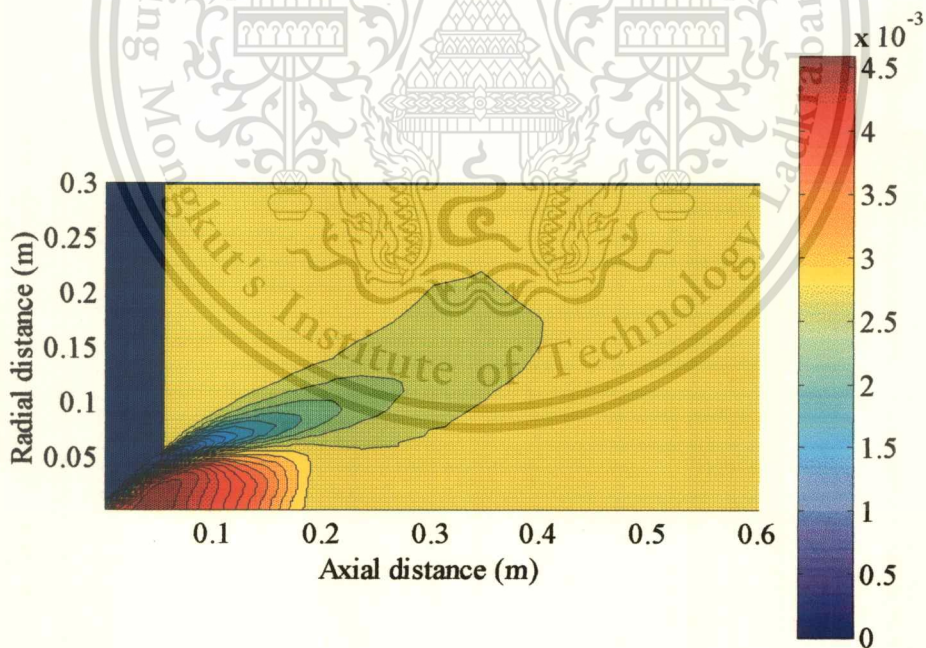


Fig.5.25 Concentration of sulfur oxides (in % $m_{\text{SO}_2} / m_{\text{mixture}}$) in the near burner zone under modified wall temperature

5.6 Modified simulation for adsorption

Cases 5,6 and 7 will be discussed in this section for a study on the effect of wall temperature on SO₂ adsorption. The operating conditions are given from Table 5.8 to 5.10. The wall temperature profile near the burner was kept constant at 500 K. The diameter of CaCO₃ is 0.0096 cm. In case 5, the particles were injected from side wall, whereas in cases 6 and 7 the particles were injected from top wall but different in inlet locations. The results of these cases are discussed as follow:

Fig.5.26 shows a 0.0096 cm. particle trajectory of case 5. It is found that the particles generally have a longer residence time in the external recirculation zone than that of the case performed under insulated wall, given in Fig.5.13. This effect leads to an increase in time for SO₂ adsorption (see Figs.5.32 and 5.15). However, lower rate of sorption occurs because the particle moves in the lower temperature zone, see Figs.5.29 and 5.14.

Figs.5.27 and 5.28 show the particle trajectories, Figs.5.30 and 5.31 show temperature distributions of cases 6 and 7, respectively. Figs.5.32, 5.33 and 5.34 show the sorption of SO₂ of cases 5, 6 and 7, respectively. Both cases have low sorption levels in common with case 5 due to comparatively low temperature levels throughout the furnace. Moreover, concentration of SO₂ from the cases 5, 6 and 7 can be illustrated in Figs.5.35, 5.36 and 5.37.

Table 5.8 Numerical set – up for desulfurization properties in case 5

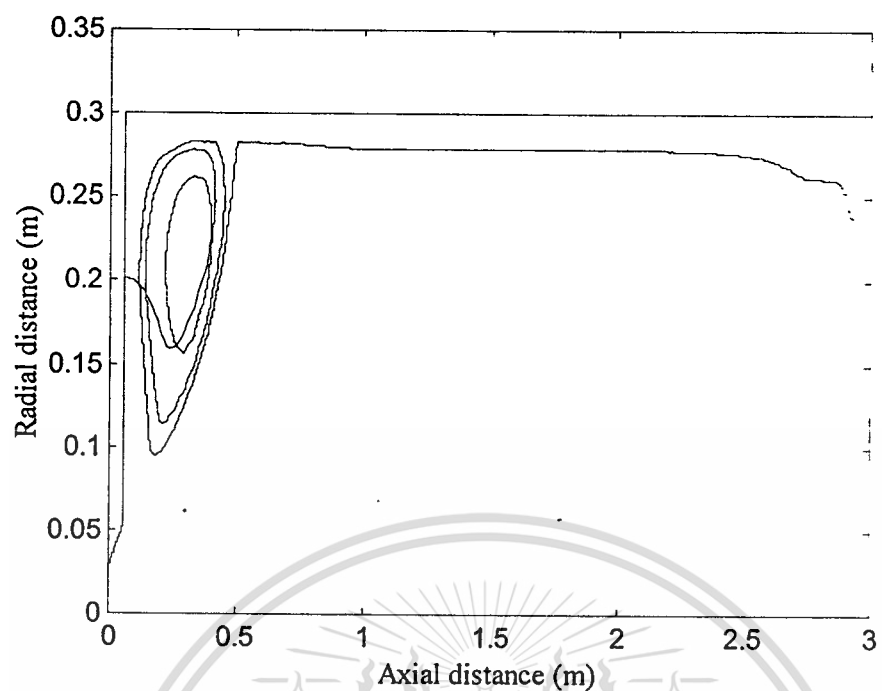
Density of CaCO ₃	kg/m ³	2710
Density of CaO	kg/m ³	1590
Particle size	m	96x10 ⁻⁴
Particle temperature	K	1143
Top wall temperature	K	500
Inlet location		Side wall
Axial distance	m	0.054
Radial distance	m	0.201
Flow rate	m ³ /s	0.006
Velocity	m/s	5.3818

Table 5.9 Numerical set – up for desulfurization properties in case 6

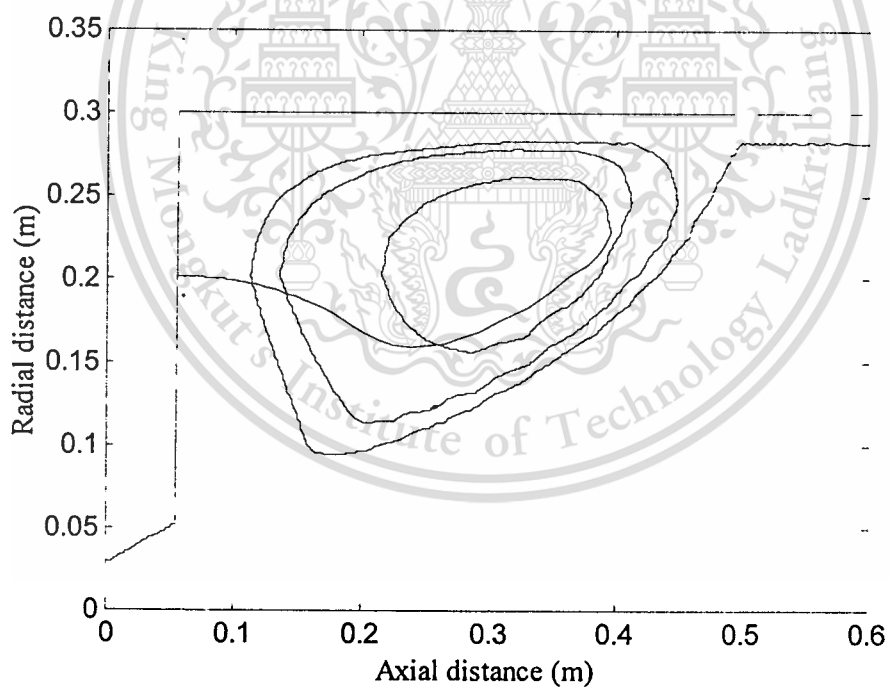
Density of CaCO ₃	kg/m ³	2710
Density of CaO	kg/m ³	1590
Particle size	m	96x10 ⁻⁴
Particle temperature	K	1143
Top wall temperature	K	500
Inlet location		Top wall
Axial distance	m	0.099
Radial distance	m	0.292
Flow rate	m ³ /s	0.005
Velocity	m/s	-3.3818

Table 5.10 Numerical set – up for desulfurization properties in case 7

Density of CaCO ₃	kg/m ³	2710
Density of CaO	kg/m ³	1590
Particle size	m	96x10 ⁻⁴
Particle temperature	K	1143
Top wall temperature	K	500
Inlet location		Top wall
Axial distance	m	0.304
Radial distance	m	0.292
Flow rate	m ³ /s	0.005
Velocity	m/s	-3.3818



(a)



(b)

Fig.5.26 CaCO_3 particle trajectories in case 5 (a) entire furnace (b) in the near burner zone

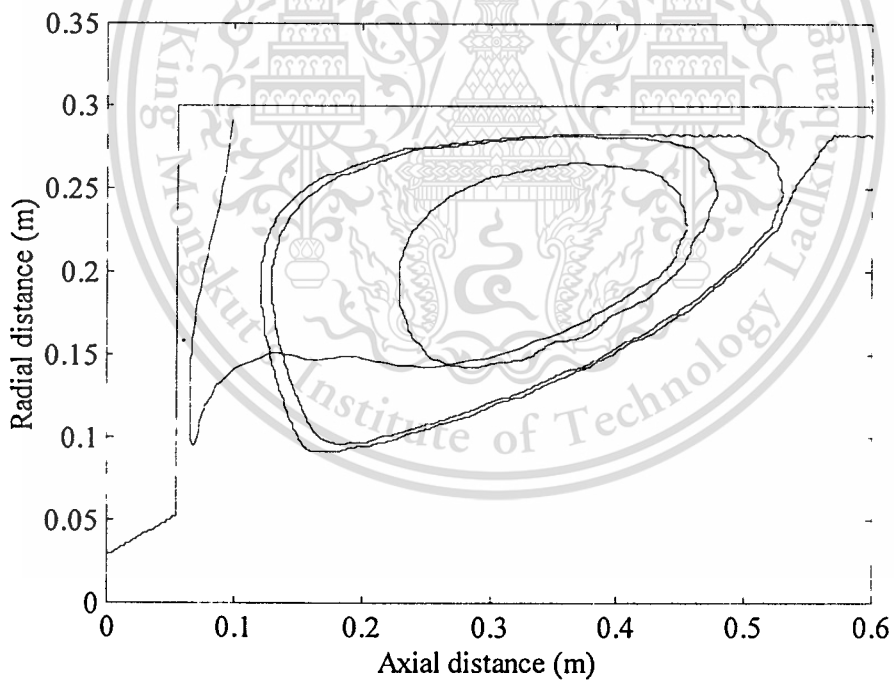
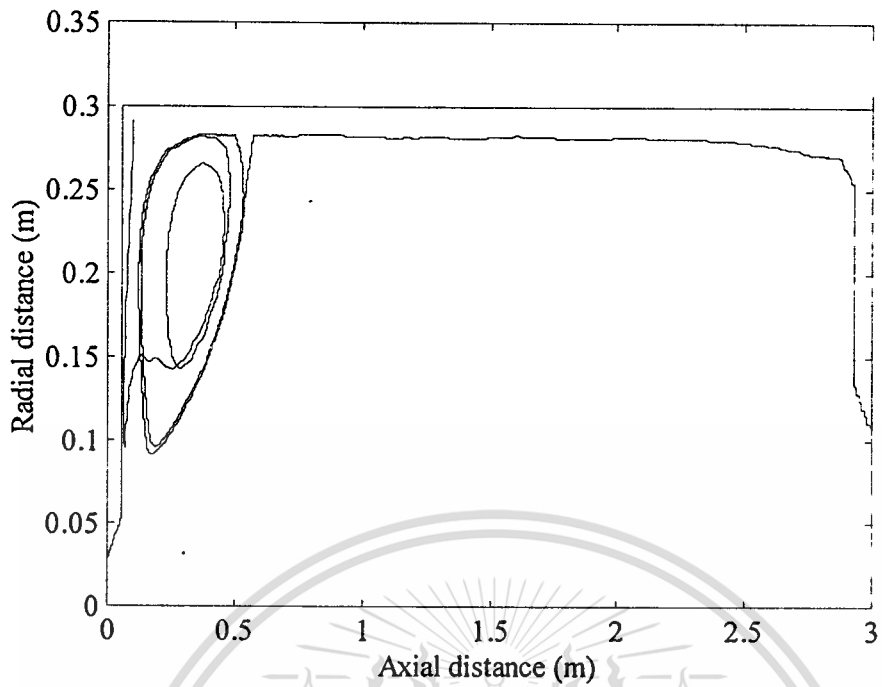


Fig.5.27 CaCO_3 particle trajectories in case 6 (a) entire furnace (b) in the near burner zone

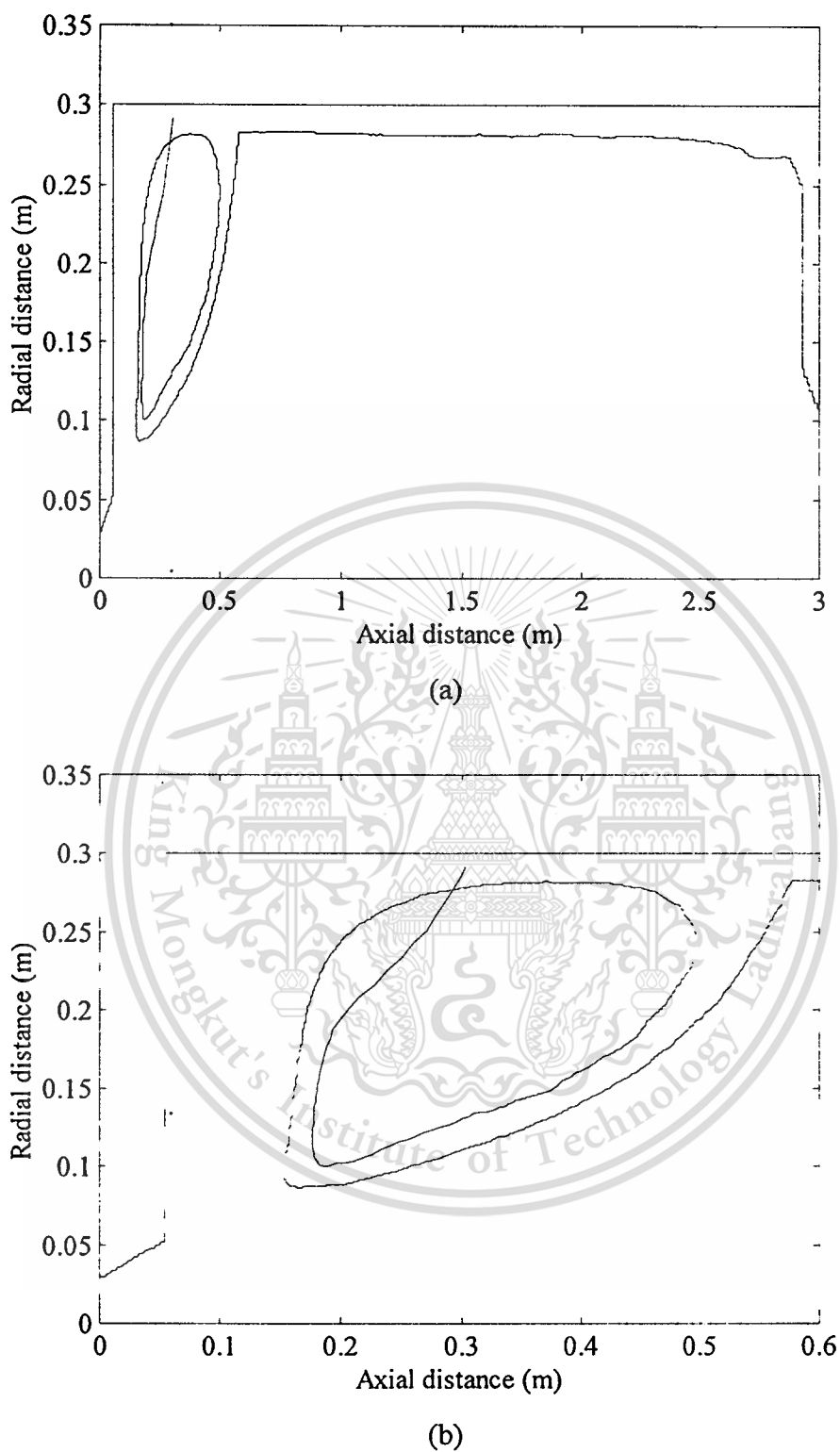
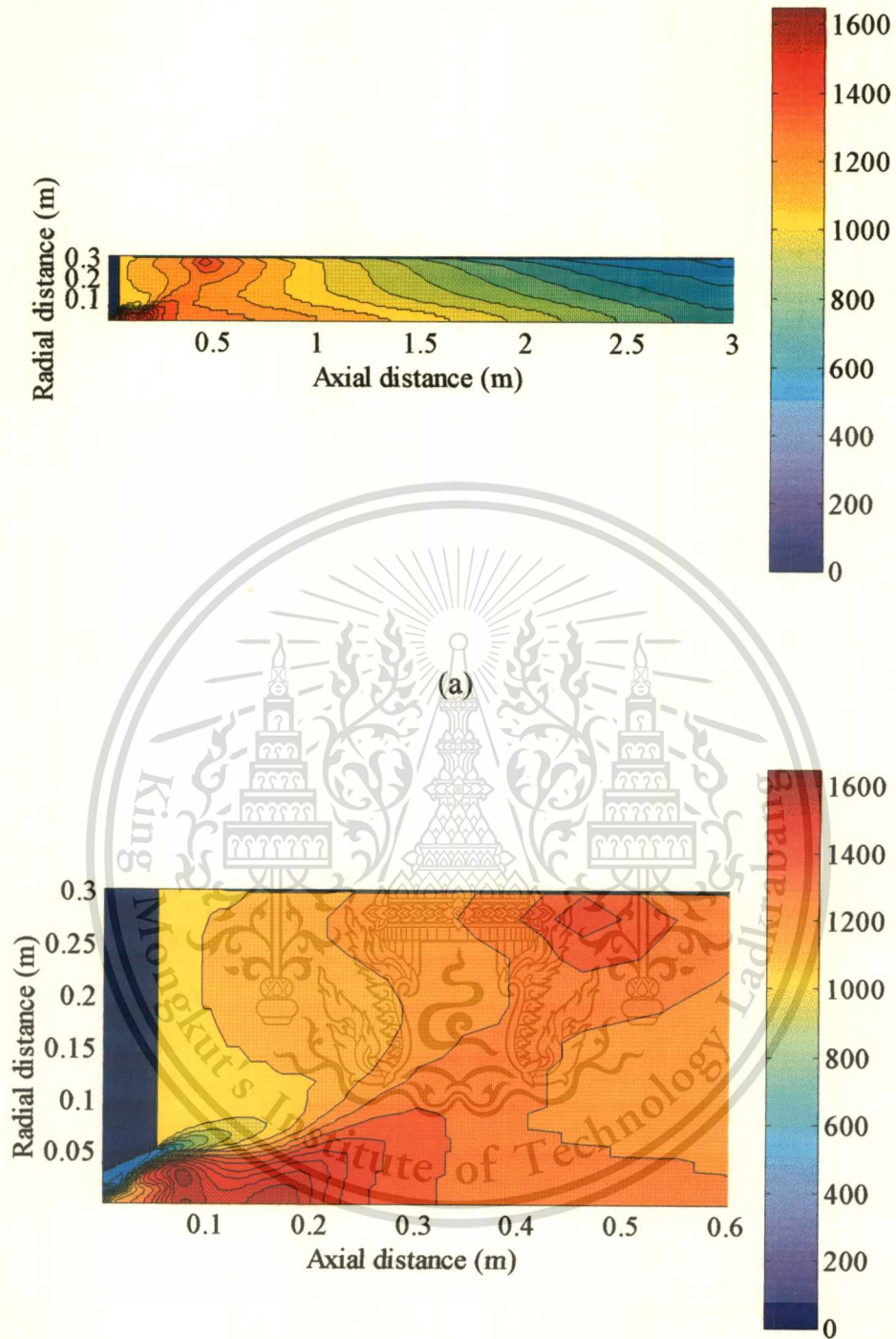
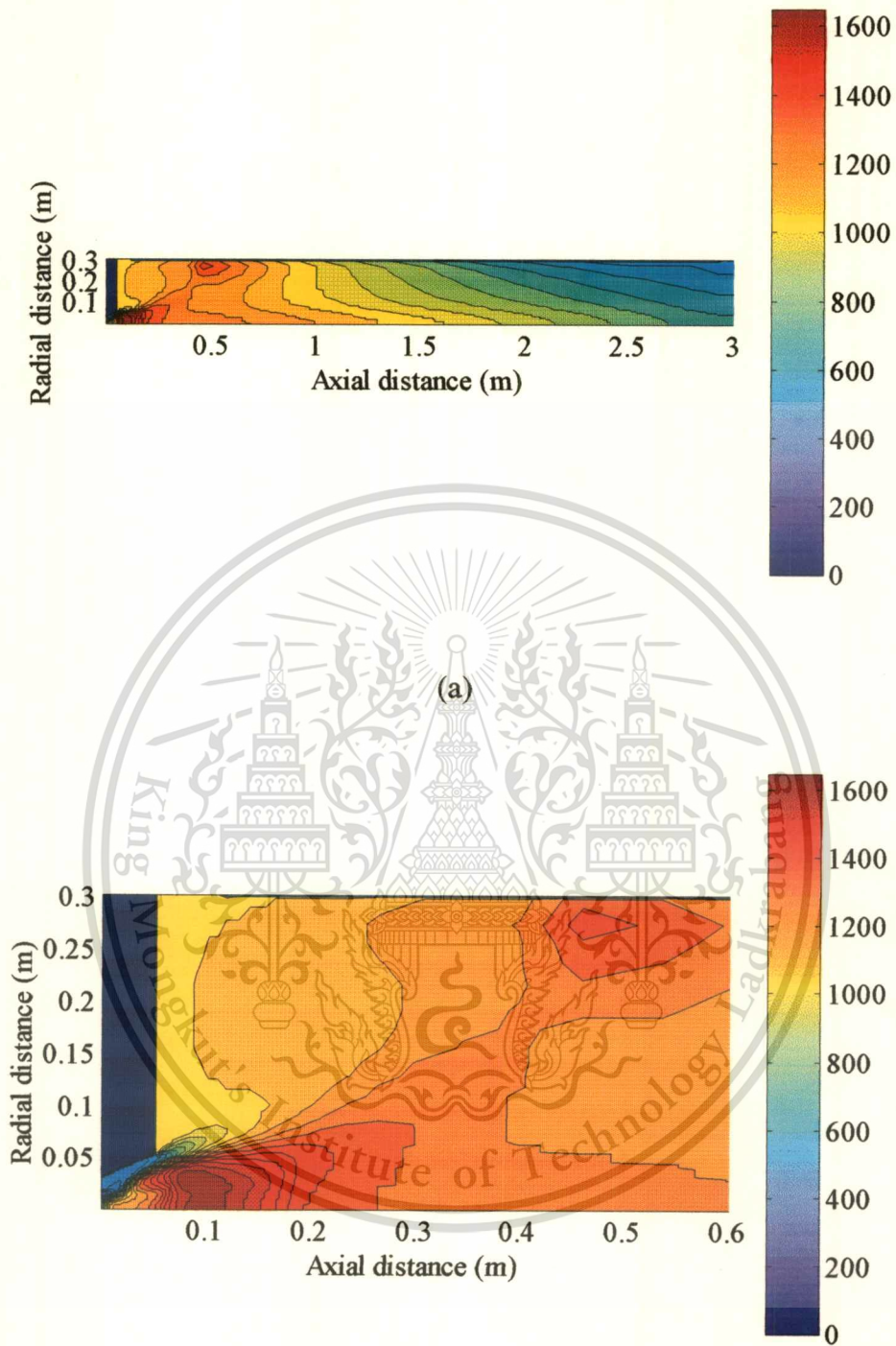


Fig.5.28 CaCO_3 particle trajectories in case 7 (a) entire furnace (b) in the near burner zone



(b)

Fig.5.29 Distribution of temperature (K) in case 5 (a) entire furnace (b) in the near burner zone



(b)

Fig.5.30 Distribution of temperature (K) in case 6 (a) entire furnace (b) in the near burner zone

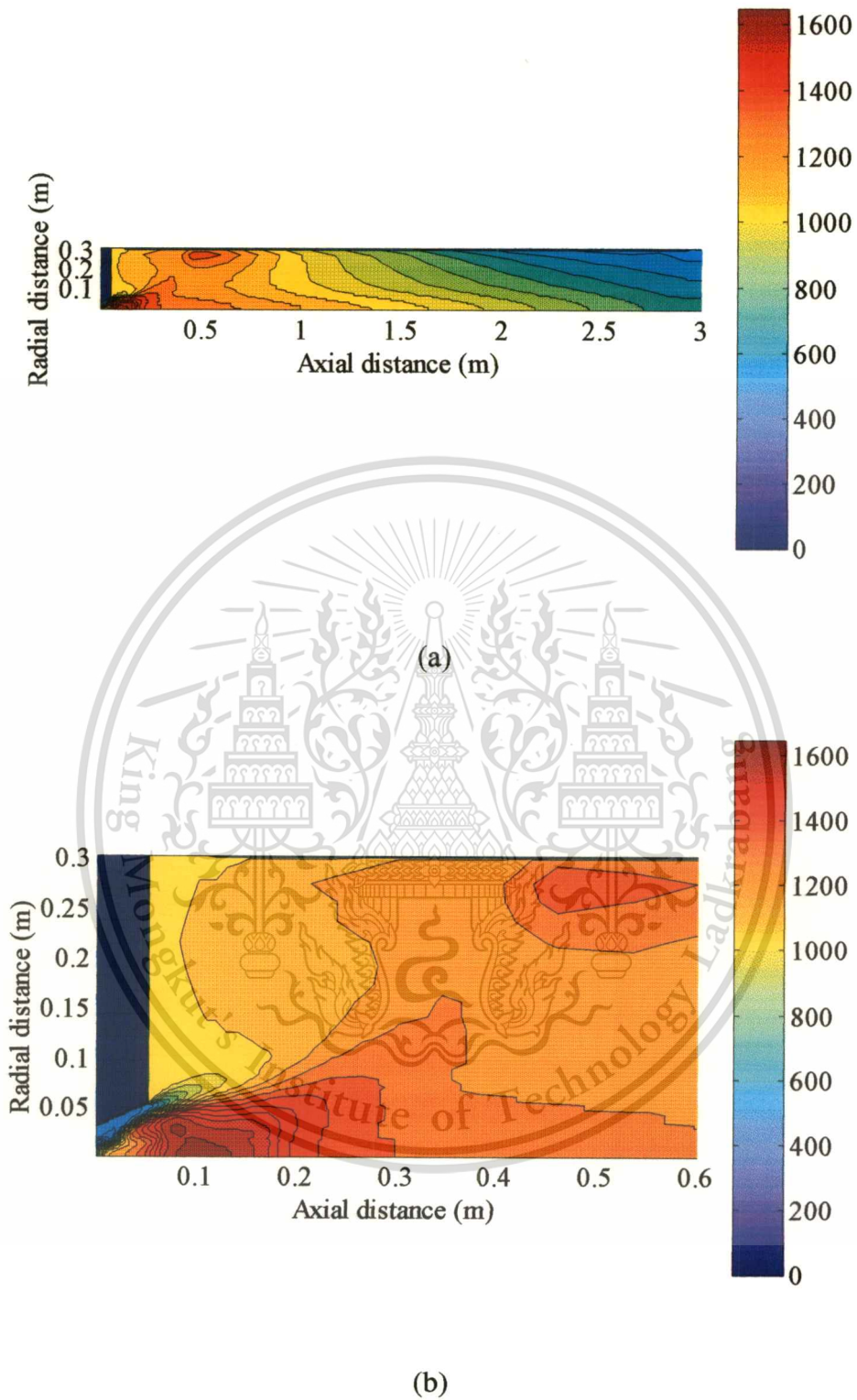


Fig.5.31 Distribution of temperature (K) in case 7 (a) entire furnace (b) in the near burner zone

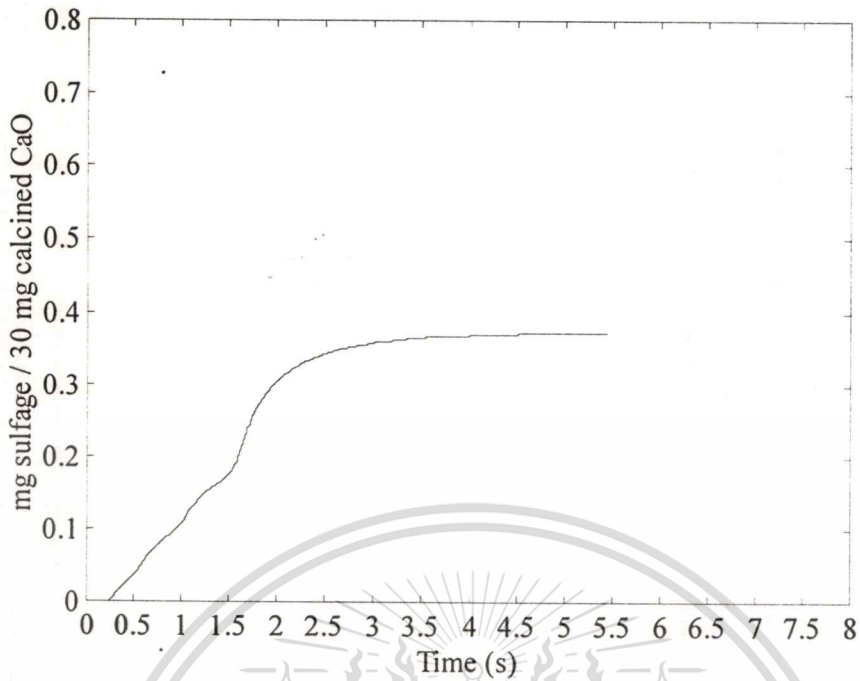


Fig.5.32 Sorption of sulfur dioxide for dolomite 1351 diameter of 0.0096 cm. (case 5)

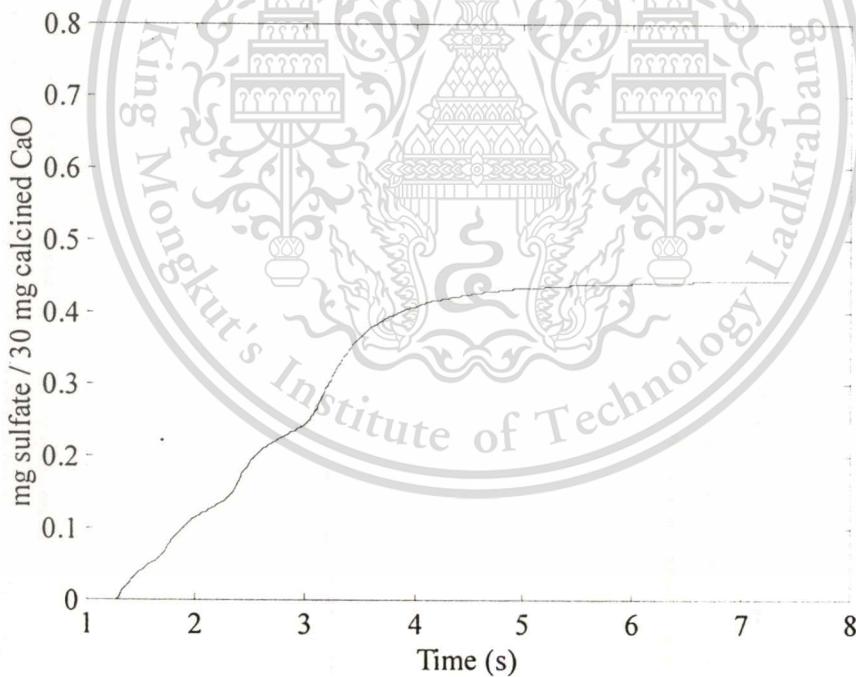


Fig.5.33 Sorption of sulfur dioxide for dolomite 1351 diameter of 0.0096 cm. (case 6)

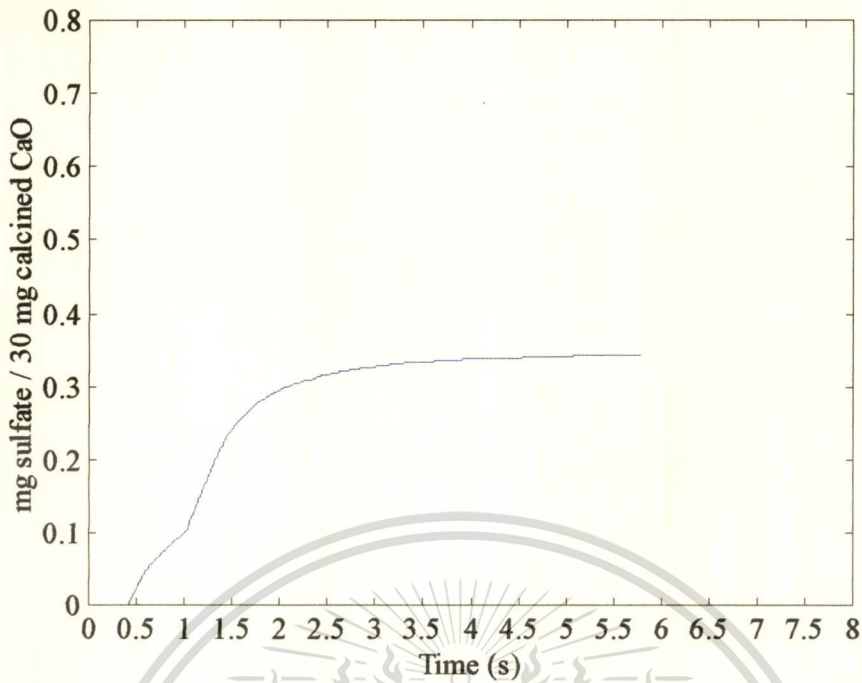


Fig.5.34 Sorption of sulfur dioxide for dolomite 1351 diameter of 0.0096 cm. (case 7)

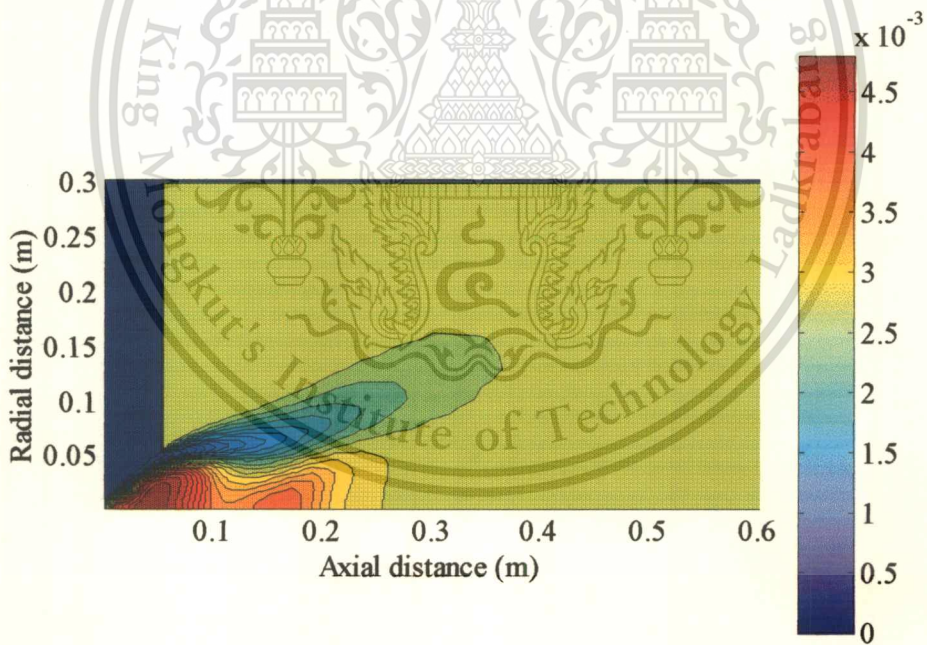


Fig.5.35 Concentration of sulfur oxides, case 5 (in % $m_{SO_2} / m_{mixture}$), in the near burner zone

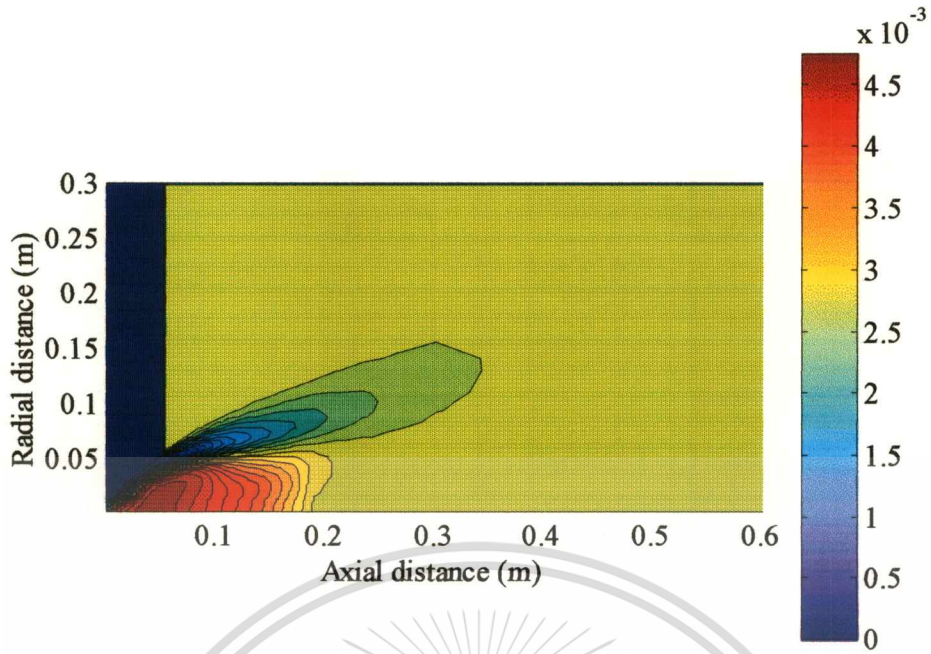


Fig.5.36 Concentration of sulfur oxides, case 6 (in % $m_{SO_2} / m_{mixture}$), in the near burner zone

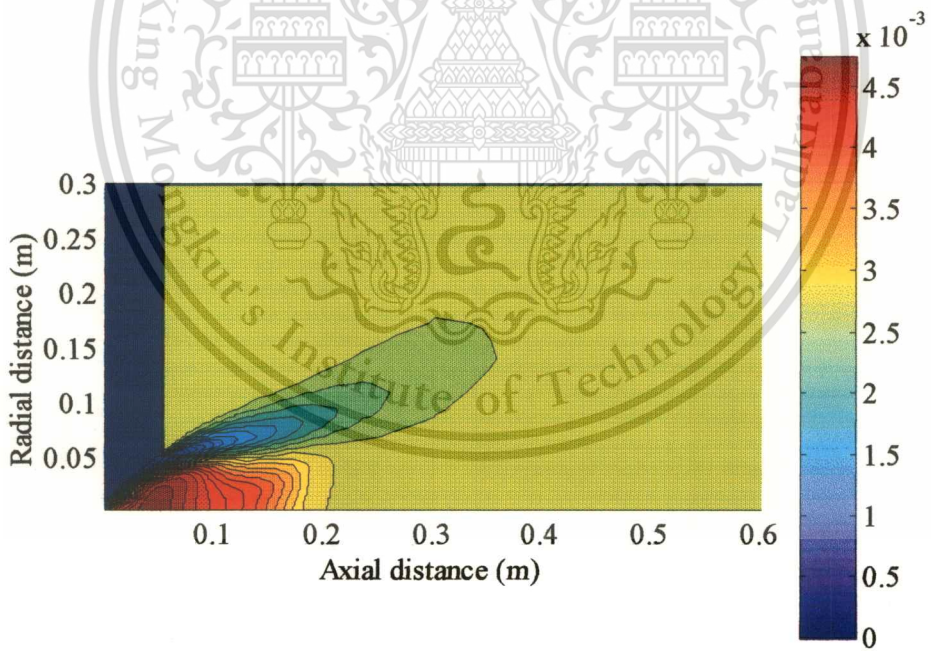


Fig.5.37 Concentration of sulfur oxides, case 7 (in % $m_{SO_2} / m_{mixture}$), in the near burner zone

5.7 Summary

There are 9 case studies performed in this thesis including two base cases. Parametric studies have been carried out involving changing in inlet locations, particle sizes and decreasing in wall temperatures. The results may be concluded as follows:

1. Calcination process rapidly takes place when the particles move through the high temperature zone. The calcination time is not observable in the case of insulated wall where gas temperature is high. In the case under temperature-controlled boundary condition, however, it occupies a time span of 0.5 and up to 1.3 seconds under of gas temperature about 1000 K.
2. The kinetic of sorption is high when the small particles move through the high temperature zone. This is related to the rate constant, which proportionally varies with temperature. However, this mathematical model does not render the effect of chemical instability of SO₂ sorption at temperature above 1300 °C [19], the sorption rate under such condition is therefore higher than the value observed at lower temperature. To overcome unrealistic representation of this model the gas temperature in the furnace is kept under 1300 °C.
3. Apart from the sorption rate, the particle residence time also play an important role on the total amount of SO₂ adsorption. However, the particles no longer adsorb SO₂ after a certain period due to insufficiently low temperature in the far burner region, despite the particles are yet to saturate. The maximum residence time of 8 seconds is observed in case 6 where the particles are injected from top wall, and the accumulative amount is 0.45 mg/mg particles, whereas this figure could be as high as 9 mg/mg particles within 120 second in a bench-top experiment [3].
4. Generally, from Figs. 5.19 – 5.22 and 5.35 – 5.37, less emissions are observed when introducing calcium carbonate particles, but this improvement is insignificant. Moreover, the effects of inlet locations and particle sizes on emission level are also negligible. From these results and the statement given in the above paragraph, reduction of SO₂ emissions rather has strong relationships with the particle residence time and temperature. Changing in inlet locations and particle sizes do not significantly alter such primary factors. It can be concluded that the configuration for pulverized coal combustor and furnace used in this study

This material is reserved for educational use only, not allowed for commercial use.

yields the unfavorable environment for in-situ dry-type desulfurization. More study on furnace configuration in order to lengthen the residence time is required in order to improve the adsorption efficiency.

5. The effect of decreasing temperature at top wall has caused a decrease in gas density in the internal recirculation zone. Such change causes the significant effect in momentum transfer between the gaseous phase and the CaCO_3 particles. As the temperature decreases, CaCO_3 particles seem to have better penetration into the central part of the external recirculation zone, resulting in longer residence time therein. However, due to lower temperature, lower adsorption rate is observed. Such effect has already been discussed above.



CHAPTER 6

CONCLUSIONS AND DISCUSSIONS

Synopses of this thesis and discussions of the further studies are included in this chapter.

6.1 Summary of the preceding chapters

Chapter 1 describes coal utilization in Thailand and objective of this thesis which is an establishment of mathematical model for simulation of SO₂ adsorption by CaCO₃ particles. This model consists of calcination and sulfation processes, which generally included with mathematical model for sulfur oxide formation. A number of terms have been added into the original model to render the effects of temperature, concentration of sulfur dioxide in the surrounding gas, particle sizes and trajectories of particles.

Chapter 2 reviews the desulfurization technologies and the suggestion of previous researchers for establishment of mathematical model, especially Silcox [2] and Borgwardt, [3] which are the main contributors for model of calcination and sulfation processes, respectively.

Chapter 3, the numerical formulations for the simulation of flow aerodynamics, combustion and heat transfer in pulverized fuel combustion systems in the model and those describing the formation of SO₂ are presented.

Chapter 4 the calcination and sulfation models are validated in this chapter. Parametric studies based on the modified equations show that good agreement with the experimental data can be achieved via the adjustments of two empirical parameters for the sulfation model.

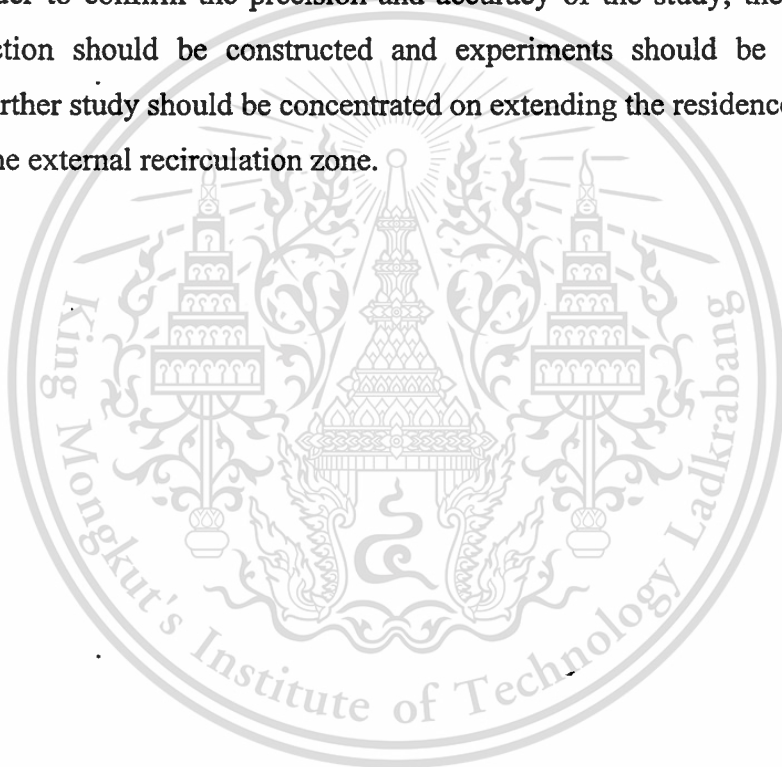
Chapter 5 contains the results and discussions for the SO₂ adsorption. The residence time and temperature surrounding CaCO₃ particles are the primary parameters for adsorption, whereas, the inlet locations and particle sizes of CaCO₃ have less effect.

6.2 Conclusions

The objective of this thesis has been achieved. The adsorption model comprising of calcination and sulfation models for pulverized coal combustion has been established. The results of this model presented in chapter 5 are sensible. The primary parameters for adsorption are residence time and temperature surrounding of CaCO_3 particles. This study is an informative data for further study about the reduction of sulfur dioxide emissions from the pulverized coal combustion.

6.3 Remarks for further studies

In order to confirm the precision and accuracy of the study, the furnace for CaCO_3 injection should be constructed and experiments should be carried out. Moreover, further study should be concentrated on extending the residence time of the particles in the external recirculation zone.

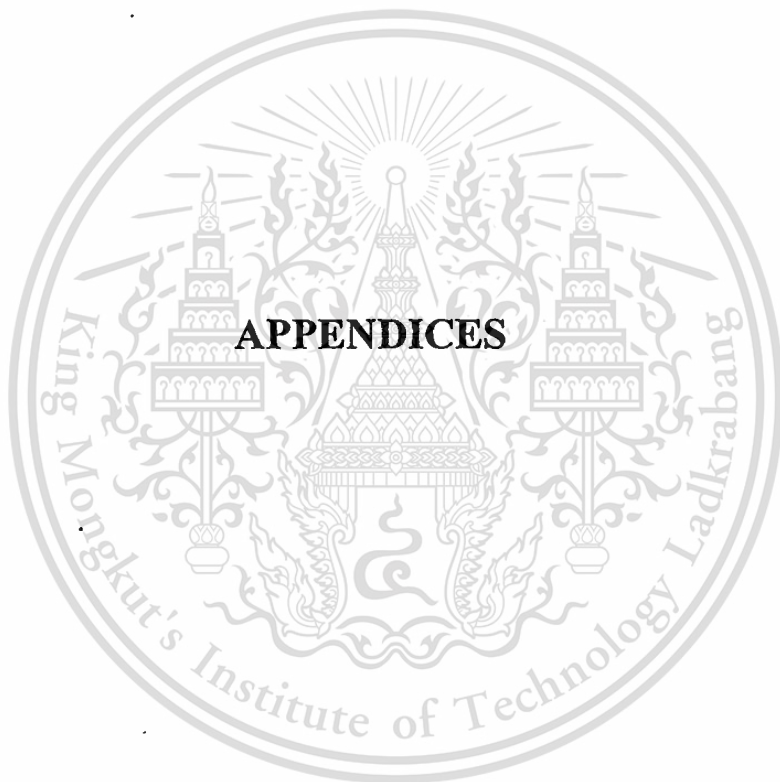


REFERENCES

- [1] Eiichi Y. "Research Survey on Efficient and Environmentally Friendly Coal Utilization Systems in Thailand." Clean Coal Technology Seminar in Thailand. Feb 1999. pp. 1-12.
- [2] Geoffrey D. Silcox. "Mathematical Model for the Flash Calcination of Dispersed CaCO_3 and Ca(OH)_2 Particles." Ind. Eng. Chem. Res, vol. 28, 1999. pp.155-160
- [3] Borgwardt, R.H., "Kinetics of the Reaction of SO_2 with Calcined Limestone." AIChE J, vol. 4, no. 1, Jan. 1970. pp. 59-64.
- [4] Charoensuk J. "The Application of Mathematical Model for Scaling Pulverised Coal Combustors." Ph.D.Thesis of University of London and the Diploma of Membership of the Imperial College. 1996.
- [5] Daungvilailux P. "Mathematical Model of Sulfur Oxide Formation in Pulverised Coal Combustion." Mater of Engineering in Mechanical Engineering School of Graduate Studies King Mongkut's Institute of Technology Ladkrabang. 2000.
- [6] Tetsuo K. "Flue Gas Desulfurization Technology." Clean Coal Technology Seminar in Thailand. Feb 1999. pp. 26-36.
- [7] Magnussen B.F. and Hjertager B.H. "On Mathematical Modeling of Turbulent Combustion with Special Emphasis on Soot Formation and Combustion." Sixteenth Symposium (Int.) on Combustion. The Combustion Institute. 1976. p. 719.
- [8] Salooja A.P. "Mathematical Modeling of and experimental Studies in Axi – Symmetrical Combustors." Ph.D.Thesis of University of London and the Diploma of Membership of the Imperial College. 1979.
- [9] Lockwood F.C., Rizvi S.M.A., Lee F.K. and Whalet K. "Coal Combustion Model Validation Using Cylindrical Furnace Data." Twentieth Symposium (Int.) on Combustion. The Combustion Institute. 1994. p. 513.
- [10] Sloan D.F., Smith P.F., and Smoot L.D. "Modeling of Swirl in Turbulent Flow System." Progress in Energy Combustion Science, vol. 12, 1986. p. 163.
- [11] Romo – Millares C.A. "Mathematical Modeling of Fuel NO Emissions from PF Burners." Ph.D.Thesis of University of London and the Diploma of Membership of the Imperial College. 1992.

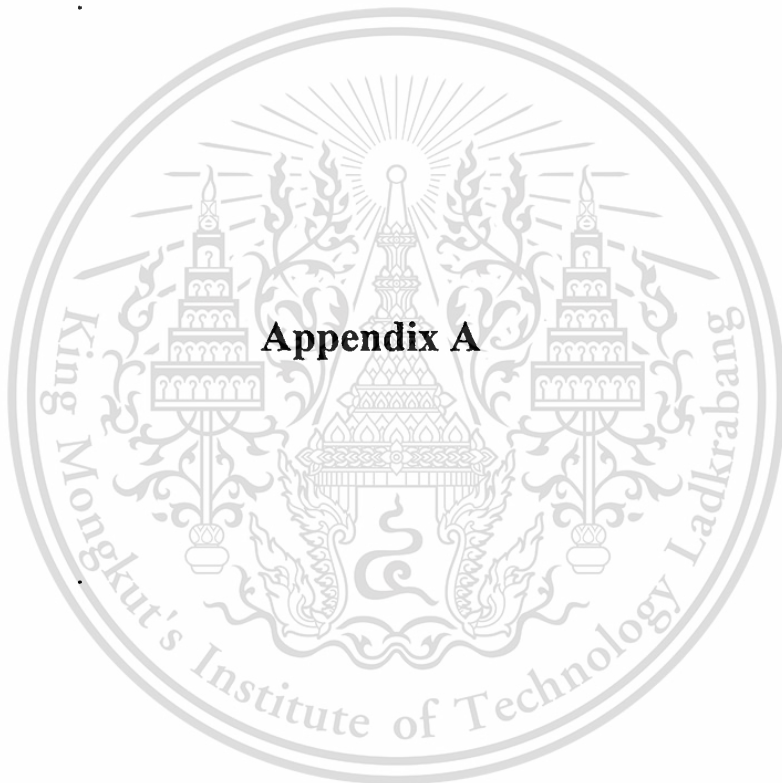
- [12] Lockwood F.C. and Jones W.P. "The Mathematical Modeling of Combustion Chambers." Furnaces and Fires: Prediction of NO emissions from a staged burner. Outline of Lecture notes. Post Experience Course Lectures. Department of Mechanical Engineering. ICSTM. London. 1993.
- [13] Shen B. "The Application of Second – Moment Turbulence Closures to 2D Pulverised –Coal Flames." Ph.D.Thesis of University of London and the Diploma of Membership of the Imperial College. 1994.
- [14] De Soete F.F. Fundamentals of NO Formation and Destruction (Gas phase). Course on combustion of solid fuels. IFRF, Noordwijkerhout, The Netherlands, 1988.
- [15] Alvfors, P. and Svedberg, G. "Modeling of the Sulphation of calcined Limestone and Dolomite – A Gas – Solid Reaction with Structural Changes in the Presence of Inert Solids" Chem. Engng. Sci, vol. 43, no. 5. pp. 1183-1193.
- [16] Borgwardt, R.H. "Calcination Kinetics and Surface Area of Dispersed Limestone Particles." AIChE J, vol. 31, no. 1, Jan. 1985. pp. 103-111.
- [17] Borgwardt, R.H., and Bruce, K.R. "Effect of Specific Surface Area on the Reactivity of CaO with SO₂." AIChE J, vol. 32, no. 2, Feb. 1986. pp. 239-246.
- [18] Zarkanitis, S., and Sotirchos, S. V. "Pore Structure and Particle Size Effects on Limestone Capacity for SO₂ Removal." AIChE J, vol. 35, no, 5, May 1989. pp. 821-830.
- [19] Newton, G. H., Chen, S. L., and Kramlich, J.C. "Role of Porosity Loss in Limiting SO₂ Capture by Calcium Based Sorbents." AIChE J, vol. 35, no. 6, Jun. 1989. pp. 988-994.
- [20] Georgakis, C., C.W. Chang, and J. Szekely. "A Changing GrainSize Model for Gas – Solid Reactions." Chem. Eng. Sci, vol. 34, 1979. p. 1072.
- [21] Lee, D.C., and C. Georgakis. "A Single – Particle Size Model for Sulfur Retention in Fluidized Bed Coal Combustors." AIChE J, vol. 27, 1981. p. 472.
- [22] Hartman, M., and R. W. Coughlin. "Reaction of Sulfur Dioxide with Limestone and the Influence of Pore Structure." Ind. Eng. Chem. Proc. Des. Dev, vol. 13, 1974. p. 248.
- [23] Hartman, M., and R. W. Coughlin. "Reaction of Sulfur Dioxide with Limestone and the Grain Model." AIChE J, vol. 22, 1976. p. 490.

- [24] Hartman, M., and R. W. Coughlin. "Influence of Porosity of Calcium Carbonates on Their Reactivity with Sulfur Dioxide." *Ind. Eng. Chem. Proc. Des. Dev.*, vol. 17, 1978. p. 411.
- [25] Bhatia, S.K., and D.D. Perlmutter. "The Effect of Pore Structure on Fluid – Solid Reactions. I : Application to the SO₂ – lime Reaction." *AIChE J.*, vol. 27, 1981a. p. 226.
- [26] Christman, P.G., and T. F. Edgar. "Distributed Pore – Size Model for Sulfation of Limestone." *AIChE J.*, vol. 29, 1983. p. 388.
- [27] Bardakci, T. "Diffusional Study of the Reaction of Sulfur Dioxide with Reactive Porous Matrices." *Thermochimica Acta*, vol. 76, 1985. p.287.
- [28] Marsh, D.W., and D. L. Ulrichson. "Rate and Diffusional Study of the Reaction of Calcium Oxide with Sulfur Dioxide." *AIChE Ann. Meet.*, Los Angeles, 1982.
- [29] Ramachandran, P.A., and J. M. Smith. "A Single – Pore Model for Gas – Solid Monocatalytic Reactions." *AIChE J.*, vol. 23, 1977. p. 353.
- [30] Simons, G. A. "The Pore Tree Structure of Pore Char." 19th Int. Symp. Combustion, Combustion Institute, 1982.
- [31] Simons, G.a., and Garman, A.R. "Small Pore Closure and the Deactivation of the Limestone Sulfation Reaction." *AIChE J.*, vol. 32, no. 9, Sept. 1986. pp. 1491-1499.
- [32] Sotirchos, S. V., and H. C. Yu. "Mathematical Modeling of Gas – Solid Reactions with Solid Product." *Chem. Eng. Sci.*, vol. 40, no. 11, 1985. pp. 2039-2052.
- [33] Suhas K. Mahuli, Rajeev Agnihotri, Raja Jadhav, Shriniwas Chauk and L. S. Fan. "Combined Calcination, Sintering and Sulfation Model for CaCO₃ – SO₂ Reaction." *AIChE J.*, vol. 45, no. 2, Feb. 1999. pp. 367-382.
- [34] Rizvi S.M.A.. "Prediction of flow, Combustion and Heat Transfer in Pulverised Coal Flames." Ph.D.Thesis of University of London and the Diploma of Membership of the Imperial College. 1985.
- [35] Steven C. and Raymond P. Canale. **Numerical Methods for Engineers.** 2nd Ed. Singapore : McGraw-Hill. 1989.
- [36] Abbas T. "In – frame Measurement of N – Pollutant and Burnout in a Pulverised – Coal – Fired Furnace." Ph.D.Thesis of University of London and the Diploma of Membership of the Imperial College. 1993.



This material is reserved for educational use only, not allowed for commercial use.

Forbidden to modify the content, and cite the document when use.



This material is reserved for educational use only, not allowed for commercial use.

Forbidden to modify the content, and cite the document when use.

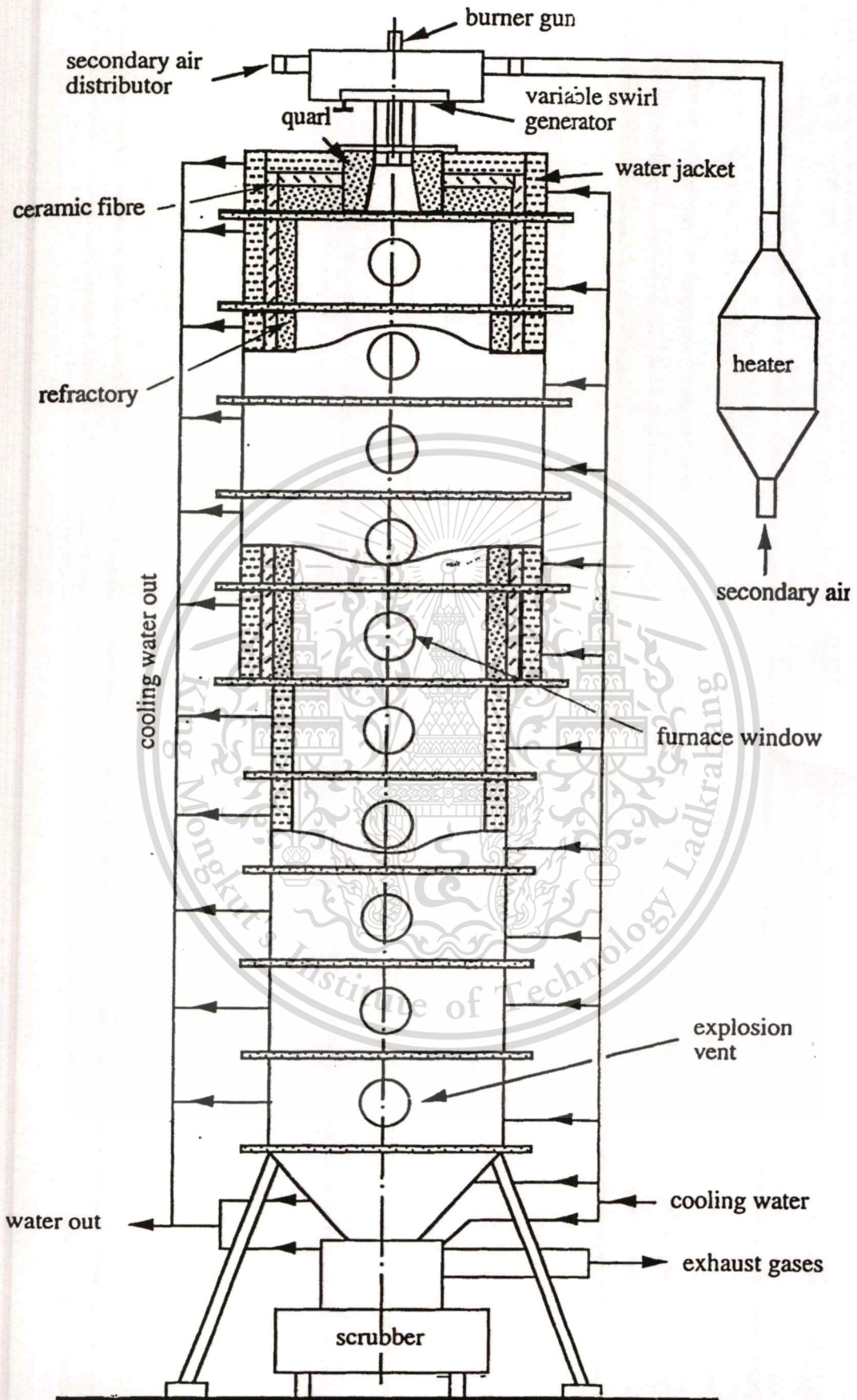


Fig.A-1 Schematic diagram of the ICSTM furnace

This material is reserved for educational use only, not allowed for commercial use.

Forbidden to modify the content, and cite the document when use.

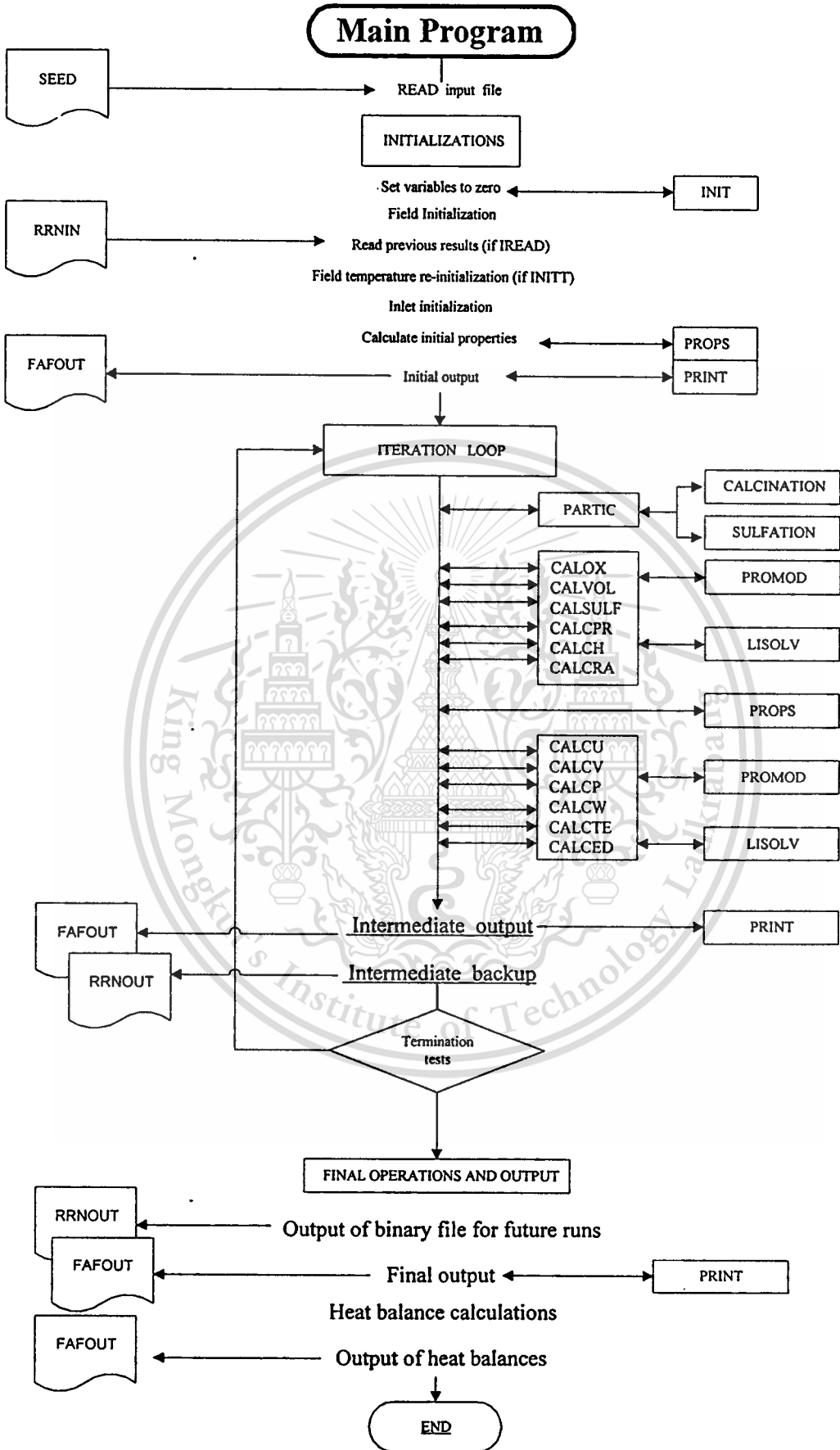


Fig.A-2 Flowchart for FAFNIR and additional calcination and sulfation processes

This material is reserved for educational use only, not allowed for commercial use.

Forbidden to modify the content, and cite the document when use.



This material is reserved for educational use only, not allowed for commercial use.

Forbidden to modify the content, and cite the document when use.

แบบจำลองทางคณิตศาสตร์สำหรับการดูดซับก๊าซซัลเฟอร์ไดออกไซด์ด้วยแคลเซียมออกไซด์

Mathematical Model for Sulfur Dioxide (SO₂) Absorption by Calcine (CaO) Particle

จารุวัตร เจริญสุข, วิชา ศรีสืบสาย

ภาควิชาวิศวกรรมเครื่องกล คณะวิศวกรรมศาสตร์ สถาบันเทคโนโลยีพระจอมเกล้าเจ้าคุณทหารลาดกระบัง

ถ.ฉลองกรุง เขตลาดกระบัง กรุงเทพฯ 10520

โทร 66(2)326-9987, โทรสาร66(2)326-9053, E-Mail: kswipoo@kmitl.ac.th

บทคัดย่อ

บทความนี้เป็นรายงานการศึกษาและกล่าวถึงแบบจำลองทางคณิตศาสตร์สำหรับปฏิกิริยาดูดซับก๊าซซัลเฟอร์ไดออกไซด์ของแคลเซียมออกไซด์ (CaO) ซึ่งเกิดจากการแตกตัวของแคลเซียมคาร์บอเนต ผลการลดปริมาณแก๊ซซัลเฟอร์ไดออกไซด์ด้วยแบบจำลองทางคณิตศาสตร์ที่สร้างขึ้นจะถูกต้องเปรียบเทียบกับข้อมูลที่ได้จากการทดลอง ทั้งยังแสดงถึงผลของการเปลี่ยนแปลงขนาดแคลเซียมออกไซด์ (CaO) ต่อการดูดซับปริมาณแก๊ซซัลเฟอร์ไดออกไซด์สำหรับเทคนิคที่ใช้แก้ปัญหาจะใช้วิธีวิเคราะห์เชิงตัวเลขแบบออยเลอร์ โดยเปรียบเทียบการอัตราการดูดซับก๊าซซัลเฟอร์ไดออกไซด์กับเวลา

Abstract

This paper concerns about a formulation of the semi-empirical mathematical model for sulfur dioxide (SO₂) absorption by Calcine (CaO) particle, dissociated from Calcium Carbonate. Euler's method is utilized for the time-domain solution of the absorption level. The model is able to predict the effect of particle size on SO₂ absorption level. Eventually, the numerical results are in good agreement with the experimental data

1. บทนำ

การพัฒนาทางด้านคอมพิวเตอร์นำไปสู่การสร้างวิธีการหาค่าตอบของสมการคณิตศาสตร์ที่ซับซ้อนด้วยวิธีวิเคราะห์เชิงตัวเลข เช่น การหาค่าตอบของแบบจำลองทางคณิตศาสตร์ของการไหล การเผาไหม้ และการถ่ายเทความร้อน ซึ่งมีประโยชน์อย่างยิ่งสำหรับกระบวนการในการศึกษาห้องเผาไหม้อุตสาหกรรม ค่าตอบที่ถูกคำนวณมาได้จะถูกเปรียบเทียบกับการทดลองเพื่อเป็นข้อมูลสำหรับวิศวกรหรือนักวิจัยเห็นประเด็นความแตกต่างระหว่างข้อสมมติทางทฤษฎี และสิ่งที่เกิดขึ้นจริงในการเผาไหม้ ซึ่งจะช่วยให้สามารถเข้าใจกระบวนการต่าง ๆ ที่เกิดขึ้นได้ดียิ่งขึ้น อย่างไรก็ตามแบบจำลองทางคณิตศาสตร์ยังต้องมีการปรับปรุงเพื่อให้มีประสิทธิภาพที่ดียิ่งขึ้นไป เพื่อให้การคำนวณด้วย

แบบจำลองทางคณิตศาสตร์มีความถูกต้องมากขึ้นเมื่อเทียบกับผลที่ได้จากการทดลอง

ถ่านหินเป็นเชื้อเพลิงที่เกิดจากการทับถมของซากพืชซากสัตว์และมีราคาถูกที่สุดเมื่อเทียบกับก๊าซธรรมชาติและน้ำมัน ถ่านหินถูกใช้เป็นตัวนำแก๊ซซัลเฟอร์ไดออกไซด์มาตั้งแต่อดีตจนถึงปัจจุบัน แต่มันก็มีผลกระทบต่อสิ่งแวดล้อม เช่น ก่อให้เกิดมลพิษทางอากาศ ในหลายปีที่ผ่านมาแบบจำลองทางคณิตศาสตร์ถูกนำมาใช้เพื่อพัฒนาระบบการเผาไหม้ถ่านหิน (Magnussen et al., 1976; Salooja, 1979; Lockwood et al., 1984; Sloan et al., 1986; Romo – Millares, 1992; Lockwood et al., 1993; and Shen., 1994) และเมื่อไม่นานมานี้ผลงานของ Millares (Millares., 1992) ได้รวมกลไกการเกิดและสลายตัวของไนโตรเจนออกไซด์ (De Soete, 1988) เข้าไปในแบบจำลองทางคณิตศาสตร์ของการเผาไหม้ การถ่ายเทความร้อนรวมถึงการปล่อยก๊าซไนโตรเจนออกไซด์จากการเผาไหม้ ก๊าซซัลเฟอร์ไดออกไซด์เป็นผลผลิตอีกชนิดหนึ่งจากการเผาไหม้ถ่านหิน ซึ่งทำให้เกิดการหมักของเขม่า ถึงแม้จะได้มีการพัฒนาแบบจำลองทางคณิตศาสตร์ของปฏิกิริยาดูดซับซัลเฟอร์ไดออกไซด์โดยอนุภาคหินปูนขึ้นมาในอดีต แต่แบบจำลองก็มีความซับซ้อนและมีข้อจำกัดสูงไม่สามารถนำมาใช้รวมกับแบบจำลองของการเผาไหม้ได้ (Sotirchos and Yu 1985) จึงอาจเป็นเหตุผลว่า ก่อนหน้านั้นไม่มีผลงานที่รวมเอากลไกการเกิดและการสลายตัวของก๊าซซัลเฟอร์ไดออกไซด์เข้าไว้ในแบบจำลองทางคณิตศาสตร์ ดังนั้นในการศึกษารังนี้จึงมีจุดประสงค์ที่จะพัฒนาแบบจำลองทางคณิตศาสตร์ที่ง่ายแต่มีความแม่นยำในระดับที่ยอมรับได้เพื่อแสดงการดูดซับก๊าซซัลเฟอร์ไดออกไซด์

จากการศึกษาถึงอัตราการเกิดก๊าซซัลเฟอร์ไดออกไซด์ (A. Levy and E.L. merryman., 1965) แสดงให้เห็นว่าอัตราการเกิดปฏิกิริยาอยู่ในระดับเดียวกันกับปฏิกิริยาการเผาไหม้ ในการเผาไหม้ของถ่านหินในห้องเผาไหม้ที่สารตั้งต้นไม่ได้ผสมกันมาก่อนนั้น เมื่ออุณหภูมิห้องเผาไหม้สูงกว่า 1000 °C อัตราการเกิดปฏิกิริยาจะสูงกว่าอัตราการผสมกัน

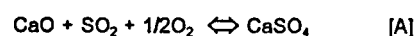
ของสารตั้งต้นทำให้สารตั้งต้นทำปฏิกิริยาอย่างรวดเร็วเมื่อผสมกัน ดังนั้นการผสมกันแบบนี้ปูนจึงมีอิทธิพลต่อปฏิกิริยาทั้งหมด อย่างไรก็ตามปฏิกิริยาของซิลิกาซัลเฟอร์ไดออกไซด์โดยมากจะเกิดขึ้นในช่วงอุณหภูมิที่ต่ำและช่วงเวลานานกว่าหลังการเผาไหม้ มีอยู่หลายวิธีที่จะลดปริมาณก๊าซซัลเฟอร์ไดออกไซด์ เช่นวิธีการกำจัดกำมะถันที่มีคุณภาพต่ำออกไปก่อนที่จะใส่เข้าไปในก้อนเผาไหม้ การผสมด้วยกำมะถันที่มีคุณภาพสูง หรือการแยกองค์ประกอบของกำมะถันด้วยวิธีการล้างหรือวิธีแรงดึงดูดของโลก เป็นต้น มีการทดลองและประสบความสำเร็จในการกำจัดเหล็กซัลไฟด์ (FeS_2) (W.D. Holstead and E. Raask, 1969) แต่ยังไม่สามารถกำจัดพันธะทางเคมีที่เป็นองค์ประกอบของกำมะถันได้ ยังมีวิธีการที่สามารถลดปริมาณก๊าซซัลเฟอร์ไดออกไซด์ได้ในระหว่างหรือหลังการเผาไหม้ เช่นการฉีดตัวดูดซับเข้าไปในเตาเผาในตำแหน่งที่ดูดซับก๊าซซัลเฟอร์ไดออกไซด์ได้ดีที่สุด ตัวดูดซับดังกล่าวที่รู้จักกันดี 2 ชนิดคือ แคลเซียมคาร์บอเนตหรือหินปูน ($CaCO_3$) และแคลเซียมไฮดรอกไซด์ ซึ่งจะมีวิธีการฉีดด้วยกัน 2 วิธีคือแบบแห้งและเปียกเพื่อให้ดูดซับก๊าซซัลเฟอร์ไดออกไซด์ที่ก๊าซไอเสีย ซึ่งการเลือกวิธีทั้ง 2 นี้ก็ขึ้นอยู่กับความต้องการหรืออุปกรณ์ที่ใช้ตามความเหมาะสมและงบประมาณ ในกระบวนการกำจัดก๊าซซัลเฟอร์ไดออกไซด์แบบแห้งจะมีราคาแพงที่สุดแต่การดูดซับก๊าซซัลเฟอร์ไดออกไซด์จะต่ำโดยสามารถลดปริมาณซัลเฟอร์ได้เพียง 50 % (Tetsuo KAWAMURA, 1999) เนื่องจากเวลาที่อยู่ในเตาเผาสั้น ฉะนั้นการเพิ่มประสิทธิภาพการดูดซับก๊าซซัลเฟอร์ไดออกไซด์จึงเป็นหัวข้อที่น่าสนใจในการท้าววิจัยเพื่อการพัฒนา

แคลเซียมคาร์บอเนตหรือหินปูน ($CaCO_3$) เมื่อใส่เข้าไปในที่อุณหภูมิสูงจะแตกตัวเป็นอนุภาคของแคลเซียมออกไซด์ที่มีรูพรุน (CaO) และปลดปล่อยก๊าซคาร์บอนไดออกไซด์อย่างรวดเร็ว จากนั้นจะจับตัวกับก๊าซซัลเฟอร์ไดออกไซด์และโมเลกุลของออกซิเจนกลายเป็นแคลเซียมซัลเฟต ($CaSO_4$) อัตราความร้อนที่สูงจากเตาเผาจะทำให้เกิดแคลเซียมออกไซด์ซึ่งมีพื้นที่จำเพาะสูงถึง 90 ตารางเมตรต่อกรัม (Borgwardt, R.H., 1985) ในการดูดซับก๊าซซัลเฟอร์ไดออกไซด์ของแคลเซียมคาร์บอเนตเมื่อเปลี่ยนเป็นแคลเซียมออกไซด์แม้ว่าจะมีประสิทธิภาพต่ำกว่าการดูดซับของแคลเซียมไฮดรอกไซด์ ($Ca(OH)_2$) (Bruce et al., 1989) แต่ก็ยังใช้กันอย่างกว้างขวางเนื่องจากง่ายต่อการใช้งาน การศึกษาด้วยวิธีการทดลองอันหนึ่งของ Zarkaniitis, S. และ Sotirchos S.V. ให้เห็นว่าอนุภาคจะมีช่องว่างสำหรับดูดซับก๊าซซัลเฟอร์ไดออกไซด์และสิ่งนี้จะสัมพันธ์กับการกระจายตัวของขนาดรูพรุนของอนุภาคและความสามารถในการส่งถ่ายมวลภายในอนุภาค ซึ่งสรุปไว้ว่าการกระจายตัวของขนาดและรูพรุนซึ่งติดต่อกันและกันเป็นปัจจัยสำคัญในการดูดซับแคลเซียม มากกว่าปัจจัยในแง่ความพรุนของอนุภาค ผลของการดูดซับก๊าซซัลเฟอร์ไดออกไซด์ต่อเวลาจะลดลงเมื่อขนาดของอนุภาคใหญ่ขึ้นในขณะที่อุณหภูมิการเกิดแคลเซียมออกไซด์สูงขึ้นและอุณหภูมิการเกิดก๊าซซัลเฟอร์ไดออกไซด์สูงขึ้น โดยสามารถอธิบายได้ในรูปของการแพร่ที่ถูกจำกัดด้วยการดูดซับของรูพรุนที่ผิวด้านนอก การศึกษานี้ยังแสดงให้เห็นว่าอุณหภูมิในช่วง 750 – 850 °C ซึ่งเป็นช่วงที่ดีที่สุดของการดูดซับก๊าซซัลเฟอร์ไดออกไซด์ ซึ่งอุณหภูมิจะต่ำกว่าบริเวณที่มีการเผาไหม้ (1000 °C)

โครงสร้างของรูพรุนนั้นจะเปลี่ยนไปเมื่อเกิดปฏิกิริยากับก๊าซซัลเฟอร์ไดออกไซด์ Newton et al., 1989 กล่าวไว้ว่าอุณหภูมิเป็นตัวแปรที่ก่อให้เกิดการลดลงของความพรุนของแคลเซียมออกไซด์เนื่องจากคาร์บอนไดออกไซด์ทำให้เกิดผลึกในช่วงอุณหภูมิสูงประมาณ 900 – 1300 °C ในเวลาอันสั้น (< 1 วินาที) ระหว่างดูดซับก๊าซซัลเฟอร์ไดออกไซด์ ในกระบวนการนี้ (ประมาณ 970 °C) ผลึกเล็ก ๆ จำนวนมากในอนุภาคแคลเซียมออกไซด์จะรวมตัวกันเป็นผลึกที่มีขนาดใหญ่ขึ้นซึ่งจะมีจำนวนลดลง ซึ่งมีผลต่อการลดลงของพื้นที่ผิวจำเพาะและการลดลงของอัตราการดูดซับ ผลดังกล่าวเป็นไปในแนวทางเดียวกันกับผลของ Borgwardt และ Bruce ในปี 1986 ซึ่งได้แสดงความสัมพันธ์ระหว่างพื้นที่ผิวจำเพาะและอัตราการเกิดแคลเซียมซัลเฟต ($CaSO_4$) ในปี 1970 Borgwardt แสดงให้เห็นถึงการลดลงของก๊าซซัลเฟอร์ไดออกไซด์และการเพิ่มขึ้นของการดูดซับก๊าซซัลเฟอร์ไดออกไซด์ซึ่งสัมพันธ์กันแบบเอ็กโปเนนเชียล ในแบบจำลองเชิงการทดลองส่วนมากจะบรรยายถึงกระบวนการดูดซับของรูพรุนที่ผิวด้านนอกเนื่องจากการแพร่ก๊าซซัลเฟอร์ไดออกไซด์ผ่านรูของแคลเซียมออกไซด์ (Georgakis et al., 1979; Lee and Goergakis, 1981; Hartman and Coughlin, 1974, 1976, 1978; Bhatia and Perlmutter, 1981; Christman and Edgar, 1983; Bardakci, 1984, Marsh and Uirichson, 1982 and Ramachandran and Smith, 1977.) หลังจากนั้น Simons, 1982; Simons and German, 1986 พบว่าการเกิดการดูดซับที่รูพรุนของอนุภาคจะลดปริมาณการแพร่ซึ่งทำให้เกิดปฏิกิริยาได้น้อยลง ก๊าซซัลเฟอร์ไดออกไซด์จะถูกดูดซับได้ระหว่างช่วงอุณหภูมิ 900 °C ถึง 1300 °C เนื่องมาจากการแพร่และจลนพลศาสตร์เคมีของพันธะเคมีเกิดขึ้นน้อยที่อุณหภูมิต่ำกว่า 900 °C ในขณะที่จะเกิดความไม่เสถียรของการเกิดปฏิกิริยาขึ้นที่อุณหภูมิสูงกว่า 1300 °C (Cole et al., 1987; Newton, 1987) การศึกษาของ Sotirchos and Yu 1985 ได้พัฒนาแบบจำลองโครงสร้างของรูพรุนแบบสุ่มรวมเข้ากับแบบจำลองการเกิดปฏิกิริยาเพื่อจะจำลองการเกิดปฏิกิริยาของของแข็งและก๊าซ ซึ่งได้จำลองการดูดซับก๊าซซัลเฟอร์ไดออกไซด์ที่มีความเข้มข้น 0.3 % โดยปริมาตรด้วยแคลเซียมที่อุณหภูมิ 850 °C และได้มาเปรียบเทียบกับผลการทดลองของ Cole et al., 1987; Newton, 1987 เป็นที่น่าสังเกตว่าอุณหภูมิที่ใช้จะต่ำกว่าอุณหภูมิที่ได้มีการแนะนำไว้ในบทความของ Cole et al., 1987; Newton, 1987 ได้มีการเปรียบเทียบผลที่ได้จากการคำนวณกับผลที่ได้จากการทดลองไว้ในรายงานนั้นเช่นกัน

2. แบบจำลองทางคณิตศาสตร์สำหรับการดูดซับก๊าซซัลเฟอร์ไดออกไซด์

ปฏิกิริยาเคมีระหว่างแคลเซียมออกไซด์และซัลเฟอร์ไดออกไซด์ แสดงได้ดังสมการสมดุลเคมีดังนี้



โดยที่อัตราการเกิดปฏิกิริยา (r) (Borgwardt, R.H., 1970) คือ

$$r = \frac{1}{w} \frac{dn'}{dt} = \frac{\eta}{\rho} k_p c^m \quad [1]$$

ในหน่วยของกรัมโมลต่อกรัมของแคลเซียมออกไซด์ต่อวินาที และ w คือน้ำหนักของอนุภาค C และ m เป็นลำดับความเข้มข้นของก๊าซซัลเฟอร์ไดออกไซด์และลำดับของปฏิกิริยา ตามลำดับ k , เป็นอัตราคงที่ ซึ่งเป็นฟังก์ชันของอุณหภูมิ อธิบายด้วยสมการของ Arrhenius

$$k_v = Ae^{-E/RT} \quad [2]$$

ตารางที่ 1 ค่าพลังงานกระตุ้น, อัตราการเกิดปฏิกิริยาและ frequency factor ของหิน dolomite, Borgwardt, R.H., 1970.

Stone	Activation energy, E, cal./g. mole	Reaction rate constant, K_v , sec. ⁻¹	Frequency factor, A, sec. ⁻¹
1337	10,000	4.8×10^3	2.4×10^5
1351	18,100	7.2×10^3	9.0×10^6
1343	14,200	4.0×10^3	1.1×10^6
1360	8,100	2.3×10^3	5.5×10^4

โดยที่ T_{ref} เป็นอุณหภูมิอ้างอิงที่ 1143 K (870 °C) สมการข้างต้นจะเหมือนกับสมการที่ 7 เมื่ออุณหภูมิเท่ากับอุณหภูมิอ้างอิง นอกไปจากนี้การเพิ่มขึ้นของอัตราการเกิดปฏิกิริยาขึ้นอยู่กับเพิ่มขึ้นของก๊าซซัลเฟอร์ไดออกไซด์ ซึ่งจะได้

$$r = r_0 e^{-\beta \frac{n'}{w}} e^{(-E/RT) + (E/R_{ref})} \frac{C^m}{C_{ref}^m} \quad [10]$$

เมื่อ C_{ref} เป็นความเข้มข้นของก๊าซซัลเฟอร์ไดออกไซด์ 2.9×10^{-3} กรัมโมลต่อลูกบาศก์เซนติเมตร ค่า r_0 ของแคลเซียมออกไซด์แต่ละชนิดได้มาจากการประมาณค่าแบบเชิงเส้นตรงของการเกิดปฏิกิริยาที่มีความเข้มข้นของซัลเฟต 1×10^{-3} กรัมโมลต่อกรัม เป็นไปตามสมการ

$$\ln r_0 = \ln r_{1 \times 10^{-3}} - \beta(1 \times 10^{-3}) \quad [11]$$

β ได้มาจากที่กล่าวไว้ข้างต้นซึ่งรู้อัตราการเกิดปฏิกิริยาที่ 1×10^{-3} และ 2×10^{-3} ซึ่งได้จากการทดลอง (Borgwardt, 1970) โดยแสดงไว้ดังตารางที่ 2 และ 3

$$\beta = \frac{\ln r_{2 \times 10^{-3}} - \ln r_{1 \times 10^{-3}}}{2 \times 10^{-3} - 1 \times 10^{-3}} \quad [12]$$

η เป็นตัวแปรที่ใช้ให้เห็นถึงการลดลงของอัตราการดูดซับเนื่องจากก๊าซซัลเฟอร์ไดออกไซด์ โดยตัวแปรนี้สัมพันธ์กับ $\frac{n'}{w}$ ตามสมการ

$$\ln \eta \frac{Ac^m}{\rho} - \frac{E}{RT} = -\beta \frac{n'}{w} + \ln r_0 \quad [3]$$

β เป็นตัวแปรที่ได้จากการทดลอง n' เป็นอนุภาคของซัลไฟด์ในหน่วยกรัมโมล r_0 เป็นการเกิดปฏิกิริยาในสภาวะเริ่มต้น (ไม่มีซัลเฟต) ดังสมการ

$$r_0 = \eta_0 \frac{A_0 c^m}{\rho_0} e^{-E/RT} \quad [4]$$

จากสมการ 3 และ 4 จะได้

$$A = \frac{\eta_0 \rho}{\eta \rho_0} A_0 e^{-\beta \frac{n'}{w}} \quad [5]$$

จากสมการที่ 2, 4 และ 5 จะได้

$$r = \frac{\eta \rho}{\rho \rho_0} r_0 \frac{\rho_0 e^{E/RT}}{\eta_0 c^m} \eta_0 e^{-\beta \frac{n'}{w}} e^{-E/RT} C^m \quad [6]$$

ดังนั้น $r = r_0 e^{-\beta \frac{n'}{w}} \quad [7]$

สมการที่ 7 แสดงให้เห็นว่าอัตราการเกิดปฏิกิริยาเป็นฟังก์ชันตัวแปรไม่กี่ตัวซึ่งไม่สัมพันธ์กับการสังเกตจากการทดลอง จากข้อมูลเมื่อมีปริมาณซัลเฟต 1×10^{-3} กรัมโมลต่อกรัม ผู้ศึกษาได้แสดงให้เห็นถึงความสัมพันธ์แบบเชิงเส้นตรงระหว่าง $\ln(r)$ และส่วนกลับของอุณหภูมิ $1/T$ (K⁻¹) ดังนั้นสมการที่ 7 จะถูกเปลี่ยนเป็น

$$r = r_0 e^{-\beta \frac{n'}{w}} e^{\frac{-E}{RT} + c_0} \quad [8]$$

$$c_0 = \frac{E}{RT_{ref}} \quad [9]$$

ตารางที่ 2 ผลของอนุภาคกับอัตราการเกิดปฏิกิริยาสภาวะ sulfate loading ที่ 2×10^{-3} g mole/g, 870 °C.

Stones	Reaction rate (g mole/g sec) X 10 ⁵		
	D _s 0.0096 cm.	D _p 0.025 cm.	D _p 0.13 cm.
1337	4.2	3.2	1.4
1351	3.2	2.1	1.3
1343	2.1	1.4	0.7
1360	2.5	1.8	1.1

ตารางที่ 3 ค่าที่ได้จากการทดลองของอัตราการเกิดปฏิกิริยาที่อุณหภูมิ 870 °C สภาวะ sulfate loading ที่ 1×10^{-3} g mole/g ของอนุภาคขนาด 0.0096 ซม.(150/170-mesh particle size).

Stones	Reaction rate (g mole/g sec) X 10 ⁵
1337	6.4
1351	5.9
1343	3.6
1360	3.1

จากความสัมพันธ์ข้างต้นตัวอย่างของกราฟสำหรับอนุภาคของแคลเซียมออกไซด์ 1337 แสดงไว้ดังรูปที่ 1 ค่าของ r_0 และ β ของอนุภาคแคลเซียมออกไซด์แต่ละชนิดได้มาในทำนองเดียวกัน โดยสรุปไว้ในตารางที่ 4

ตารางที่ 4 อัตราการเกิดปฏิกิริยาที่ภาวะไม่มีซัลเฟอร์ (Zero sulfation)

Type	lnr ₀	β		
		0.0096cm.	0.025cm.	0.13cm.
1337	-9.24	-420	-550	-970
1351	-8.97	-690	-900	-1140
1343	-9.69	-540	-740	-1090
1360	-10.16	-220	-385	-630

สมการที่ 3 สามารถเขียนได้เป็น

$$\ln \eta_0^* \eta A \frac{c^m}{\rho} - \frac{E}{RT} = -\beta \frac{n'}{w} + \ln r_0 \quad [13]$$

หรือ

$$\ln \eta_0^* + \ln \eta A \frac{c^m}{\rho} - \frac{E}{RT} = -\beta \frac{n'}{w} + \ln r_0 \quad [14]$$

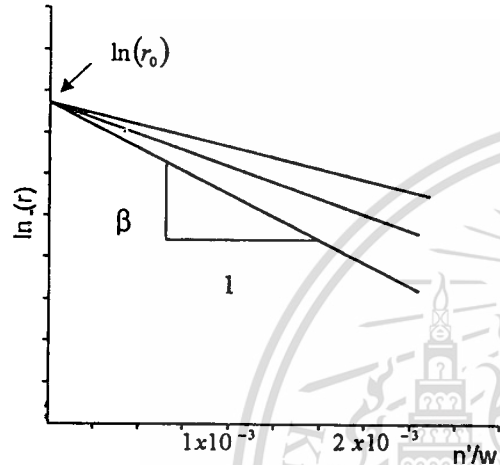
หรือ

$$\ln \eta A \frac{c^m}{\rho} - \frac{E}{RT} = -\beta \frac{n'}{w} + \ln \left(\frac{r_0}{\eta_0^*} \right) \quad [15]$$

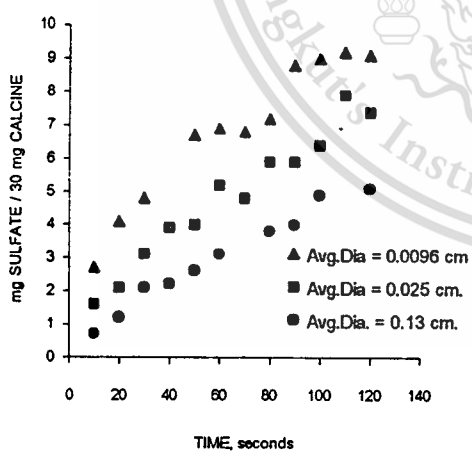
ทุกเทอมยกเว้นสมการที่ 15 ทางด้านขวามือจะเหมือนกันสมการที่ 3 ดังนั้นสมการเชิงเส้นตรงระหว่าง ln(r) และ 1/r ยังคงอยู่ ค่าของ η₀^{*} แสดงถึงการแพร่ที่ภาวะเริ่มต้นซึ่งต่างจาก η ซึ่งแสดงถึงประสิทธิภาพของอัตราการเกิดปฏิกิริยาตลอดช่วงเวลา ค่า η₀^{*} นี้จะคงที่สำหรับอนุภาคแต่ละชนิดแต่ η จะลดลงเรื่อยๆ เนื่องจากการเกิดซัลเฟตในอนุภาค สำหรับสมการในรูปทั่วไปของ β อาจเขียนได้ดังนี้

$$\beta = \frac{\ln r_{2 \times 10^{-3}} - \ln \left(\frac{r_0}{\eta_0^*} \right)_{0.0}}{2 \times 10^{-3}} \quad [16]$$

r₀ เป็นอัตราการเกิดปฏิกิริยาที่สภาวะเริ่มต้น ตัวแปรนี้สะท้อนให้เห็นถึงอัตราการเกิดปฏิกิริยาโดยรวม [A] โดยปราศจากผลของการแพร่และการอุดตันภายในอนุภาค ซึ่งได้ให้ไว้ในตารางที่ 4 ในรูปของค่า β ดังรูปที่ 3

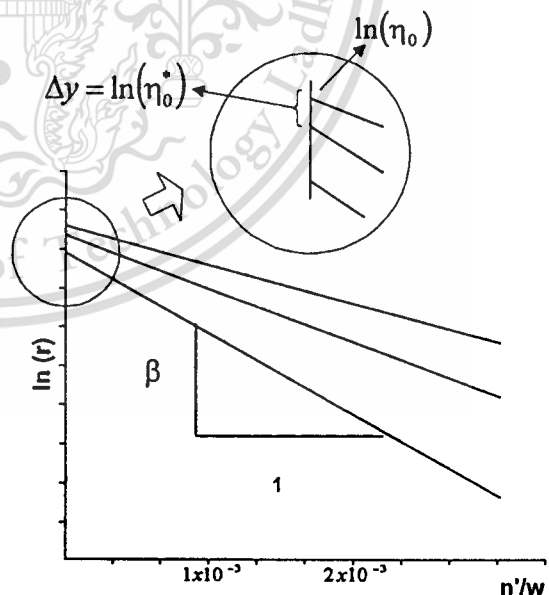


รูปที่ 1 ความสัมพันธ์ของ sulfation load กับอัตราการเกิดปฏิกิริยา รวมทั้งการหาค่า r₀ และ β



รูปที่ 2 การดูดซับของซัลเฟอร์ไดออกไซด์ที่ขนาดของอนุภาคชนิด 1351 ต่าง ๆ กัน, Borgwardt, R.H., 1970.

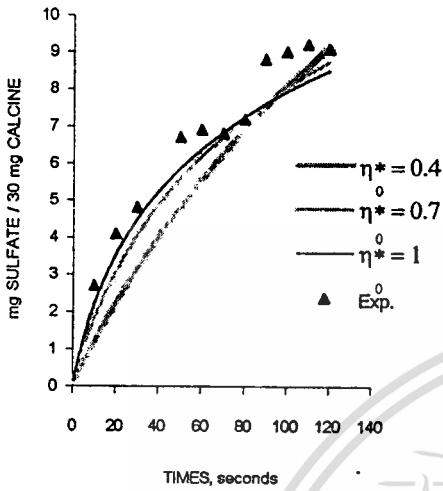
ผลจากการทดลองดังรูปที่ 2 พบว่าการดูดซับก๊าซซัลเฟอร์ไดออกไซด์ต่อหน่วยมวลของอนุภาคที่มีขนาดเล็กกว่าจะดูดซับได้ดีกว่าอนุภาคที่มีขนาดใหญ่ซึ่งสังเกตได้อย่างชัดเจนในตอนเริ่มของการเกิดปฏิกิริยา ซึ่งเกิดขึ้นเนื่องจาก รูพรุนของอนุภาคตอนเริ่มต้นมีมากกว่าอนุภาคที่มีขนาดใหญ่



รูปที่ 3 ผลของ η₀^{*} ต่ออัตราการเกิดปฏิกิริยาที่ Sulfation loading ต่าง ๆ

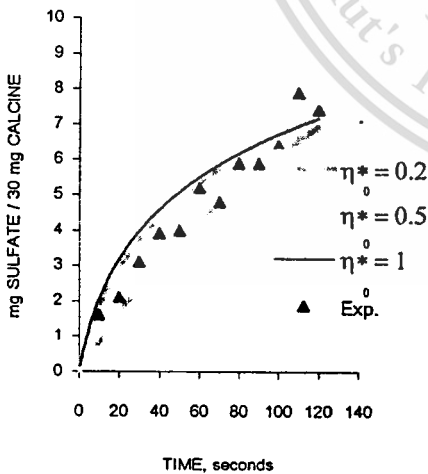
รูปที่ 4 แสดงผลของการแพร่ในช่วงการดูดซับก๊าซซัลเฟอร์ไดออกไซด์ ด้วยการเปลี่ยนค่า η₀^{*} จาก 1 (ตอนภาวะเริ่มต้น) ลดลงถึง 0.1

สำหรับแคลเซียมออกไซด์ต่างๆ กัน ข้อมูลที่ได้จากการทดลองถูกนำมาเปรียบเทียบกับผลการคำนวณ จากสมการที่ 10 ด้วยพลังงานการกระตุ้นจากตารางที่ 1 r_0 และ β จากตารางที่ 4



รูปที่ 4 ผลของความต้านทานการแพร่ที่ภาวะไม่มีซิลเฟอร์ของอนุภาคชนิด 1351, $dp = 0.0096$ cm. เปรียบเทียบกับข้อมูลที่ได้จากการทดลอง

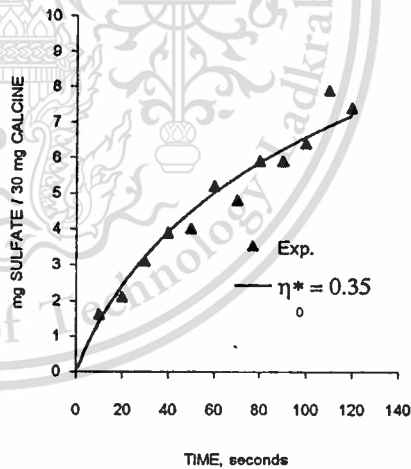
จากสมการที่ 16 หึ่งสังเกตว่าค่าของ β ถูกแสดงในตารางที่ 4 นั้นหาได้จากสมการที่ 12 ภายใต้สมมติฐานที่ว่าในภาวะเริ่มต้นปฏิกิริยา r_0 ไม่เปลี่ยนแปลงในอนุภาคชนิดเดียวกันที่มีขนาดต่างกันดังนั้น ค่าเหล่านี้จะถูกระบุเฉพาะความสัมพันธ์ระหว่าง $\ln(r)$ และ ปริมาณซิลเฟด g/w ในกรณีที่ไม่มีผลจากการแพร่ ($\eta_0^* = 1$) ในภาวะเริ่มต้น



รูปที่ 5 ผลของความต้านทานการแพร่ที่ภาวะไม่มีซิลเฟอร์ของอนุภาคชนิด 1351, $dp = 0.025$ cm เปรียบเทียบกับข้อมูลที่ได้จากการทดลอง

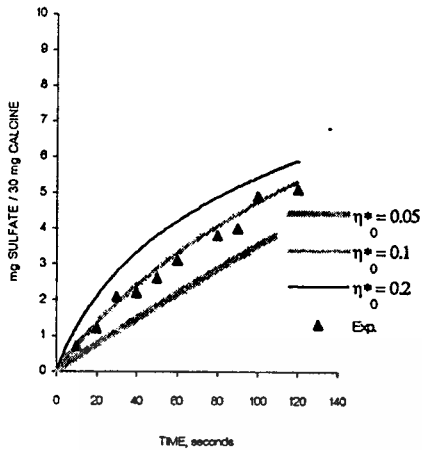
โดยทั่วไปจะสังเกตเห็นว่าผลที่ได้จะต่ำกว่าข้อมูลที่ได้จากการทดลอง การเปลี่ยนความต้านทานในการแพร่มีผลต่อการดูดซับ การลดลงของอัตราการเกิดปฏิกิริยาที่สภาวะแรก ๆ ของการเกิดปฏิกิริยาในสภาวะที่มีซิลเฟด 2×10^3 กรัมต่อ 1 กรัมของน้ำหนักอนุภาค อัตราการเกิดปฏิกิริยาจะเท่ากับค่าที่แสดงไว้ในตารางที่ 2 ในขณะที่พจน์ที่เป็นลอคกาลีทิมของอัตราการเกิดปฏิกิริยาลดลงแบบเชิงเส้นต้องการเพิ่มขึ้นของซิลเฟดจึงทำให้อัตราการลดลงนี้สำหรับกรณี $\eta_0^* < 1$ จะน้อยกว่าในกรณีที่ $\eta_0^* = 1$ เป็นผลให้เกิดปฏิกิริยาที่สูงกว่าเมื่อมีซิลเฟดมากกว่า 2×10^3 กรัมต่อ 1 กรัมของน้ำหนักอนุภาค การเพิ่มขึ้นของซิลเฟดในกรณี $\eta_0^* < 1$ จะมากกว่าในกรณี $\eta_0^* = 1$ หลังระยะเวลาหนึ่ง

ในรูปที่ 5 แสดงถึงสิ่งที่เกิดขึ้นในลักษณะเดียวกันในการเปลี่ยน η_0^* อัตราการเกิดปฏิกิริยาจะน้อยเมื่ออนุภาคมีขนาดเล็ก ($dp = 0.0096$ เซนติเมตร) เนื่องจากขนาดของ β มีค่าน้อย ที่เวลา 0 วินาที และ $\eta_0^* = 1$ นั้น ทั้ง 2 กรณีมีอัตราการเกิดปฏิกิริยาเท่ากันหากแต่ว่าสำหรับเวลาที่มากกว่า 0 วินาที อัตราการเกิดปฏิกิริยาสำหรับอนุภาคขนาด 0.25 เซนติเมตร จะน้อยกว่าอนุภาคขนาด 0.0096 เซนติเมตร และความแตกต่างจะเห็นได้ชัดเจนเมื่อเวลาเพิ่มขึ้น เนื่องมาจากการเพิ่มขึ้นของซิลเฟดดังนั้นเมื่อใช้ค่า $\eta_0^* = 0.35$ จะเป็นค่าที่ดีที่สุด ดังรูปที่ 6



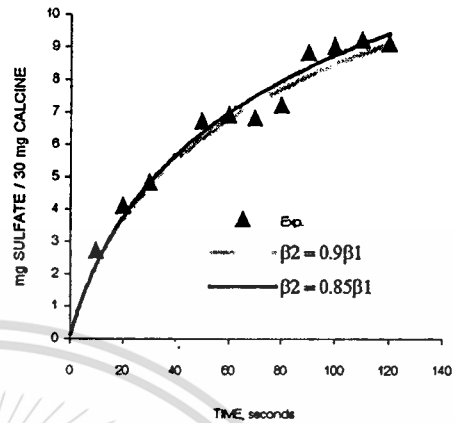
รูปที่ 6 เปรียบเทียบระหว่างแบบจำลองทางคณิตศาสตร์เมื่อใช้ $\eta_0^* = 0.35$ กับผลที่ได้จากการทดลองของอนุภาคชนิด 1351, $dp = 0.025$ cm

ในขณะที่การดูดซับด้วยอนุภาคขนาด 0.13 เซนติเมตร ค่า η_0^* ที่ 0.09 เป็นค่าที่ดีที่สุด ที่ η_0^* มีค่าเป็น 0.05 จะเพิ่มความเป็นเส้นตรงเทียบกับเวลาที่ผ่านไป ซึ่งแสดงให้เห็นว่าอิทธิพลของ $\frac{n'}{w}$ มีน้อยมากที่สภาวะดังกล่าว

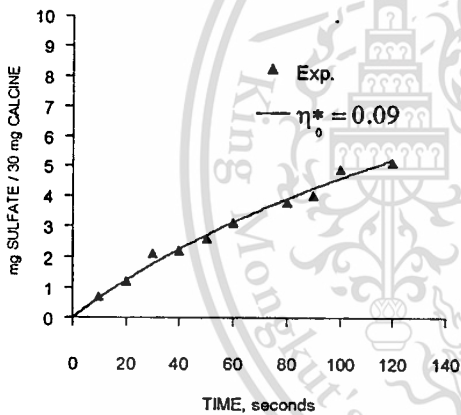


รูปที่ 7 ผลของความต้านทานการแพร่ที่ภาวะไม่มีซัลเฟอร์ของอนุภาคชนิด 1351, $d_p = 0.13$ cm เปรียบเทียบกับข้อมูลที่ได้จากการทดลอง

เป็นสิ่งที่แตกต่างกัน ดังนั้น η_0^* และ β ควรถูกกำหนดขึ้นสำหรับอนุภาคแต่ละชนิด



รูปที่ 9 ผลของ β ต่อการดูดซับก๊าซซัลเฟอร์ไดออกไซด์เปรียบเทียบกับผลที่ได้จากการทดลอง ของอนุภาคชนิด 1351, $d_p = 0.0096$ cm



รูปที่ 8 เปรียบเทียบระหว่างแบบจำลองทางคณิตศาสตร์เมื่อใช้ $\eta_0^* = 0.09$ กับผลที่ได้จากการทดลองของอนุภาคชนิด 1351, $d_p = 0.13$ cm เมื่อใช้ β ต่าง ๆ กัน

3.บทสรุป

งานวิจัยที่นำมารายงานในบทความนี้เป็นส่วนหนึ่งของการสร้างแบบจำลองทางคณิตศาสตร์ ซึ่งยังต้องทำการพัฒนาอีกต่อไปเพื่อให้สามารถครอบคลุมช่วงของการทำปฏิกิริยาในห้องเผาไหม้อุตสาหกรรมในขั้นนี้พอจะสรุปได้ว่า แบบจำลองทางคณิตศาสตร์ได้ถูกพัฒนาขึ้นให้ผลการจำลองเป็นที่น่าพอใจสำหรับขนาดและชนิดของหินปูนที่มีผลการทดลองจากรายงานในอดีต โดยตัวแปรที่ทำการปรับแต่ง 2 ตัวคือ η_0^* และ β ซึ่งไม่ยุ่งยากในการนำไปรวมกับแบบจำลองหลักทางด้าน การเผาไหม้

4.รายการสัญลักษณ์

- A = frequency factor, $\text{sec}^{-1}(\text{g.moles/cc.})^{-m}$
- A_0 = frequency factor ในสภาวะไม่มีการทำปฏิกิริยา, $\text{sec}^{-1}(\text{g.moles/cc.})^{-m-1}$
- C = ความเข้มข้นของก๊าซซัลเฟอร์ไดออกไซด์, g.moles/cc.
- C_{sat} = ความเข้มข้นของก๊าซซัลเฟอร์ไดออกไซด์ 2.9×10^{-5} g.moles/cc.
- Dp = เส้นผ่านศูนย์กลางของอนุภาค, cm.
- E = พลังงานการกระตุ้น, cal./g.mole
- k_p = ค่าคงที่ของอัตราการเกิดปฏิกิริยาต่อหน่วยปริมาตรของของแข็ง, $\text{sec}^{-1}(\text{g.moles/cc.})^{-m-1}$
- m = ลำดับความเข้มข้นของก๊าซซัลเฟอร์ไดออกไซด์
- n' = ซัลเฟอร์ใน SO_3 , g.mole
- r = อัตราการเกิด SO_3 , g.moles/(g.sec)
- r_0 = อัตราการเกิด SO_3 ที่สภาวะไม่มีซัลเฟอร์, g.moles/(g.sec)
- v = ปริมาตร, cc.

สำหรับรูปที่ 7 แสดงให้เห็นถึงความแตกต่างของ η_0^* เช่นเดียวกับรูปที่ 5 แต่มีขนาดเส้นผ่านศูนย์กลาง 0.13 cm. และรูปที่ 8 เป็นค่าที่เหมาะสมของ η_0^* สำหรับอนุภาคชนิด 1351 ขนาดเส้นผ่านศูนย์กลาง 0.13 cm. ผลของ β ต่อการดูดซับซัลเฟอร์ไดออกไซด์แสดงได้ดังรูปที่ 9 ที่ค่าคงที่ของ $\eta_0^* = 1$ การลดลงของขนาดของ β จะทำให้อัตราการเกิด ปฏิกิริยาเพิ่มขึ้น ค่า β ที่มากขึ้นจะทำให้อัตราการเกิดปฏิกิริยา ลดลง สำหรับอนุภาคแต่ละชนิด แบบจำลองทางคณิตศาสตร์สำหรับการดูดซับก๊าซซัลเฟอร์ไดออกไซด์ ที่มีความสัมพันธ์ระหว่างการเพิ่มขึ้นของซัลเฟอร์ไดออกไซด์ตลอดช่วงเวลาและ η_0^* รวมถึง β จะหาได้จากข้างต้น อย่างไรก็ตามปฏิกิริยาเคมีและโครงสร้างของอนุภาค

w = น้ำหนัก, g.

T = อุณหภูมิ, K

T_{ref} = อุณหภูมิอ้างอิงที่ 1143K (870°C)

t = เวลา, sec

β = สัมประสิทธิ์ที่ได้จากกราฟและแสดงในตารางที่ 4

η = อัตราส่วนของอัตราการเกิดปฏิกิริยา

ρ = ความหนาแน่น, g/cc.

5. เอกสารอ้างอิง

- A. Levy and E. L. Merryman. (1965).** The Microstructure of Hydrogen Sulphide Flames. Combust. Flame. Vol. 9 p.229-240.
- Bardakci, T. (1985).** Diffusional Study of the Reaction of Sulfur Dioxide with Reactive Porous Matrices. Thermochemica Acta. Vol. 76. p. 287.
- Bhatia, S.K., and D.D. perlmutter. (1981a).** The Effect of Pore Structure on Fluid – Solid Reactions. I : Application to the SO₂ – lime Reaction. AIChE J. Vol. 27. p. 226.
- Bhatia, S.K., and D.D. perlmutter. (1981b).** A Random – Pore Model for Fluid – Solid Reactions. II : Diffusion and Transport Effects. AIChE J. Vol. 27. p. 274.
- Borgwardt, R.H. (1970).** Kinetics of the Reaction of SO₂ with Calcined Limestone. AIChE J. Vol. 4. p. 59.
- Borgwardt, R.H., and Bruce, K.R. (1986).** Effect of Specific Surface Area on the Reactivity of CaO with SO₂. AIChE J. Vol.32. p. 239.
- Christman, P.G., and T. F. Edgar. (1983).** Distributed Pore – Size Model for Sulfation of Limestone. AIChE J. Vol. 29. p. 388.
- De Soete F.F. (1988).** Fundamentals of NO Formation and Destruction (Gas phase). Course on combustion of solid fuels. IFRF, Noordwijkerhout, The Netherlands.
- Georgakis, C., c.W. Chang, and J. Szekely. (1979).** A Changing GrainSize Model for Gas – Solid Reactions. Chem. Eng. Sci. Vol. 34. p. 1072.
- Hartman, M., and R. W. Coughlin. (1974).** Reaction of Sulfur Dioxide with Limestone and the Influence of Pore Structure. Ind. Eng. Chem. Proc. Des. Develop. Vol. 13. p. 248.
- Hartman, M., and R. W. Coughlin. (1976).** Reaction of Sulfur Dioxide with Limestone and the Grain Model. AIChE J. Vol. 22. p. 490.
- Hartman, M., and R. W. Coughlin. (1978).** Influence of Porosity of Calcium Carbonates on Their Reactivity with Sulfur Dioxide. Ind. Eng. Chem. Proc. Des. Dev. Vol. 17. p. 411.
- Lee, D.C., and C. Georgakis. (1981).** A Single – Particle Size Model for Sulfur Retention in Fluidized Bed Coal Combustors. AIChE J. Vol.27. p. 472.
- Lockwood F.C. and Jones W.P. (1993).** The Mathematical Modelling of Combustion Chambers Furnaces and Fires: Prediction of NO emissions from a staged burner. Outline of Lecture notes. Vol.3. October 1993. Post Experience Course Lectures. Dept. of Mech. Eng., ICSTM, London.
- Lockwood F.C., Rizvi S.M.A., Lee F.K. and Whalet K. (1994).** Coal Combustion Model Validation Using Cylindrical Furnace Data. Twentieth Symposium (Int.) on Combustion. The Combustion Institute. p.513.
- Magnussen B.F. and Hjertager B.H. (1976).** On Mathematical Mldelling of Turbulent Combustion with Special Emphasis on Soot Formation and Combustion. Sixteenth Symposium (Int.) on Combustion. The Combustion Institute. p.719
- Marsh, D.W., and D. L. Ulrichson. (1982).** Rate and Diffusional Study of the Reaction of Calcium Oxide with Sulfur Dioxide. AIChE Ann. Meet, Los Angeles.
- Newton, G. H., Chen, S. L., and Kramlich, J.C. (1989).** Role of Porosity Loss in Limiting SO₂ Capture by Calcium Based Sorbents. AIChE J. Vol. 35. p.988.
- Ramachandran, P.A., and J. M. Smith. (1977).** A Single – Pore Model for Gas – Solid Monocatalytic Reactions. AIChE J. Vol. 23. p. 353.
- Romo – Millares C.A. (1992).** Mathematical Modelling of Fuel NO Emissions from PF Burners. Ph.D. Thesis. University of Lodon.
- Salooja A.P. (1979).** Mathematical Modelling of and experimental Studies in Axi – Symmetrical Combustors. Ph.D. Thesis. University of London.
- Shen B. (1994).** The Application of Second – Moment Turbulence Closures to 2D Pulverised –Coal Flames. Ph.D. Thesis. University of London.
- Simons, G. A. (1982).** The Pore Tree Structure of Pore Char. 19th Int. Symp. Combustion, Combustion Institute.
- Simons, G.a., and Garman, A.R. (1986).** Small Pore Closure and the Deactivation of the Limestone Sulfation Reaction. AIChE J. Vol. 32. p. 1491.
- Sloan D.F., Smith P.F., and Smoot L.D. (1986).** Modelling of Swirl in Turbulent Flow System. Progress in Energy Combustion Science. Vol.12. p.163.
- Sotirchoe, S. V., and H. C. Yu. (1985).** Mathematical Modelling of Gas – Solid Reactions with Solid Product. Chem. Eng. Sci. Vol. 40. p. 2039.
- Tetsuo KAWAMURA, (1999).** Flue Gas Desulfurization Technology. Clean Coal Technology Seminar in Thailand. p. 26.

- W.H. Holstead and E. Raask. (1969). The Behavior of Sulphur and Chlorine Compounds in Pulverized Coal – Fired Boilers. J. Inst. Fuel. Vol. 42 p. 344.
- Zarkanitis, S., and Sotichos, S. V. (1989). Pore Structure and Particle Size Effects on Limestone Capacity for SO₂ Removal. AIChE J. Vol. 35. p. 821.



This material is reserved for educational use only, not allowed for commercial use.

Forbidden to modify the content, and cite the document when use.

AUTHOR BIOGRAPHY

Author: Wipoo Sriseubsai

Date of Birth: February 7, 1976

Bachelor Degree: B.Eng. (Mechanical Engineering)

Institution: Faculty of Engineering

King Mongkut's Institute of Technology Ladkrabang

Year of Graduation: 2000

Under Graduate Research:

Development of Finite Volume Method with Fluid Flow in Circular Pipe,
1997.

Under Graduate Publication:

Charoensuk J. and Sriseubsai W. "Solution for Laminar Flow in Circular Pipe
by Finite Volume Method." National Mechanical Engineering Conference
12th. Dec.1998. pp. 159-165.

Graduate Research:

Mathematical Model for The Adsorption of Sulfur Dioxide by Calcium
Carbonate, 2000.

Graduate Publication:

Charoensuk J. and Sriseubsai W. "Mathematical Model for Sulfur Dioxide
(SO₂) Absorption by Calcine (CaO) Particle." National Mechanical
Engineering Conference 13th. Nov.1999. pp. 1-8.

Occupation: Lecturer

Department of Industrial Engineering, Faculty of Engineering

King Mongkut's Institute of Technology Ladkrabang

This material is reserved for educational use only, not allowed for commercial use.

Forbidden to modify the content, and cite the document when use.